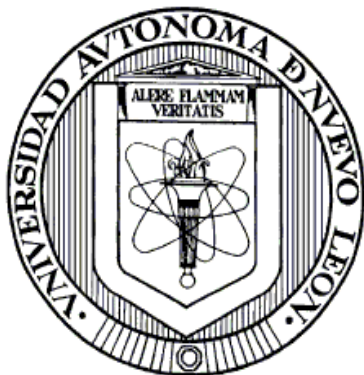UNIVERSIDAD AUTÓNOMA DE NUEVO LEÓN

FACULTAD DE CIENCIAS QUÍMICAS

ARTIFICIAL NEURAL NETWORK MODELING OF PHENOL ADSORPTION

ONTO BARLEY HUSKS ACTIVATED CARBON IN AN AIRLIFT REACTOR

Por

MARGARITA LOREDO CANCINO

Como requisito parcial para obtener el Grado de
DOCTOR EN CIENCIAS con Orientación en Procesos Sustentables

Julio, 2013

ARTIFICIAL NEURAL NETWORK MODELING OF PHENOL ADSORPTION

ONTO BARLEY HUSKS ACTIVATED CARBON IN AN AIRLIFT REACTOR

Dissertation Review Comittee:

Dr Eduardo Soto Regalado
Advisor

Dr María Teresa Garza González
Co-Advisor

Dr María Mónica Alcalá Torres
Reviewer

Dr Felipe de Jesús Cerino Cordova
Reviewer

Dr Oscar Leonel Chacón Mondragón
Reviewer

Dr Refugio Bernardo García Reyes
Reviewer

Dr Ricardo Gómez González
Reviewer

ACKNOWLEDGEMENTS

To my family, for their endless encouragement.

To David, for his remarkable patience and unwavering love and support.

By this virtue,
may all beings,
my dear family, friends,
and all my dear relations everywhere and at all times
have health,
long life,
clear minds,
peace and joy.

ABSTRACT

Margarita Loredo Cancino   Jul, 2013

Universidad Autónoma de Nuevo León

Facultad de Ciencias Químicas

Dissertation title: ARTIFICIAL NEURAL NETWORK MODELING OF PHENOL ADSORPTION ONTO BARLEY HUSKS ACTIVATED CARBON IN AN AIRLIFT REACTOR

Number of pages: 89   Doctoral candidate in the Sustainable
                                        Processes orientation.

Orientation: Sustainable Processes.

Purpose and method of the study: The production of activated carbon from barley husks (BH) by chemical activation with zinc chloride was optimized by using a 2^3 factorial design with replicates at the central point, followed by a central composite design with two responses (the yield and iodine number) and three factors (the activation temperature, activation time, and impregnation ratio). Both responses were simultaneously optimized by using the desirability functions approach to determine the optimal conditions of this process. The experimental data from the batch phenol adsorption onto barley husks activated carbon (BHAC) was represented by adsorption isotherms (Langmuir and Freundlich) and kinetic models (pseudo-first and pseudo-second order, and intraparticle diffusion models), besides the regeneration of phenol-loaded BHAC with different solvents was evaluated. Experimental data confirmed that the breakthrough curves were dependent on BHAC dosage, phenol initial concentration, air flow rate, and influent flow rate. Adaline and feed-forward back-propagation Artificial Neural Networks (ANNs) were developed to predict the breakthrough curves for the adsorption of phenol onto barley husks activated carbon (BHAC) in an airlift reactor. Feed-forward back-propagation networks were tested with different quantity of neurons at the hidden layer to determine the optimal number of neurons in the ANN architecture to represent the breakthrough curves performed at different operational conditions for the airlift reactor.

Contributions and conclusions: After the simultaneous dual optimization of BHAC production, the maximal response values were obtained at an activation temperature of 436 °C, an activation time of 20 min, and an impregnation ratio of 1.1 g $ZnCl_2$ g BH^{-1}, although the results after the single optimization of each response were quite different. At these conditions, the predicted values for the iodine number and yield were 829.58 ± 78.30 mg g^{-1} and 46.82 ± 2.64%, respectively, whereas experimental tests produced values of 901.86 mg g^{-1} and 48.48%, respectively. Moreover, activated carbons from BH obtained at the optimal conditions mainly developed a porous

structure (mesopores > 71% and micropores > 28%), achieving a high surface area (811.44 m^2 g^{-1}) that is similar to commercial activated carbons and lignocellulosic-based activated carbons. These results imply that the pore width and surface area are large enough to allow the diffusion and adsorption of pollutants inside the adsorbent particles.

Freundlich isotherm model satisfactorily predicted the equilibrium data at 25 and 35 °C, whereas the Langmuir isotherm model well represented the equilibrium data at 45 °C. The maximum phenol adsorption capacity onto BHAC was 98.83 mg g^{-1} at 25 °C and pH 7, similar to phenol adsorption onto commercial activated carbons. The kinetic data were adequately predicted by both the pseudo-first order and intraparticle diffusion models. The external mass transfer was minimized at stirring speeds greater than 400 min^{-1}, and the adsorption kinetics are affected by both initial phenol concentration and temperature. Adsorption equilibrium was reached within 40 and 200 min at initial phenol concentration of 1000 mg L^{-1} at 35 °C and 30 °C, respectively. Ethanol/water solutions at 10% V/V were the most effective regenerating agent, with desorption capacity of 47.79 mg g^{-1} after five adsorption-desorption cycles.

The breakthrough curves of phenol adsorption onto BHAC in an airlift reactor in continuous operation were adequately predicted with feed-forward back-propagation ANN architecture with 2 neurons in the hidden layer for the single-input single-output problem. Correlation coefficients higher than 0.95 were observed between the breakthrough curves predicted by the developed Adaline network and those obtained experimentally for the multiple-input single-output problem. Further improvements and generalization of the developed predictive Adaline network are discussed.

ADVISOR SIGNATURE: _____

Dr. Eduardo Soto Regalado

TABLE OF CONTENTS

Chapter   Page

LIST OF TABLES

LIST OF FIGURES

xi

CHAPTER 1

1. INTRODUCTION

1.1 Phenol Properties

Phenol (CAS No. 108-85-2) is a colorless crystalline solid at 25° C. It has a molecular formula of C_6H_5OH and a molecular weight of 94; the size of a phenol molecule could be approximated by an ellipsoid of 0.8 x 0.7 x 0.2 nm dimension [1,2] with a cross sectional area of $0.3 - 0.522$ nm^2 molecule^{-1} [3] and an approximate volume of 3.52 nm^3 [2]. At 25° C, the vapor pressure is 0.35 mm Hg. Pure solid phenol has a melting point of 43° C, a boiling point of 182 °C at standard pressure, and a very sweet tarry odor. Phenol has variable water solubility between 0 – 65° C, approximately 6.7 g in 100 mL at 16° C. Phenol is slightly acidic with a pK_a of 9.9 in aqueous solutions at 25° C [4].

1.1.1 Phenol Industrial Synthesis and Sources

Phenolic compounds are natural components of many common products such as tea, wine, and smoked food. Phenol was first isolated in 1834 from coal tar by the German chemist Runge [5]. Nowadays most of phenol is synthetically produced by the Hock process, which is based on the oxidation of cumene to form phenol and acetone; this process produce approximately 95% of the phenol used worldwide [5]. Alternatives

for phenol production include reactions of chlorobenzene with caustic soda, the oxidation of toluene via benzoic acid, and recovery by the fractional distillation of coal tar [5,6].

Phenol is also a product of the combustion of fossil fuels and tobacco, the decomposition of organic material, and it can be present in the air as a product of the photo-oxidation of benzene. Phenol is a common pollutant present in wastewaters of industries, such as refineries, coal processing, olive milling, and the manufacture of petrochemicals, fabrics, plastics, wood products, paints, paper, and resins, among others.

1.1.2 Phenol Industrial Applications

As a pure substance, phenol is used as disinfectant; for the preparation of lotions and shaving soap; in veterinary medicine as antiseptic and gastric anesthetic; as an extracting solvent in refineries; for the production of lubricants; and as reagent in chemical analysis. However, the largest use of this substance is in the production of phenolic resins (Bakelite). Also, phenol can be converted into bisphenol A, a monomer for epoxic resins, by a reaction with acetone. Phenol is also used to produce cyclohexanone, which is later converted into the monomer for nylon 6 [5].

1.2 Phenol and Health

Phenol may have harmful effects on both public health and aquatic life; for example, it has been found that metabolism, survival, growth, and reproductive system of fishes are affected when they live in phenolic polluted water [7]. In human beings, the effects of repeated oral exposure to phenol include diarrhea, mouth sores, and dark urine [6], furthermore the ingestion of 1 g of phenol is deadly for humans [5].

In addition, phenol has been evaluated in a number of tests in order to verify its potential to induce gene mutations. Bruce *et al.* [6] have reported positive results in *in vitro* tests for gene mutation in Chinese hamster cells, and also refer other studies that demonstrate fetotoxicity of phenol at high doses. Phenol may be a promoter and/or weak skin cancerigen [6]. Consequently, wastewater polluted with phenol must be treated prior to its discharge.

1.3 Abatement Technologies for Phenol in Wastewaters

Phenol is one of the most common organic water pollutants present in natural water resources polluted by effluents of a variety of chemical industries. Phenol is toxic even at low concentrations, and its presence in wastewaters can lead to the formation of highly toxic substituted phenolic compounds during disinfection and oxidation processes.

The methods to remove phenol from wastewaters can be divided into two groups: destruction and regeneration methods. Destruction methods include chemical transformation of phenol such as: oxidation, supercritical destruction, and biodegradation, while regeneration methods comprise separation by evaporation, extraction, adsorption, pervaporation, and membrane techniques. Because each method have advantages and disadvantages, in order to design the most suitable system for phenolic wastewater treatment it is necessary to take into account several factors such as initial concentration of phenol and other pollutants, the permissible limit of phenol in wastewater, and the quantity of wastewater to be treated, among others.

1.3.1 Destruction of Phenol in Water Solution

1.3.1.1 Total Oxidation of Phenol by Air or Oxygen

1.3.1.1.1 Non Catalytic Wet Air Oxidation. Wet air oxidation was first developed and applied as a commercial process by Zimmerman in 1950 [5]. Typical conditions for wet oxidation range from 180 °C and 2 MPa to 315 °C and 15 MPa. Residence times may be ranged from 15 to 120 minutes. The ortho and para dihydroxy-benzenes (catechol and hydroquinone) and ortho and para benzoquinones, are by-products of the phenol oxidation, and these are compounds of equal or greater toxicity than phenol [5].

1.3.1.1.2 Catalytic Wet Air Oxidation. Most of the catalysts proposed for catalytic wet air oxidation of phenol are alumina or carbon containing noble metals (Pt, Ru) or transition metal cations (Cu, Co, Mn, Fe). Typical reaction conditions are temperatures from 100 to 200 °C and reaction times from 1 to 3 hours, allowing phenol conversion greater than 90 to 95% [5]. The disadvantages of catalytic wet air oxidation include the formation of toxic intermediates and the leaching of the active metal species that pollutes the wastewater and leads to the progressive loss of catalytic activity of the catalyst.

1.3.1.1.3 Oxidative Polymerization with Oxygen in Presence of Enzymes. The enzymes tyrosinase and laccase use oxygen to convert phenols into o-quinones. These compounds are further converted into heavier oligomeric species that may be more easily filtered and/or adsorbed on a solid. The main disadvantage of this technique is the high cost and the difficulty to obtain isolated and purified enzymes.

1.3.1.2 Wet Oxidation with Chemical Oxidants

Different chemical oxidants have been reported to be active in the wet total oxidation of phenol in aqueous solution. The most used are ozone and hydrogen peroxide.

1.3.1.2.1 Oxidation with Ozone. Ozonation is a promising alternative for wastewater treatment through degradation of contaminants with ozone acting directly on the nucleophilic sites and unsaturated bonds of the organic compounds. However, in this method pollutant oxidation rate and the utilization efficiency of ozone are low. Subsequently, a large amount of ozone is needed for an efficient operation, which greatly limits its practical application [5,8].

1.3.1.2.2. Oxidation with Hydrogen Peroxide (Conventional Homogeneous Fenton Reaction). The conventional Fenton reaction uses hydrogen peroxide in conjunction with an iron (II) salt to produce hydroxyl radicals which can oxidize organic compounds in solution. The Fenton reaction has been reported as the most economic oxidation alternative due to the simplicity of the equipment and moderate operation conditions (atmospheric pressure and room temperature). Nonetheless, acidic pH and stoichiometric excess of hydrogen peroxide are required for an efficient reaction, and this usually implies that significant quantities of ferric salts must be disposed of after the reaction is complete. Another detriment of this method is that some intermediates such as hydroquinone and *p*-benzoquinone show toxicity levels much higher than phenol itself [5]. Finally, the application of the conventional Fenton reaction is complicated due to the typical problems associated to homogeneous catalysis, such as catalyst separation and regeneration, among others.

1.3.1.2.3. Oxidation with Other Chemical Oxidants. Alternative oxidation procedures for phenol elimination include oxidation with chlorine and chlorine dioxide, as well as with potassium permanganate. These methods are not environmentally friendly, due to the formation of chlorinated organic compounds and the dispersion of manganese compounds. These methods are also expensive due to the cost of the reagents [5].

1.3.1.3 Electrochemical Oxidation

1.3.1.3.1 Indirect Electro-oxidation Processes (Electrofenton). In this technique the oxidizing agent (hydrogen peroxide) is generated electrically from dissolved oxygen in aqueous solution with the addition of Fe^{2+} as catalyst in a continuous mode, which may be more efficient and cost-effective than conventional dosing methods. The electrofenton method has the advantage of allowing a better control of hydroxyl radical production; however, the possibility of secondary pollution from the added heavy metals limits the application of this process.

1.3.1.3.2 Direct Anodic Oxidation. Electro-oxidation of pollutants can be performed directly on anodes. The anodic oxidation does not need to add a large amount of chemicals to wastewater or to feed O_2 to cathodes, with no tendency of producing secondary pollution. Anode materials investigated include Ti/RuO_2, Ti/Pt-Ir, fiber carbon, MnO_2, Pt-carbon black, porous carbon felt, stainless steel, and reticulated vitreous carbon. Nevertheless, none of them have sufficient activity and at the same time stability [5]. The application of boron-doped diamond electrodes present a better performance with respect to previously mentioned materials, but costs associated to this electrode limits its use.

1.3.1.4 Photocatalytic Oxidation

TiO_2 photocatalysis has been intensively investigated for its application to the destruction of environmental toxic pollutants. TiO_2-anatase is non-toxic and resistant to photo-corrosion. The main drawback of this method is the possibility of catalyst leaching into the effluent, causing loss of activity during reuse [5].

1.3.1.5 Supercritical Water Gasification

Supercritical water gasification is the conversion of organic material into gaseous products (H_2, CO, CO_2, CH_4) via reactions in and with water at temperature and pressure exceeding the thermodynamic critical point of water ($T_c = 374$ °C, $P_c = 22.1$ MPa). The main detriment of this technology is its high operation cost resulting from the extreme pressure and temperature conditions needed to operate.

1.3.1.6 Biodegradation

Biological treatment involves the action of living microorganisms that utilize pollutants as food and convert it into simpler substances by natural metabolic processes. Aerobic biodegradation of many aromatic compounds is common and proceeds through a key intermediate, cathecol. Many microbial strains capable of degrading phenol have been cited such as the genus *Pseudomonas* [9-12] and *Candida tropicalis* [13,14]. Most of the cultures tested are capable of degrading phenol at low concentrations; however, phenol is toxic to most types of microorganisms at sufficiently high concentration. Consequently, phenol concentration needs to be maintained below toxic limits for microorganisms in order to achieve a satisfactory performance. Phenol concentrations lower than 500 mg L^{-1} are generally considered suitable for biological treatment techniques [15].

1.3.2 Separation of Phenol from Water Solutions

1.3.2.1 Evaporation Methods

Phenol removal from an organic media is frequently carried out by steam distillation processes, based on the steam volatility of phenol. Nevertheless, when phenol is dissolved in an aqueous solution, azeotrope properties are highly unfavorable for this technology: to remove 95% of the phenol, it is necessary to have 16 – 20 theoretical trays, as well as to distill up to 10% of the quantity of wastewater. The main disadvantage of this method is the high energy demand: about 2000 m^3 of steam are required to treat 1 m^3 of wastewater [16].

1.3.2.2 Extraction

The extraction of phenols using immiscible solvents with water is widely used in industry, particularly for phenol extraction from highly loaded phenolic wastewaters. Several organic solvents allow phenol extraction in water, such as *n*-hexane and cyclohexane, benzene, toluene, etylbenzene, cumene, acetate esters, di-isopropyl eter, metyl-*iso*-butyl ketone, etc. Once phases are separated, phenol is extracted by treating organic phase with an alkali or by distillation. With an adequate selection of solvent, most of the phenol homologues are extracted with this pollutant. The main drawbacks of this method are the high operational costs and secondary pollution of wastewaters with solvents.

1.3.2.3 Pervaporation

Pervaporation is a process where a liquid or gas mixture is separated by means of a partial vaporization through a selective membrane. The mixture contacts one side of a non-porous permselective membrane; permeate is removed as a vapor from the

other side. At present, membranes and other equipment related to this process (*i.e.,* vacuum pumping systems) are relatively expensive; hence pervaporation of phenolic wastewater is not economically feasible.

1.3.2.4 Membrane-based Solvent Extraction

Emulsion Liquid Membranes (ELM) consist of an aqueous phase (internal receptor phase) stabilized by oil soluble surfactants and dispersed as very fine droplets inside an oil phase (membrane phase). The resulting liquid membrane is further dispersed as emulsion globules in another aqueous solution (external donor phase). The target solutes in the external donor phase are transferred across the membrane phase into the internal receptor phase during an extraction process. After the desired level of extraction is achieved, the external phase and the ELM are gravimetrically separated and demulsified for separation of the internal phase from the membrane phase which is typically regenerated and reused. Advantages of this process are the relative low energy consumption and rapid extraction with relatively high efficiency; however, extensive use of ELM processes has been limited due to the instability of the emulsion globules [5].

1.3.2.5 Adsorption

Adsorption is the best suitable method for the removal of phenol at low concentration in wastewater, due to the high specific surface area and the possibility of incorporating functional groups on its surface, activated carbon could have a strong affinity for binding organic or inorganic pollutants from aqueous solutions. For these reasons, activated carbons are commonly used for wastewater treatment. However, despite these advantages, the use of commercial activated carbon as adsorbent is often limited for economic reasons, and many researchers have paid attention to the

use of alternative precursors for activated carbon production, such as agro-waste materials. A number of lignocellulosic by-products have been tested as precursors in the production of activated carbon, including: date stones [17], coffee residue [18], nutshell [19,20], agave bagasse [21], pharmaceutical herb residue [22], tamarind wood [23], coir pith [24], *oreganum* stalks [25], pistachio-nut shell [26], etc.

In addition to the high cost, the main drawback of the use of activated carbon as adsorbent is the secondary pollution generated by disposal of spent adsorbent. To overcome this disadvantage, there are numerous adsorbent regeneration techniques used to re-establish the maximum adsorbent capacity and to preserve, as much as possible, the initial weight and pore structure of the adsorbent. Thermal regeneration is one of the desorption methods most widely used. In this method, the adsorbates are desorbed by means of volatilization and oxidation at high temperature. However, this method has disadvantages such as the loss of activated carbon by attrition (5 to 10%), due to excessive burn off and washout during each cycle [27]. Chemical regeneration of adsorbents is a feasible alternative since it has some advantages; for instance, it can be performed *in situ*, there are no loss of activated carbon opposite to thermal desorption, it is possible the recovery of valuable adsorbates, and the chemical reagents can be reused [28].

1.4 Adsorption process

Adsorption is a surface phenomenon that involves the accumulation of substances on a surface; the adsorbed compound is named adsorbate and the phase where adsorption occurs is named adsorbent. Adsorption on solids is usually classified according to the type of force involved in the binding of the adsorbed molecules to the

surface molecules of the solid. When physical adsorption or physisorption takes place, the bonding forces are both the non-specific and relatively weak van der Waals forces (dispersion – repulsion) and electrostatic interactions comprising polarization, dipole and quadrupole interactions. Adsorption can also result in strong chemical bond formation between the adsorbent surface and the adsorbate molecules, by exchanging and sharing electrons, and may be considered as the formation of a surface compound. This phenomenon is called chemical adsorption or chemisorption. Although this distinction is conceptually useful there are many intermediate cases and it is not always possible to categorize a particular system unequivocally.

Since all molecules are subject to van der Waals forces, any specie can be physisorbed in a solid surface under appropriate conditions. Besides this, when adsorbent – adsorbate interactions are strong, multilayer of adsorbate are accumulated on the adsorbent, increasing its adsorption capacity [28-30]. On the other hand, chemisorption is limited to monolayer coverage of the surface because the strong bonds adsorbent–adsorbate are site-specific, thus making chemisorption systems generally viable only for trace impurity removal. These and other features which distinguish between physisorption and chemisorption are listed in Table 1 [31].

Table 1 Features of Physisorption and Chemisorption.

Physisorption	Chemisorption
Low heat of adsorption (< 2 or 3 times latent heat of evaporation).	High heat of adsorption (> 2 or 3 times latent heat of evaporation).
Non-specific.	Highly specific.
Monolayer or multilayer.	Only monolayer.
No dissociation of adsorbed species.	May involve dissociation.
Only significant at relatively low temperatures.	Possible over a wide range of temperature.
Rapid, reversible.	May be low and irreversible.
No electrons transfer although polarization of adsorbate may occur.	Electron transfer leading to bond formation between adsorbate and surface.

11

Various factors affect the extent to which a given compound will be adsorbed on the adsorbent surface. Major factors will be briefly discussed on the next paragraphs.

Temperature – In general, when raising the temperature the adsorption decreases because the adsorbed molecules have greater vibrational energies and they are therefore more likely to desorb from the surface [28,32].

Nature of the solvent – Due to the solvent competing with the adsorbent surface in attracting the solute, adsorption of a solute from a compatible solvent is less than its adsorption from another kind of solvent.

Particle size – Particle size is generally not a factor that affects adsorption capacity unless part of the surface area becomes inaccessible to adsorbate of certain size due to surface bottlenecks created by micropores. In such case, milling can contribute to the pore widening and facilitate adsorbate access. Therefore, particle size affects adsorption kinetics.

Surface area – Adsorption capacity is usually proportional to accessible internal surface area, and the availability of the aforementioned area is function of pore-size distribution.

Pore size distribution – Pores are often classified as macropores (pores with widths exceeding about 50 nm), mesopores (pores of widths between 2 nm and 50 nm) and micropores (pores with widths not exceeding about 2 nm) [33]. According to Efremenko and Sheintuch [1], phenol adsorption in pores lower than 0.94 nm in diameter is limited by steric restrictions. Therefore, only micropores with diameter higher than 1 nm are available for phenol adsorption.

Nature of the solute – As for organic substances, an increase in size of the solute molecule usually enhances adsorption, until the molecular sizes becomes large enough so that a significant number of pores become inaccessible. Also aromatic

compounds are usually more adsorbable tan aliphatic compounds of a similar molecular size [28].

pH of the solution – It is well known that when the pH is such that an adsorbable compound exists in ionized form, adjacent molecules of the adsorbed species on the carbon surface will repel each other to a significant degree, because they carry the same electrical charge.

Point of zero charge (PZC) and charge distribution – PZC is related to the pH value where net surface charge is zero, in other words the point where the total concentration of surface anionic sites is equal to the total concentration of surface cationic sites. Surface charge of adsorbent is positive for pH values lower than PZC and negative for pH values higher than PZC.

Functional groups – Depending on pH of the solution, some functional groups on the adsorbent surface are proton donors (acidic sites) and others are proton acceptors (basic sites). Cations are adsorbed in acidic sites whereas anions are adsorbed in basic sites, due to electrostatic attraction that allows the accumulation of the ion on the surface.

Presence of inorganic salts – The presence of inorganic salts (*e.g.*, NaCl) can enhance the adsorption of organic species to carbon, given that salt ions which carry a charge opposite to that of the adsorbed organic ions are attracted to the spaces between adjacently adsorbed organic ions, and reduce the strength of repulsion of the adjacently adsorbed organic ions [28].

Competing solutes – In general, the presence of other solutes will reduce the adsorption of any given solute, but it should be considered that because some adsorption sites can adsorb only certain solutes, not all solutes compete for exactly the same sites.

1.4.1 Lignocellulosic By-products as Activated Carbon Precursors

The basic structure of all lignocellulosic by-products is mainly composed by three natural polymers: cellulose, hemicelluloses, and lignin. Lignin is a mononuclear aromatic polymer found in the cell wall of certain biomass, whose function is to cement cellulose fibers in plants. This polymer is rich in carbon and its molecular structure is similar to bituminous coal which makes it a suitable precursor for activated carbon production [34].

The manufacture of activated carbon consist of the pyrolysis of the precursor material followed by a controlled oxidation stage (in case of physical activation) or the pyrolysis of the precursor material in a single step with activating agents such as KOH, K_2CO_3, NaOH, $ZnCl_2$ or H_3PO_4. The production of activated carbon by physical activation requires high temperatures (800 to 1000 °C) which involves high power consumption and a low yield of carbon [28,35]. On the contrary, chemical activation requires low temperatures (400 to 600ºC) and, consequently, the power consumption is significantly reduced and yield can be increased. However, there are also some disadvantages of the chemical activation, such as the generation of acidic wastewater containing the residual activating agent from the washing process of the final product. For this issue, some authors have investigated the reuse of the filtrate from the washing step as activating solution, with promising results [19,25,36]. Depending on the conditions of the manufacturing process, the typical surface areas for activated carbon vary from 500 to 1400 m^2 g^{-1}, although values as high as 2500 m^2 g^{-1} have been reported [1].

The final properties of the carbon will depend significantly on the nature of the raw material and the production conditions. To select the optimal conditions (*e.g.,* the temperature, impregnation ratio, and activation time, among other factors) for the

production of activated carbon, various researchers have carried out the optimization using the one-factor-at-time strategy [19,20,25,26]. This single-dimensional search is laborious and time-consuming, especially for a large number of variables. In recent years, some authors have used experimental designs to optimize and to study the effects of the process parameters and their possible interactions [37]; in particular, the factors that affect the activated carbon production from lignocellulosic by-products have been studied using Taguchi experimental designs for the optimization of one response [38,39] and the response surface methodology when two or more responses were optimized [21-23]. According to recent literature, there are not reported studies related to simultaneous optimization of yield and iodine number for the production of activated carbon from barley husks.

1.4.2 Phenol Adsorption onto Activated Carbon

Phenol adsorption on activated carbon is one of the most developed areas in the liquid phase adsorption field, because activated carbon exhibits a high affinity for phenolic compounds [18-20,25,40-46]. The raw materials for activated carbon are carbonaceous materials such as wood, peat, coals, petroleum coke, bones, coconut shell, fruit nuts, and lignocellulosic waste, among others. These waste materials have little or no economic value and often present a disposal problem, and their conversion into activated carbon would add economic value, could help to reduce the cost of waste disposal, and provide a potentially inexpensive alternative to the existing commercial activated carbons.

Several studies have tried to elucidate the mechanism of phenol adsorption on activated carbon, and the following interactions has been proposed: (a) donor-receptor interactions between the phenol aromatic ring and basic functional groups that contain oxygen, such as carbonyl groups; (b) the dispersion effect between the phenol aromatic

ring and π-electron of the carbon structure, and (c) the electrostatic attraction and repulsion when ions are involved [1-3,5,46-48].

The infrared studies indicates that the most common oxygen functional groups onto carbon materials are C=O in lactones and carboxylic anhydrides (stretching frequency 1750 cm^{-1}), quinone and ceto-enol groups (1600 cm^{-1}), and C-O group in ethers, lactones, phenols, and carboxylic anhydrides (a broad band centered around 1250 cm^{-1}) [1].

1.4.3 Adsorption Isotherms

In a state of equilibrium, the number of adsorbed molecules is the same that the numbers of desorbed molecules. The equilibrium state is characterized by the solute concentration in the adsorbent (q_e) and an associated final solute concentration in the liquid phase (C_e). These values of q and C_e often can be fitted to one or more standard isotherm equations; in this way, the q vs. C_e relationship can be expressed in mathematical form.

Adsorption isotherm is the expression of the relationship between the quantity of solute adsorbed and the concentration of the solute in the liquid phase, at a constant temperature. This relationship allows designing batch adsorption systems according to established methods. It is important to note that the adsorption isotherm does not provide systematically any information about the reactions involved in the sorption phenomenon. So, mechanistic interpretations must be carefully verified.

1.4.3.1 Henry's law

At sufficiently low adsorbed-phase concentrations on a homogeneous surface, the equilibrium isotherm for physical adsorption should always approach linearity (Henry's law). Henry's law corresponds physically to the case where the adsorbed

phase is so dilute that there is neither competition for adsorption sites nor interaction between adsorbed molecules. However, at higher loadings both effects become significant, leading to curvature of the above-mentioned relationship.

1.4.3.2 Langmuir Isotherm Equation

At higher loadings (beyond the Henry's law region) the equilibrium isotherms for microporous adsorbents are generally of Type I form in Brunauer's classification [33]. The Langmuir equation development has four important underlying assumptions. First, adsorption occurs at definite localized "sites" on the surface. Second, each site can bind only one molecule of the adsorbate species. Third, the energy of adsorption is the same for all sites, and, fourth, there are no forces of interaction between adjacently adsorbed molecules. The Langmuir isotherm equation has a hyperbolic form represented in Eq. 1:

$$q = \frac{b q_m C_e}{1 + b C_e} \qquad (1)$$

where b represents the equilibrium constant of adsorption reaction and q_m is the maximum adsorption capacity [49]. In the development of the original Langmuir equation q_m represents the concentration of the adsorbed species on the surface when one complete monomolecular layer of coverage is achieved [28,29]. The constants b and q_m can be determined from experimental data on a plot of adsorption capacity vs. equilibrium concentration of solute. Although the Langmuir expression provides a useful qualitative representation of the equilibrium behavior of many systems is generally not quantitatively reliable, especially at higher loadings [29].

1.4.3.3 Freundlich Isotherm Equation

It is frequently found that adsorption data from a liquid phase are well represented by the Freundlich isotherm equation:

$$q = KC_e^{1/n} \tag{2}$$

where K is the Freundlich isotherm constant related to adsorption capacity and n is a constant usually higher than 1, that represent the intensity of adsorption [29].

Freundlich model does not impose any requirement that the coverage must approach a constant value corresponding to one complete monomolecular layer as C_e increases. This behavior is physically impossible, and it means that Freundlich equation should fail to fit experimental data at very high C_e values.

1.4.4 Adsorption kinetics

The study of batch adsorption kinetics is relevant to design continuous systems. The solute uptake rate obtained from the kinetic analysis determines the residence time to achieve the equilibrium in an adsorption process, and it is useful for the scale up of adsorption equipment.

Several mathematical models have been proposed to describe adsorption data, which can be classified as adsorption diffusion models and adsorption reaction models. In one hand, adsorption reaction models are based on the whole process of adsorption without considering the mass transfer. On the other hand, adsorption intraparticle diffusion models are based on [50]: (1) bulk diffusion becoming significant for the adsorbent macropores, (2) Knudsen diffusion becoming predominant when the mean free path of the molecular species is much larger than the pore diameter (mesopores), and (3) surface diffusion of adsorbed molecular species along the pore wall surface.

18

1.4.4.1 Adsorption Reaction Models

The pseudo-first order kinetic equation [51] is given by Eq. 3

$$q_t = q_e\left(1 - e^{k_1 t}\right) \tag{3}$$

in which q_t is the amount of adsorbate adsorbed at time t, q_e is its value at equilibrium, and k_1 is a constant.

Pseudo-second order kinetic equation [52] can be expressed as follows:

$$q_t = \frac{q_e^2 k_2 t}{1 + q_e k_2 t} \tag{4}$$

1.4.4.2 Adsorption Intraparticle Diffusion Models

The intraparticle diffusion model can be derived from Fick's second law assuming that the intraparticle diffusivity (D_i) is constant and the uptake of adsorbate by the adsorbent is small relative to the total quantity of adsorbate present in the solution. Crank [53] developed Eq. 5 for the dimensionless fractional uptake of solute in the solid phase, q_t/q_∞.

$$F(t) = 1 - \frac{6}{\pi^2} \sum_{z=1}^{\infty} \frac{1}{z^2} \exp\left[\frac{-z^2 \pi^2 D_i t}{r_0^2}\right] \tag{5}$$

where $F(t) = q_t/q_\infty$ is the fractional attainment of equilibrium at time t, D_i is the internal diffusion coefficient, r_0^2 is the radius of the adsorbent particle assumed to be spherical, and z is an integer. Vermeulen's approximation of Eq. 5 fits the whole range $0 < F(t) < 1$

for adsorption on spherical particles. The simplified Vermeulen's approximation is given in Eq. 6 [54].

$$\ln\left[\frac{1}{1-F^2_{(t)}}\right]=\frac{\pi^2 D_i t}{r_0^2} \tag{6}$$

Thus the slope of the plot of $\ln[1/(1-F^2(t))]$ versus time would give D_i. Moreover, for small times Eq. 5 may be written as follows:

$$F(t)=6\left(\frac{D_i t}{r_0^2}\right)^{\frac{1}{2}}\left(\pi^{-\frac{1}{2}}+I\right) \tag{7}$$

Thus a plot of $F(t)$ vs. $t^{1/2}$ should give a straight line. Since q_∞ is a constant equal to the final value of q_t, then a plot of q_t alone vs. $t^{1/2}$ should also be linear. Therefore, the equation describing Weber & Morris [55] intraparticle diffusion model is represented by Eq. 8:

$$q_t=k_p t^{0.5}+I \tag{8}$$

where I is the intercept that could be associated to the thickness of the boundary layer [17]. A value of I around zero indicates that diffusion is the only controlling step of the adsorption process [17]. The slope of the plot has been defined as a rate parameter (k_p) which characterizes the rate of adsorption, given in Eq. 9.

$$k_p=\left(\frac{3q_e}{d_p}\right)\sqrt{\frac{D_i}{\pi}} \tag{9}$$

where d_p is the mean particle diameter, and from which D_i can be determined.

1.4.5 Airlift Reactors: Application in Adsorption Process

Commonly, the process of adsorption in liquid phase has been carried out mostly in mixed contacting vessels in batch operation and, also, using fixed-bed columns in a continuous-flow operation. Nevertheless, operational complexity and the limitation of the efficiency of removal have led to search for new and efficient equipment which can give better removal efficiency without additional mechanical complications. Airlift reactors are drawing increased attention as possible alternatives to current adsorption units because of their basic advantages such as a simple construction without moving parts, a high liquid phase content, and good mixing properties at low energy consumption [56]. Therefore, a few researchers have conducted adsorption experiments in airlift reactors; in 2004 and 2008 Filipkowska and Waraksa [57,58] studied the adsorption of dyes onto chitin on batch and continuous-flow operation, whereas in 2008 Mohanty *et al.* [56] studied the adsorption of phenol onto activated carbon on batch operation. More recently, Mohammed *et al.* [59] studied a process for continuous dye adsorption onto a graphite intercalation compound and electrochemical regeneration using an airlift reactor.

Airlift reactors belong to the category of buoyancy induced flow reactors in which compressed air is used to simultaneously aerate and agitate the liquid phase with controlled recirculation. Airlift reactors can be divided into two classes namely, the internal loop airlift reactors (ILALR) and the external loop airlift reactors (ELALR). The main difference is due to the presence of a separate gas disengagement section in ELALRs, which enables, if needed, a complete deaeration, whereas in the ILALR the downcomer is incorporated in the riser itself resulting in incomplete gas–liquid separation.

1.4.6 Modeling of Adsorption Process in an Airlift Reactor in Continuous Operation

Batch experiments provide a measure of the effectiveness of adsorption for removing specific adsorbates, as well as the maximum adsorption capacity. However, the continuous treatment of wastewater poses problems of hydrodynamics and mass transfer. A continuous adsorber does not run under equilibrium conditions and the flow conditions (hydrodynamics) affect the adsorbent mass transference. The breakthrough characteristics of the adsorber play a major role in the evaluation of the efficacy of the operation during continuous adsorption.

In continuous operations the feed to an adsorber is stopped when the concentration of solute in the effluent stream reaches a prescribed value named the breakthrough concentration, C_b. The time corresponding to this concentration is the breakthrough time, T_b. The breakthrough time can be estimated by the empirical process knowledge or by a model that describe the behavior of the breakthrough curves. Although Filipkowska and Waraksa [58] have recently reported the breakthrough curves of the adsorption of a reactive dye onto chitosan in airlift reactors, they did not reported a model for breakthrough curves prediction.

This could be because the basic knowledge needed for the design of an airlift reactor is not widely available in the literature. Moreover, the accessible information frequently shows wide variations, resulting in a lack of reliable design basis for airlift reactors. The difficulties associated in rigorous mathematical modeling of an airlift reactor due to the complexities of the process often makes the development of pure black-box artificial neural network (ANN) models particularly useful in this field.

Artificial neural networks are nets of simple functions that can provide satisfactory empirical models of complex nonlinear processes useful for a wide variety

22

of purposes. Some of the advantages in using ANNs as models are as follows: (1) ANNs can represent a highly nonlinear process with a complex structure in some cases better than many other empirical models, (2) ANNs are quite flexible models, and (3) once developed and their coefficients determined, they can provide a rapid response for a new input [60].

An ANN is a highly interconnected network of many simple processing elements or neurons that can perform massively parallel computation for data processing and knowledge representation. Two or more neurons can be combined in a layer, and a particular network could contain one or more of such layers. In a one layer network (Fig. 1) with R input elements and S neurons, each element of the input vector **p** is connected to each neuron input through the weight matrix **W**. The ith neuron gathers its weighted inputs and bias to form its own scalar output $n(i)$. The various $n(i)$ taken together form an S-element net input vector n. Finally, the neuron layer outputs form a column vector **a**. In the adsorption process, input data typically represent the adsorbent and adsorbate characteristics and the hydrodynamic conditions under which the adsorption unit is operating. On the other hand, the outputs represent the breakthrough curves of a number of adsorption experiments covering a certain domain of the input parameters.
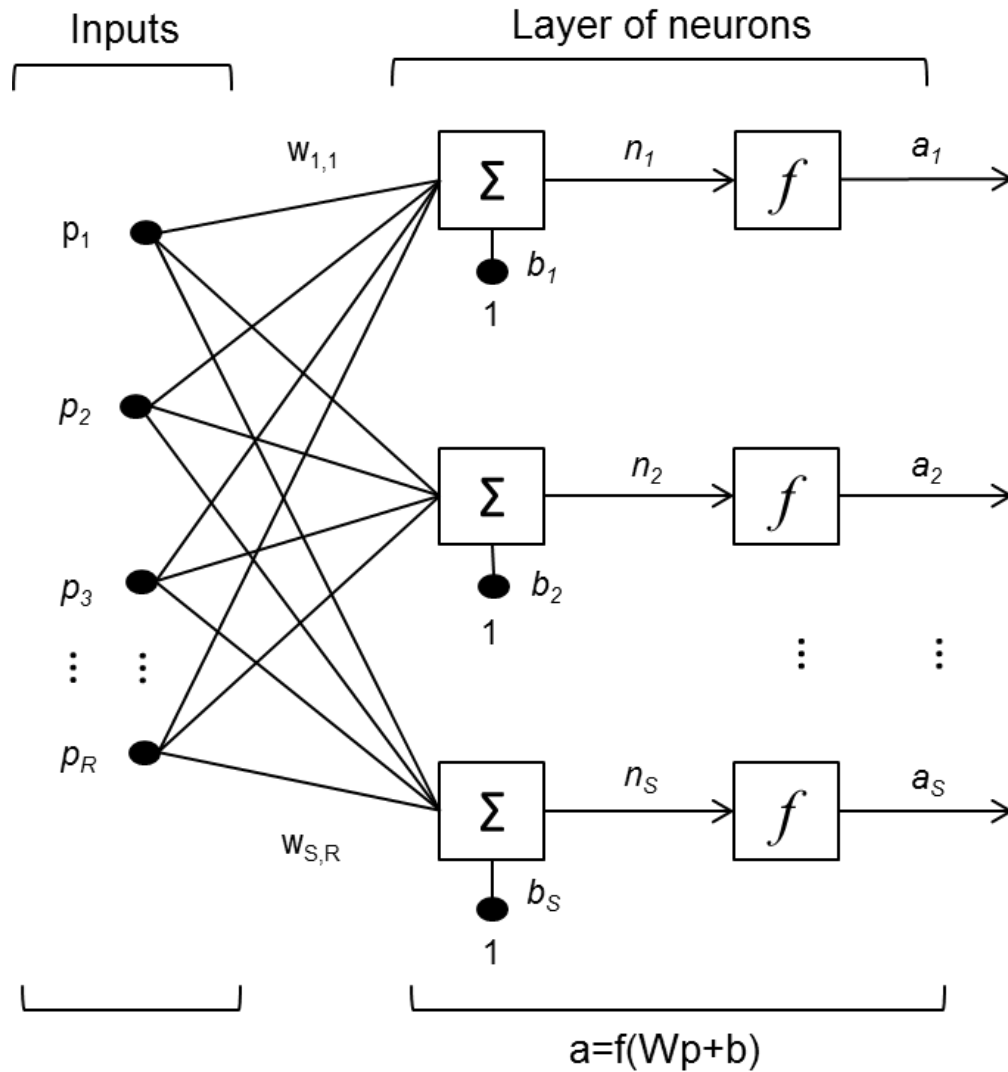
Fig. 1 A One-layer Artificial Neural Network. *R* is the number of elements in input vector and *S* the number of neurons in layer.

Neurons with a linear transfer function are used as linear approximators in Adalines (Adaptive Linear Neuron), which respond to changes in its environment as it is operating. Linear networks that are adjusted at each time step based on new input and target vectors can find weight and biases that minimize the network's sum square error for recent input and target vectors. The learning rule of Adalines is the least mean square error (LMSE) algorithm or Widrow-Hoff rule, in which the learning rule is provided with a set of examples of desired network behavior. The LMSE algorithm

24

adjusts the weights and biases of the linear network so as to minimize the average of this mean square error. Fortunately, the mean square error performance index for the linear network is a quadratic function. Thus, the performance index will either have one global minimum, a weak minimum, or no minimum, depending on the characteristics of the input vector. Specifically, the characteristics of the input vectors determine whether or not a unique solution exists.

Feedforward networks often have one or more hidden layers of sigmoid neurons followed by an output layer of linear neurons. Backpropagation is the generalization of the Widrow-Hoff learning rule to multiple-layer networks and nonlinear differentiable transfer functions. Input vectors and the corresponding target vectors are used to train a network until it can approximate a function. Networks with biases, a sigmoid layer, and a linear output layer are capable of approximating any function with a finite number of discontinuities. Multilayer networks often use the log-sigmoid transfer function.

The performance of a neural network, in terms of its generalization and prediction qualities, significantly depends on the training cases (or the input patterns) it is presented with, and the domain this training cases cover. For phenomena that are difficult to model mathematically, a best source of data is experimental investigations in which a large number of cases are tested. The input data are only those input variables that influence the output data.

1.5 Scope of the Study

In this study, barley husks (BH) were used as precursor for activated carbon production. It was recently reported that barley production in México was about 487,488 tons per year [61] and it is also reported that around 70% of this crop is used in the beer industry [62]. Prior to the fermentation process, barley husks (which represent between

10 to 20% of the whole crop) are removed from the grain and large quantities of waste are generated [63,64].

The production of activated carbon from barley husks by chemical activation with zinc chloride was simultaneously optimized using a factorial design with two responses (the yield and iodine number). The factors included in the experimental design were the activation temperature, activation time, and impregnation ratio of the activating agent. To establish the optimal conditions for the production of barley husks activated carbon (BHAC), a 2^3 factorial design with replicates at the central point was followed by a central composite design with axial points to build a quadratic model and to explore the response surface space. Finally, the BHAC produced at the optimal conditions was characterized by N_2 physisorption, Fourier Transform Infrared (FTIR) analysis and scanning electron microscopy (SEM).

The potential of BHAC as adsorbent of phenol from aqueous solution was evaluated observing the effect of pH solution value, temperature, and adsorbent dosage on adsorption capacity. In order to determine the effectiveness of BHAC, the performance of this adsorbent was compared with a commercial activated carbon (CAC). Besides, kinetic and isotherm models were used to represent the kinetic and equilibrium adsorption, respectively, and the regeneration of the adsorbent was proved by the use of distilled water, 0.1 N HCl, 0.1 N NaOH, and 10% V/V ethanol/water solution.

The scope of this study additionally included the use of artificial neural network to model the process of phenol adsorption with BHAC in an airlift reactor. An important reason for the development of this research was the need to obtain a process model that allows the prediction of the system at different operational conditions.

CHAPTER 2

2. MATERIAL AND METHODS

2.1 Precursor

Barley husks were used as the activated carbon precursor; this material, a by-product of the beer industry, was obtained from a local brewery. The precursor was washed five times with distilled water until a colorless solution was obtained. After that, BH was dried at 60 °C for 24 h and sieved to obtain 0.6 – 1 mm particle size (18/30 mesh screen) before zinc chloride impregnation and pyrolysis processes.

2.2. Adsorbents

The BHAC used in this study was produced according to the procedure described in Section 2.4, and the CAC was purchased from Jalmek (México). Prior to adsorption experiments, both BHAC and CAC were ground and sieved to obtain 0.074 – 0.150 mm particle size (100/200 mesh screen).

2.3 Chemicals

All used chemicals were of analytical reagent grade. Phenol was obtained from Sigma-Aldrich, $ZnCl_2$, KI, I_2 and $Na_2S_2O_3 \cdot 5H_2O$ were obtained from DEQ, HCl was obtained from PQM, NaOH and NaCl were obtained from Fisher chemical, KIO_3 was obtained from Merck, and nitrogen of ultra-high purity was obtained from AOC Mexico. Distilled water was used throughout this work.

2.3.1. Adsorbate

A stock solution of 1000 mg L^{-1} was prepared with phenol (Sigma-Aldrich). Appropriate dilutions were performed to obtain initial concentrations of phenol ranging from 50 to 1000 mg L^{-1} that were used in adsorption experiments. Phenol solutions were prepared using distilled water.

2.4 Activated Carbon Production

The precursor was impregnated with $ZnCl_2$ at three different weight ratios: 0.5, 1.0, and 1.5 g $ZnCl_2$ g BH^{-1}. Known quantities of zinc chloride (5, 10 or 15 g) were first dissolved in distilled water, 10 g of the precursor were then added to $ZnCl_2$ solution, mixed with a magnetic stirrer (200 min^{-1}) and heated at the boiling point for 6 h. The wet mixture was then dried at 60 °C for 12 h. A mass of 10 g of the impregnated precursor was heated at a rate of 5 °C min^{-1} in an electrical furnace (length, 30.5 cm; inner diameter, 5 cm) to reach the activation temperature (300, 500, and 700 °C) under a nitrogen flow of 60 mL min^{-1}. Once the activation temperature was reached, the samples were kept at constant temperature for different activation times (20, 100, and 180 min). The carbonization experiments were carried out in duplicate in order to provide an estimate of the repeatability of each experimental run. The BHAC was then

washed with a 0.1 N HCl solution to remove the activating agent from the porous material. The BHAC was separated from the solution by filtration and was washed several times with distilled water until a non-turbid solution was obtained. To verify the complete removal of the activating agent, 10 mL of 0.1 M NaOH solution were added to a 10 mL of filtrate sample for each washing stage. Then, the BHAC was dried at 60 °C for 12 h and stored in a desiccator.

The BHAC yield percentage (Y) was calculated by Eq. 10 as follows:

$$Y = \frac{M}{M_0} \times 100 \tag{10}$$

where M (g) is the mass of BHAC and M_0 (g) is the mass of BH.

2.5 Materials Characterization

In order to apply pyrolysis, the precursor must be properly characterized for elemental and fixed carbon, volatile matter, ash, and moisture content. The elemental analysis (C, H, N, and S) was performed using an elemental analyzer (2400 Series II, Perkin Elmer). The proximate analysis was carried out according to the method described in ASTM D3172 [65].

Thermal degradation characteristics of barley husks were studied using a thermogravimetric method. Experiments were performed on a TA Instruments SDT 2960 Simultaneous DSC – TGA analyzer. Each sample was heated from room temperature to a final temperature of 800 °C at a heating rate of 10 °C min^{-1} under nitrogen atmosphere.

The surface area is a very important property of activated carbons for adsorption processes, and it can be determined by a N_2-physisorption method or estimated by the iodine number. The former property is measured as the quantity of iodine adsorbed on activated carbon (mg g^{-1}) in equilibrium with iodine solutions (0.02 N I_2–KI) according to the ASTM D4607 procedure [66]. Although the iodine method only indicates the surface area which exists in pores of widths equal to or greater than 1 nm [28], the surface area is quickly determined and special equipment is not needed as for the N_2-physisorption method.

The pore size distribution is an important parameter that is useful in determining whether an adsorbate could diffuse towards the functional groups inside the activated carbon particle. The pore size distribution and specific surface area were obtained from the adsorption isotherm of nitrogen at −197.54 °C and 32 different partial pressures (0.01 to 0.995), using the BET equation. The adsorption isotherm of nitrogen was determined using an ASAP 2020 (Micromeritics) analyzer after out-gassing BHAC at 500 µm of Hg for 240 min. The surface morphology of BHAC was studied by SEM (NanoSEM 200, Nova) with a 15 kV accelerating voltage.

The identification of the functional groups on activated carbon is useful for understanding the interactions between the adsorbate and adsorbent. The surface functional groups were qualitatively identified using a FTIR spectrometer (Spectrum One, Perkin Elmer) and a scanning was recorded in the range of 4000 – 650 cm^{-1}.

An adsorbent in an aqueous solution acquires a positive or negative surface charge as a result of the interactions between the functional groups in the adsorbent and the H^+ or OH^- ions present in solution. When the positive and negative charges are equal, the adsorbent net surface charge is neutral; this pH value is commonly called the point of zero charge (pH_{PZC}). The pH_{PZC} of BHAC was determined based on the method reported by Noh and Schwarz [67]. Sixteen different volumes of 0.1 M NaOH or HCl

were placed into 25 mL volumetric flasks and filled to the mark with 0.1 M NaCl. Then, 50 mg of BHAC were added to the solutions and stirred continuously for 5 days at room temperature. The final pH was measured at the end of the experiment. Blank tests were simultaneously performed without BHAC under the same conditions.

It is well known that the adsorption can be strongly affected by the nature and quantity of surface oxygenate groups. The surface acidity studies were determined based on the method reported by Al-Degs *et al.* [68]. Triplicate samples (0.5 g) of BHAC and CAC were shaken in 50 mL of 0.01 M NaOH for 24 h, at room temperature. Thereafter, the samples were filtered and the remaining NaOH was titred with 0.01 M HCl. The results were expressed in mEq of H^+ per g of adsorbent.

2.6 Experimental Design

The optimal conditions in the production of activated carbon from BH were determined using a 2^3 factorial design with central points followed by a central composite design. Two responses (the yield and iodine number) were simultaneously optimized by studying three factors (the activation temperature, activation time, and impregnation ratio) at different levels as listed in Table 2.

Table 2 Factors and Levels used in the Experimental Design.

Independent variable	Coded factor	Coded levels		
		-1	0	1
		Actual levels		
Activation time (min)	A	20	100	180
Temperature (°C)	B	300	500	700
Impregnation ratio (g $ZnCl_2$ g BH^{-1})	C	0.5	1.0	1.5

A linear model (Eq. 11) was initially used to represent the experimental data obtained from the full 2^3 factorial design:

$$Y = \beta_0 + \sum_{i=1}^{I} \beta_i x_i + \sum_{i=1}^{I} \sum_{j>i}^{I} \beta_{ij} x_i x_j + \sum_{i=1}^{I} \sum_{j>i}^{I} \sum_{k>j}^{I} \beta_{ijk} x_i x_j x_k + \varepsilon \qquad (11)$$

where Y is the independent variable or response, β_0 is a constant coefficient, β_i, β_{ij}, β_{ijk} are the coefficients for the linear, double, and triple interaction effects, respectively, x_i, x_j, x_k are the independent variables or factors, and ε is the random error.

After the linear model was applied, replicates of the central point were added to full 2^3 factorial design to test curvature on response surface. Subsequently, axial points were added to the existing data to build the quadratic model represented by Eq. 12:

$$Y = \beta_0 + \sum_{i=1}^{I} \beta_i x_i + \sum_{i=1}^{I} \sum_{j>i}^{I} \beta_{ij} x_i x_j + \sum_{i=1}^{I} \sum_{j>i}^{I} \sum_{k>j}^{I} \beta_{ijk} x_i x_j x_k + \sum_{i=1}^{I} \beta_{ii} x_i^2 + \varepsilon \qquad (12)$$

where β_{ii} is the coefficient for the quadratic effect and x_i^2 represents the quadratic independent variables.

An analysis of variance was used to measure the magnitude of the effects of the factors for the two studied response variables: the yield and iodine number. The adjusted determination coefficient (R_{adj}^2) was used as a measurement of the proportion of the total observed variability described by the model [69]. Quadratic models were used to build the surfaces of the response variables and to find the maximal value of responses by using the *Design expert* software (version 7.0.0, Stat-Ease, Inc., USA).

2.7 Optimization Method

The iodine number and yield were simultaneously optimized by using the desirability functions approach included in the *Design expert* software. This method first

32

converts each estimated response y_i (the iodine number or yield) into an individual scale-free desirability function d_i that varies over the range of 0 to 1. When a response is to be maximized, the partial desirability of y_i at condition x^* can be defined as:

$$d_i(x)= \begin{cases} 0 & \text{if } y_i(x) \leq y_{i,min} \\ \left(\frac{y_i(x)-y_{i,min}}{y_{i,max}-y_{i,min}} \right)^r & \text{if } y_{i,min} \leq y_i(x) \leq y_{i,max} \\ 1 & \text{if } y_i(x) \geq y_{i,max} \end{cases} \tag{13}$$

where $y_{i,min}$ and $y_{i,max}$ are the lower and upper acceptability bounds for response i, respectively, and r is the weight. The lower and upper acceptability bounds were set at the extreme values of the individual estimated response, since the response surface had been reasonably explored in the range of studied variables. The weights for the response variables were set to one, because both variables (yield and iodine number) were considered equally important.

The design variables are then chosen to maximize the overall desirability D, which is another value between 0 and 1 and is defined by combining d_i using a weighted geometric mean as presented in Eq. 14.

$$D=\left(d_1^{r_1} \times d_2^{r_2} \times \ldots \times d_n^{r_n} \right)^{\frac{1}{\sum r_i}} \tag{14}$$

where the r_i are the relative importance among the n variables and responses with target i = 1, 2, …, n. The objective is then to find the input variable setting x^* which maximizes the value of D [69,70]. The overall desirability function was maximized using the *Design expert* software by a penalty function approach in a downhill simplex search [71].

2.8 Equilibrium Adsorption Experiments

To determine an appropriate adsorbent dosage to be used in equilibrium adsorption experiments, a known mass of BHAC (0.02 to 0.25 g) was added to flasks of 50 mL containing 25 mL of 500 mg L^{-1} phenol solutions at pH 5, 6, and 7, stirred at 200 min^{-1}, and kept at 25 °C during 24 h. After that, the selected dosage was used in the equilibrium experiments varying phenol initial concentrations from 50 to 1000 mg L^{-1} and temperatures of 25, 35, and 45 °C. These flasks were continuously stirred at 200 min^{-1} at the selected temperature until the equilibrium was achieved. Solution pH was adjusted during the experimentation to the selected value by adding NaOH and/or HCl as required. The initial and final phenol concentrations were determined by UV spectrophotometer (Varian Cary 50) at a wavelength of 290 nm. All experiments were conducted by triplicate. The quantity of phenol adsorbed onto the activated carbon (q) and the percentage removal (R) of phenol were calculated according to Eq. 15 and Eq. 16, respectively.

$$q = \frac{(C_0 - C)V}{W} \tag{15}$$

$$R = \frac{C_0 - C}{C_0} \times 100 \tag{16}$$

where C_0 is the initial phenol concentration, V is the volume of the solution, W is the mass of activated carbon, and C is the residual phenol concentration at equilibrium or at any time t, which defines q_e or q_t, respectively.

2.9 Adsorption Kinetic Experiments

A rotating-basket reactor [72,73] was used for kinetic experiments. This basket contained the adsorbent and it was submerged in a beaker containing the phenol solutions. It is important to mention that the rotating-basket reactor was equipped with six equally spaced baffles to prevent the vortex formation, and a stirrer for complete mixing. The beaker was partially immersed in a water bath to keep constant the temperature of the phenol solution. A known mass of BHAC (0.8 g) was placed into the basket and it was attached to the shaft of the stirrer, while 1000 mL of a solution of a known initial concentration of phenol (250, 500, or 1000 mg L^{-1}) were poured into the beaker; the pH solution value was kept at 7 by adding NaOH or HCl as required. Afterwards, the basket was immersed in the beaker, and the timer and the motor of the stirrer were simultaneously turned on. Once the experiments were initiated, the contents were mixed at the chosen stirring speed (300, 400, or 500 min^{-1}). Samples of the solution were withdrawn at selected intervals of time, and adsorption capacity at time t was calculated with Eq. 15 taking into account the withdrawn sample volume. The initial and final phenol concentrations were determined by UV spectrophotometer (Varian Cary 50) at a wavelength of 290 nm.

2.10 Regeneration of Spent Activated Carbons

Distilled water, 0.1 N HCl, 0.1 N NaOH, and 10% V/V ethanol/water solution were selected as the regenerating agents. Samples of 0.02 g of activated carbon were added to 25 mL of phenol solutions containing 1000 mg L^{-1} at 30 °C. These experiments were continuously stirred at 200 min^{-1} and the solution pH was adjusted to 7 by adding NaOH and/or HCl as required, until the equilibrium was achieved.

Adsorption capacity at equilibrium was calculated with Eq. 15. The adsorbent was separated from phenol solutions by filtration, and phenol was desorbed from phenol-loaded activated carbons by 25 mL of the tested eluents at 30 °C for 4 hours at 200 min^{-1}. The initial and final phenol concentrations were determined by UV spectrophotometer (Varian Cary 50) at a wavelength of 290 nm. The regenerated activated carbon was separated by filtration and it was used for adsorption of phenol at the above described conditions.

2.11 Phenol adsorption studies in an airlift reactor

The dynamic adsorption of phenol onto BHAC was performed in a stainless steel airlift reactor from Applikon Biotechnology (The Netherlands). The reactor consists of a vertical cylindrical stainless steel column of 5 cm diameter and 38 cm length, fitted concentrically into another vertical cylindrical stainless steel column of 6 cm and 60 cm length, as shown in Fig. 2. The temperature of the airlift reactor was monitored with a temperature sensor located at the bottom of the reactor, and maintained at 30 °C with a heating blanket. The airlift reactor was loaded with 6 or 15 g of BHAC. Two Masterflex peristaltic pumps enable synthetic phenolic wastewater to flow through the airlift reactor with a flow rate of 2 or 3 L h^{-1}. The feed port was located at the bottom center of the reactor; consequently, the solution flowed upward. Sampling port and a stainless steel air outlet condenser were provided at the top of the reactor to collect samples and prevent the loss of phenolic solutions by evaporation, respectively. Samples were collected at selected time intervals and analyzed for phenol concentration using an UV-vis spectrophotometer (Varian Cary 50) at a wavelength of 290 nm.. The value of the initial phenol concentration was 40 or 250 mg L^{-1}, for a sampling period of 516 min.
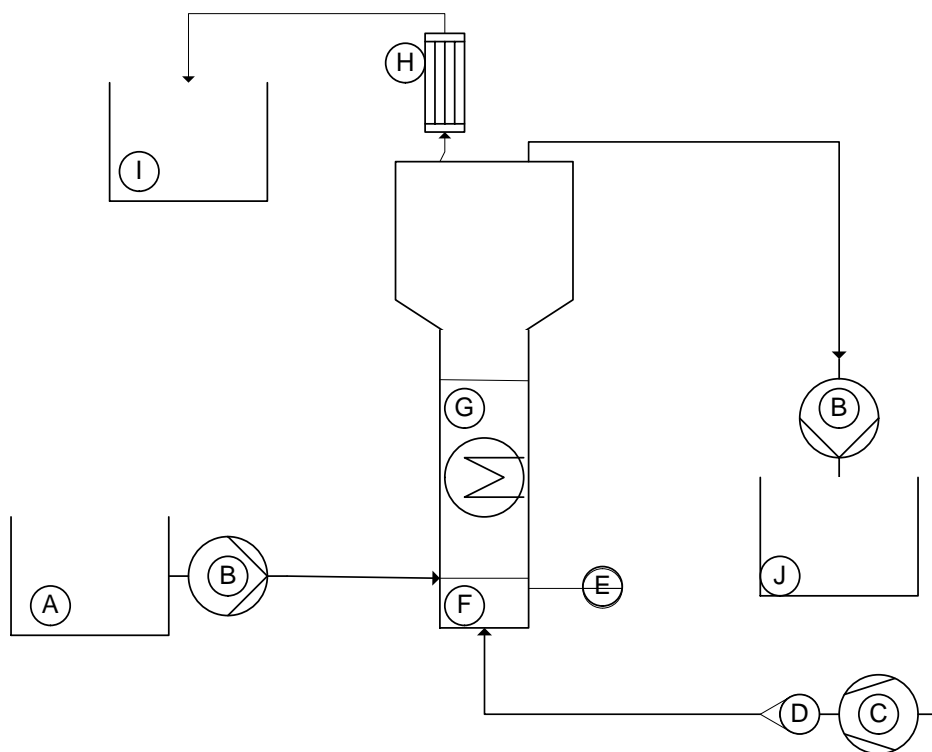
Fig. 2 Schematic Representation of the Airlift Reactor Used to Conduct the Dynamic Adsorption of Phenol onto BHAC. A: Phenolic Solution Reservoir; B: Peristaltic Pump; C: Compressor; D: Rotameter; E: Thermometer; F: Airlift Reactor; G: Heating Blanket; H: Condenser; I: Condensation; J: Treated Effluent.

2.12 Artificial Neural Network

In the adsorption process in an airlift reactor in continuous operation, the breakthrough curve shape is affected by several factors pertaining to adsorbent-adsorbate interaction mechanisms and the hydrodynamic conditions. For the present investigation, four input variables are known to affect the continuous operation. These variables were the influent concentration, the influent flow rate, the air flow rate, and the BHAC dosage.

The values tested for the influent concentration, the influent flow rate, the air flow rate, and the BHAC dosage were divided into 7 sets, each of one representing a breakthrough curve with 87 experimental points (Table 3, C/C_0 values listed in Appendix

37

B). The experimental sets summarized in Table 3 were used for training the artificial neural network and to verify the efficiency of the ANN simulation.

Table 3 Seven Experimental Sets Used in Modeling Phenol Adsorption onto BHAC with Artificial Neural Network. All experiments were carried out at pH 7 and 30 °C.

Set	BHAC dosage (g L^{-1})	Phenol initial concentration (mg L^{-1})	Influent flow rate (L h^{-1})	Air flow rate (L min^{-1})
1	5	250	2	10
2	5	40	2	10
3	5	40	2	1
4	5	40	3	10
5	2	40	2	10
6	2	40	3	3
7	2	40	3	1

The capacity of ANN to fit a function was studied as a single-input single-output problem, where time was the input and C/C_0 was the output. Each data set listed in Table 3 was fitted using a two-layer feed-forward network with sigmoid hidden neurons and linear output neurons, trained with Levenberg-Marquardt back propagation algorithm by using Matlab® of *MathWorks*. The 87 samples were randomly divided up as follows: 70% for training, 15% for validation, and 15% for testing. Several ANN varying the number of hidden neurons were tested and the final architecture was selected based in the mean square error and the regression values.

Experimental sets 2, 5, 6, and 7 listed listed in Table 3 were also used to study the capacity of ANN to provide generalization in a multi-input single-output problem. The inputs were four vectors (the influent concentration, the influent flow rate, the air flow rate, and the BHAC dosage), while the outputs was one vector of the variations of effluent phenol concentration at time *t* respect to the initial phenol concentration (the breakthrough curve). Each input is a 1 by 1 vector and the output is a 87 by 1 vector. Four Adaline networks were created by using Matlab® of *MathWorks,* to simulate

experimental sets 2, 5, 6, and 7 individually by training the net with the remaining experimental sets. The experimental sets were presented as sequences of inputs during the training.

2.13 Error Analysis

The average relative error (ARE) was used as error function to determine the accuracy of the non-lineal regression which was performed to fit the isotherm and kinetic models to the experimental data. This error function attempts to minimize the fractional error distribution across the entire studied range. The model parameters were obtained by using Solver® of *Microsoft Excel*, minimizing the ARE according to Eq. 17.

$$\text{ARE}=\left(\frac{1}{N}\sum_{t=1}^{N}\left|\frac{q_{exp}-q_{cal}}{q_{exp}}\right|\right)\times100 \tag{17}$$

where N is the number of experimental points and q_{exp} and q_{calc} are the experimental and predicted phenol concentration, respectively.

The ANN performance was measured according to the least mean square error algorithm according to Eq. 18.

$$\text{MSE}=\frac{1}{N}\sum_{k=1}^{N}e(k)^2=\frac{1}{N}\sum_{k=1}^{N}\left(t(k)-a(k)\right)^2 \tag{18}$$

where $t(k)$ is the target output and $a(k)$ the output predicted by the neuron.

2.14 Waste disposal

The wastes generated during this project were disposed according to internal procedures of Facultad de Ciencias Químicas of the Universidad Autónoma de Nuevo León.

CHAPTER 3

3. RESULTS AND DISCUSSION

3.1 Precursor Properties

Several factors could be taken into account in the selection of raw material for the manufacturing of activated carbon; for instance, high carbon content, low inorganic content (ash), and sufficient volatile matter content, among others. Barley husks can be considered a viable alternative for the production of activated carbon due to the aforementioned properties, which are listed in Table 4. Similar values have been reported for other lignocellulosic precursors, with fixed carbon in the range of 14.2 to 76% [19,74], ash from 0.4 to 17.1% [74,75], and volatile matter from 20 to 85.4% [19,74].

Table 4 Proximate and Elemental Analyses of Barley Husks.

Analysis	Content	Weight percentage (%)
Proximate	Moisture	8.86
	Ash	6.78
	Volatile matter	75.02
	Fixed carbon	18.19
Elemental	C	41.16
	H	6.83
	N	0.045
	S	0.65

Thermogravimetric analysis of the barley husks revealed that major thermal decomposition occurred in the range of 300 to 700 °C as shown in Fig. 3. This weight loss corresponds to the evolution of light volatile compounds from the degradation of cellulose, hemicelluloses, and lignin [76,77]. The release of volatile matter from the precursor causes the formation of the pores in the activated carbon. Therefore, temperatures of 300, 500, and 700 °C were selected to the pyrolysis of the precursor.
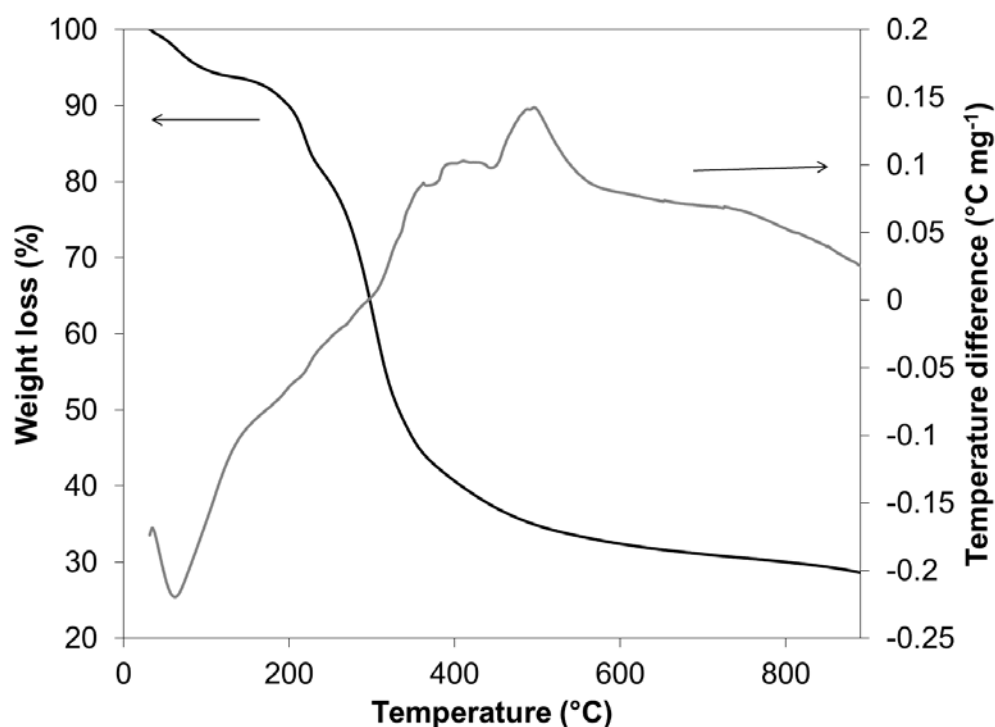
Fig. 3 Thermogravimetric Analysis of the Barley Husks.

3.2 Statistical Analysis

Table 5 lists the conditions and the experimental results for the production of BHAC. The analysis of variance (ANOVA) used to determine the significance of the curvature in the iodine number and yield responses at a confidence level of 99% are listed in Table 6 and Table 7, respectively. In both cases, the p-value for the lack of fit is

higher than 0.0001, which means that the curvature is significant and consequently there is an inflection point on the studied range of variables. Therefore, the linear model is not appropriate to represent the design space and, for this reason, a central composite design was used to fit the quadratic model considering the 18 experimental runs (listed in Table 5).

Table 5 The Design Matrix and Experimental Responses.

Run	Coded values			Iodine number (mg g^{-1})				Yield (%)			
	A	B	C	Replicate		Average	Predicted	Replicate		Average	Predicted
				1	2			1	2		
1	-1	-1	-1	221.70	374.63	298.16	293.83	65.00	59.79	62.40	60.11
2	+1	-1	-1	336.48	313.48	324.98	293.83	54.19	62.62	58.40	60.11
3	-1	+1	-1	270.25	309.83	290.04	247.56	30.79	31.52	31.16	29.25
4	+1	+1	-1	288.09	110.31	199.20	247.56	29.91	27.11	28.51	29.25
5	-1	-1	+1	452.54	452.54	452.54	513.23	51.51	48.53	50.02	49.25
6	+1	-1	+1	537.66	541.97	539.82	513.23	46.77	48.57	47.67	49.25
7	-1	+1	+1	736.10	670.72	703.41	757.23	11.89	11.77	11.83	10.33
8	+1	+1	+1	788.38	682.81	735.60	757.23	10.28	6.92	8.6	10.33
9	-1	0	0	1011.06	*	1011.06	854.74	49.02	*	49.02	42.82
10	+1	0	0	885.37	*	885.37	854.74	38.65	*	38.65	42.82
11	0	-1	0	400.74	*	400.74	403.53	56.66	*	56.66	60.26
12	0	+1	0	665.06	*	665.06	502.40	19.48	*	19.48	25.37
13	0	0	-1	448.66	*	448.66	672.47	41.19	*	41.19	44.68
14	0	0	+1	1091.54	*	1091.54	1037	31.88	*	31.88	29.79
15[a]	0	0	0	712.74	813.86	844.65	854.74	42.80	41.54	43.75	42.82
				870.83	730.10			42.90	45.25		
				1009.96	871.21			47.29	41.65		
				1019.30	792.19			45.62	42.95		

*Axial points did not require duplicate samples.
[a]Central point has 8 replicates

Table 6 The Analysis of Variance for Iodine Number, Determined from a Factorial Design with Central Points.

Variation Source	Sum of square	Degree of freedom	Mean Square	F-value	p-value
Model	4.349×10^5	1	4.349×10^5	35.74	<0.0001
Curvature	8.946×10^5	1	8.946×10^5	73.51	<0.0001
Residual	2.555×10^5	21	12168.93		
Lack of fit	1.263×10^5	6	21056.14	2.44	0.0751
Pure error	1.292×10^5	15	8614.05		
Total	1.585×10^6	23			

Table 7 The Analysis of Variance for Yield, Determined from a Factorial Design with Central Points.

Variation source	Sum of square	Degree of freedom	Mean square	F-value	p-value
Model	58.25	3	19.42	276.25	<0.0001
Curvature	2.2	1	2.2	31.34	<0.0001
Residual	1.34	19	0.070		
Lack of fit	0.39	4	0.097	1.54	0.2416
Pure error	0.95	15	0.063		
Total	61.79	23			

After discarding the insignificant terms, the ANOVA data for the coded and hierarchical quadratic models of the iodine number and yield are reported in Table 8 and 9, respectively. According to the ANOVA data for the iodine number, the most significant individual factors were the temperature (B) and impregnation ratio (C), the most significant double interaction was between the temperature and the impregnation ratio (BC), and the most significant quadratic term was for temperature (B^2) (Eq. 19). Similar results were reported by Nieto-Delgado and Rangel-Mendez [21]. Because the activation time was not a significant factor for the iodine number, it was not included in final coded model (Eq. 19). The individual factors and the double interaction had a positive effect on the response of the iodine number in contrast with the quadratic term for the temperature.

Table 8 The Analysis of Variance for Iodine Number, Determined from a Central Composite Design.

Variation source	Sum of square	Degree of Freedom	Mean Square	F-value	p-value
Model	1.89×10^6	4	4.721×10^5	45.41	< 0.0001
B	43986.97	1	43986.97	4.23	0.0503
C	5.980×10^5	1	5.980×10^5	57.51	< 0.0001
BC	84260.74	1	84260.74	8.10	0.0087
B^2	1.162×10^6	1	1.162×10^6	111.78	< 0.0001
Residual	2.599×10^5	25	10397.27		
Lack of fit	1.307×10^5	10	13072.09	1.52	0.2254
Pure error	1.292×10^5	15	8614.05		
Total	2.148×10^6	29			

Table 9 The Analysis of Variance for Yield, Determined from a Central Composite Design.

Variation source	Sum of Square	Degree of freedom	Mean square	F-value	p-value
Model	6763.75	4	1690.94	160.72	< 0.0001
B	5476.72	1	5476.72	520.56	< 0.0001
C	997.73	1	997.73	94.83	<0.0001
BC	64.99	1	64.99	6.18	0.0200
C^2	224.31	1	224.31	21.32	0.0001
Residual	263.02	25	10.52		
Lack of fit	168.32	10	16.83	2.67	0.0422
Pure error	94.70	15	6.31		
Total	7026.77	29			

$$\text{Iodine number} = 854.74 + 49.43B + 182.27C + 72.57BC - 401.77B^2 \qquad (19)$$

$$\text{Yield} = 42.82 - 17.44B - 7.45C - 2.02BC - 5.58C^2 \qquad (20)$$

Based on the ANOVA data for the yield response (Table 9), the most significant individual factors were the temperature (B) and impregnation ratio (C), the most significant double interaction was between the temperature and the impregnation ratio (BC), and the most significant quadratic term was for the impregnation ratio (C^2) (Eq.

20). The above-mentioned factors had a negative effect on the yield response. Additionally, the activation time did not have a significant effect on the yield response.

The adjusted determination coefficients (R^2_{adj}) for the iodine number and the yield were 0.8597 and 0.9566, respectively. These results indicate that the models could represent approximately 86% and 96% of the observed variability for the iodine number and yield responses, respectively.

The mathematical models for the iodine number (Eq. 19) and the yield (Eq. 20) were used to build response surfaces and contour plots, as well as to determine the optimal conditions of the process. For all of the above-mentioned purposes, the lowest activation time in the studied range (20 minutes) was selected to reduce the energy consumption in the pyrolysis process, because this factor was not significant in either response. Fig. 4 a and b show that the iodine number increased with increasing impregnation ratio when temperature is fixed, and a maximal iodine number is observed in the range of 500 to 600 °C regardless of the impregnation ratio. Fig. 4 c and d show that when increasing both temperature and impregnation ratio, the yield response decreases.
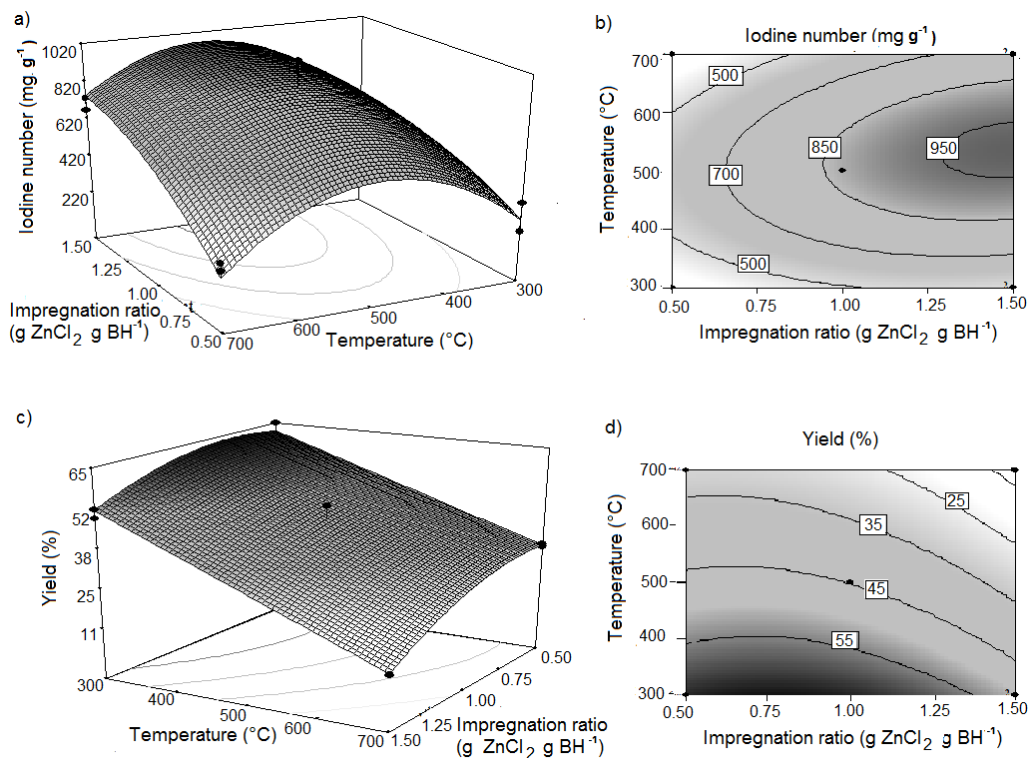
Fig. 4 The Surface Response and Corresponding Contour Plot for the Iodine Number (a and b) and the Yield (c and d).

To determine the optimal conditions, Eq. 19 and Eq. 20 were used to maximize the iodine number and yield, respectively. The maximum iodine number (1046.26 ± 105.52 mg g^{-1}) was predicted at 530 °C and an impregnation ratio of 1.5 g ZnCl$_2$ g BH^{-1}. The maximal yield (61.58 ± 3.32%) was predicted at 300 °C and an impregnation ratio of 0.76 g ZnCl$_2$ g BH^{-1}.

The effect of temperature on the iodine number and yield could be explained because an increase in the carbonization temperature increases the release of volatile matter from the precursor, causing an increase in the dimensions of the pores and, therefore, causing an increase in the iodine number up to the optimal conditions but a decrease in the yield. When the temperature is higher than 530 °C, a decrease in the iodine number could be associated with the sintering effect of the volatiles and the

shrinkage of the carbon structure, resulting in the narrowing and closing-up of the pores [26,78], as well as the widening of the pores, which means that many micropores were enlarged to mesopores [79]. At temperatures higher than 600 °C, a decrease in the iodine number is caused by both the temperature effect (as described above) and the progressive evaporation of $ZnCl_2$, which leads to a reduction in the degradation of the tars that are responsible for the shrinkage of the pores [80]. Regarding the effect of the impregnation ratio on the iodine number, in the range of studied temperatures, the $ZnCl_2$ assumes a role as a dehydration agent during activation, inhibiting the formation of tars and other liquids that could clog up the pores of the carbons. In this way, the movement of the volatiles through the pores will be enhanced, increasing iodine number, but the yield is decreased.

According to the results, the maximum iodine number (1046.26 ± 105.52 mg g^{-1}) and maximum yield (61.58 ± 3.32%) were found at different optimal conditions, and both responses depend on the temperature and impregnation ratio. For instance, when using the optimal conditions for the iodine number (530 °C and impregnation ratio of 1.5 g $ZnCl_2$ g BH^{-1}), a low yield (26.84 ± 3.05%) was predicted by Eq. 20. In contrast, if the optimal conditions for the yield (300 °C and impregnation ratio of 0.76 g $ZnCl_2$ g BH^{-1}) were used, a low iodine number (350.87 ± 105.7 mg g^{-1}) was predicted by Eq. 19. Therefore, both responses were optimized simultaneously by using the desirability functions approach included in the *Design expert* software.

The surface response and the corresponding contour plot for desirability can be observed in Fig. 5 a and b. The maximum value of the desirability function (0.779) was obtained at a temperature of 436 °C, an activation time of 20 min, and an impregnation ratio of 1.1 g $ZnCl_2$ g BH^{-1}. At these conditions, the predicted responses for the iodine number and yield were 829.58 ± 78.30 mg g^{-1} and 46.82 ± 2.64%, respectively. To validate the predicted responses, experiments were conducted at the optimal

conditions, obtaining an iodine number of 901.86 mg g^{-1} and yield of 48.48%. The iodine number obtained in this research is similar to or higher than those reported by other researchers studying lignocellulosic precursors (Table 10).
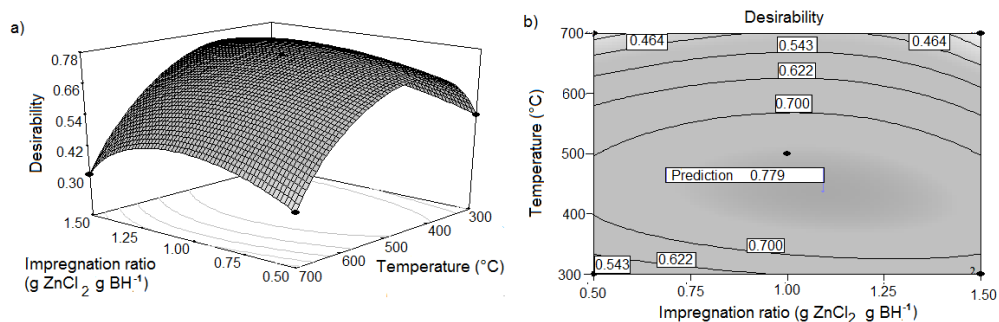
Fig. 5 The Surface Response and Contour Plot for the Desirability Function for the Simultaneous Optimization of the Iodine Number and Yield.

Table 10 Examples of Lignocellulosic Activated Carbon Properties and Operational Conditions Reported in Literature.

Precursor	Impregnation ratio (g ZnCl$_2$ g BH^{-1})	Temperature (°C)	Activation time (min)	Iodine number (mg g^{-1})	Surface area (m^2 g^{-1})	Yield (%)	Reference
Dates stones	0.5	700	180	-	951	-	[17]
Coffee residue	0.25	110	1440	-	520	-	[18]
Nuts of Terminalia Arjuna	2	500	60	-	1260	-	[19]
Nutshells of Sterculia Alata	1	500	60	1122	712	46	[20]
Agave bagasse[a]	1.08	456.1	23.8	-	1593.4	-	[21]
Herb residues[a]	1.105	467	60	896	1125	34	[22]
Tamarind wood[a]	2.95	439.76	40.26	-	1322	45.26	[23]
Coir pith	0.5	700	-	203	910	-	[24]
Oreganum stalks	1	600	120	-	944	36	[25]
Pistachio-nut shell	0.75	400	60	-	1635.37	-	[26]
Barley husks (this research)	1.1	436	20	901.86	811.44	48.48	[81]

[a]Optimal production conditions determined using the response surface methodology.

3.3 Physical Chemical Properties

3.3.1 Surface Area and Pore Volume

Fig. 6 shows the isotherms of the adsorption/desorption of nitrogen at 77 K on the BHAC produced at different conditions. These isotherms exhibit typical Type IV adsorption/desorption isotherm shape with hysteresis loop and steep rises at low relative pressure indicating the presence of both mesopores and micropore structures [33] and, at the highest impregnation ratio, the hysteresis effect is more evident, indicating an increase in the percentage of mesopores. Additionally, an increase in the

impregnation ratio results in an increase in the adsorbed volume; for example, at a relative pressure of 1, the adsorbed volume increases almost twofold when the impregnation ratio shifts from 1.0 to 1.5 g $ZnCl_2$ g BH^{-1} (Fig. 6).
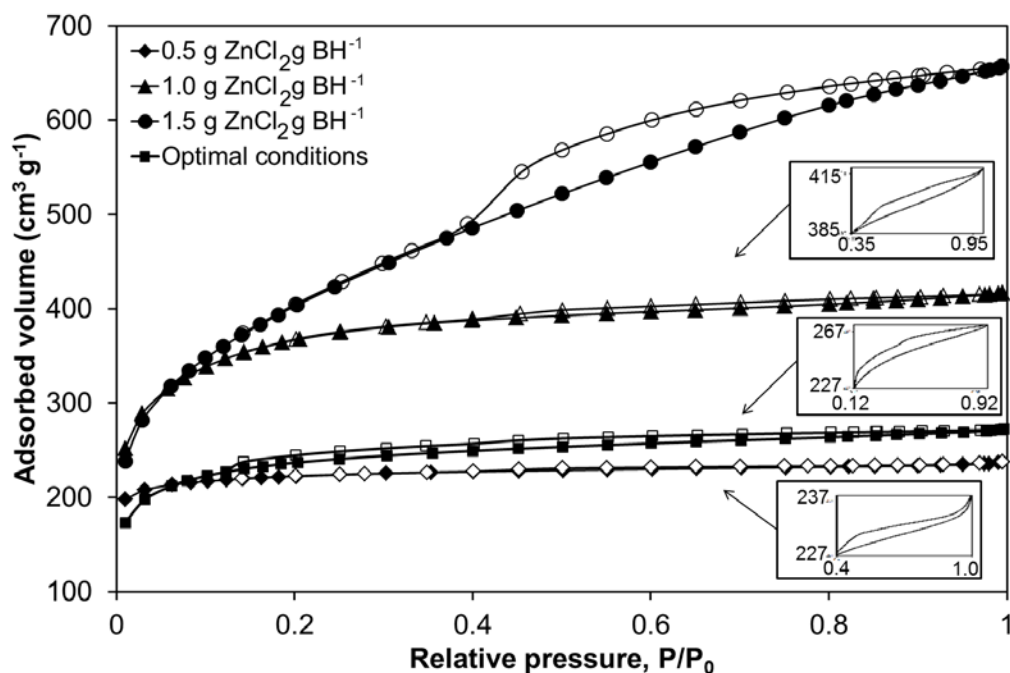
Fig. 6 The Adsorption/Desorption Isotherms of N_2 at 77K on BHAC Produced Under Optimal Conditions (Activation time of 20 min, Temperature of 436 °C, and Impregnation Ratio of 1.1 g $ZnCl_2$ g BH^{-1}) and under Different Impregnation Ratios (with Activation Time of 100 min and Temperature of 500 °C).

The specific surface area was calculated using the BET model for selected operational conditions to produce activated carbon. The activated carbon produced under the optimal conditions has a surface area of 811.44 m^2 g^{-1}, which is similar to the commercial and lignocellulosic activated carbons listed in Table 10. Additionally, the surface areas of carbons produced at different impregnation ratios (0.5, 1.0, and 1.5 g $ZnCl_2$ g BH^{-1}, at 500 °C and 100 min) were calculated to validate the assumption that the iodine number could be used as an indicator of the surface area. Fig. 7 shows that surface area and iodine number follow the same trend, where both increase as the

impregnation ratio increases. Nevertheless, the surface area of BHAC produced at the optimal conditions is not as high as the BHAC produced with an impregnation ratio of 1.5 g $ZnCl_2$ g BH^{-1} (1445.52 m^2 g^{-1}). However, the last conditions were not selected because of the low activated carbon yield (31.88%), while optimal conditions were determined by simultaneously taking into account the surface area and activated carbon yield.
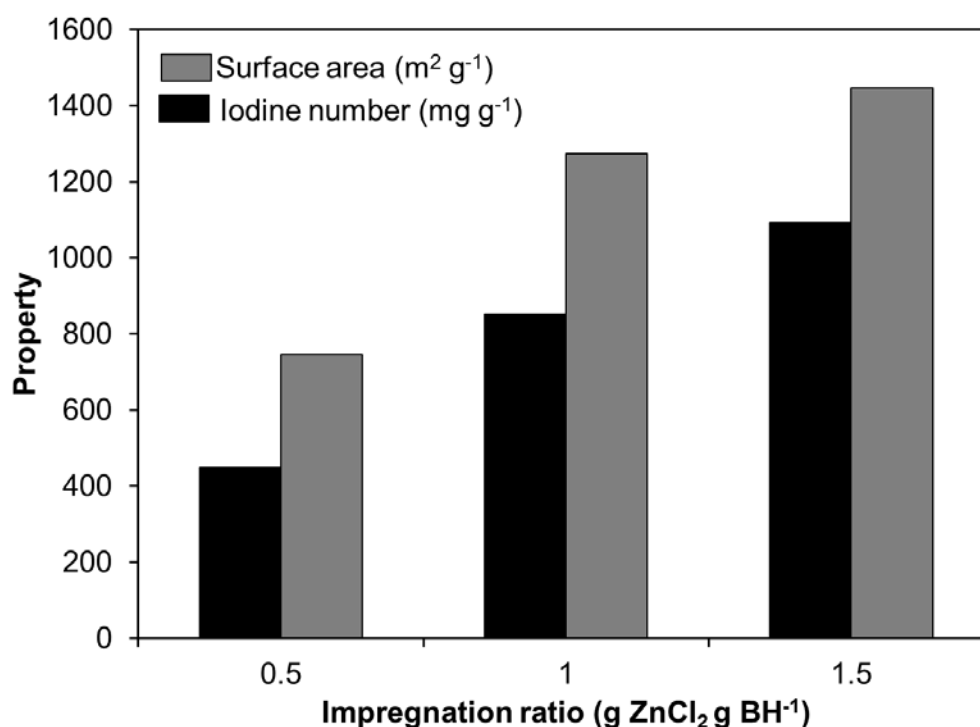
Fig. 7 The Effect of the Impregnation Ratio on the Iodine Number (mg g^{-1}) and Surface Area (m^2 g^{-1}) (with Activation Time of 100 min and Temperature of 500 °C).

Fig. 8 shows the pore size distribution of the BHAC produced under different conditions. Activated carbon has a mesoporous structure, with a significant fraction of the volume corresponding to micropores (< 2 nm) and mesopores (2 − 50 nm). The average pore increased as the impregnation ratio increased, suggesting that there was

a widening of existing pores into larger pores through the gasification of carbon in the pore walls.
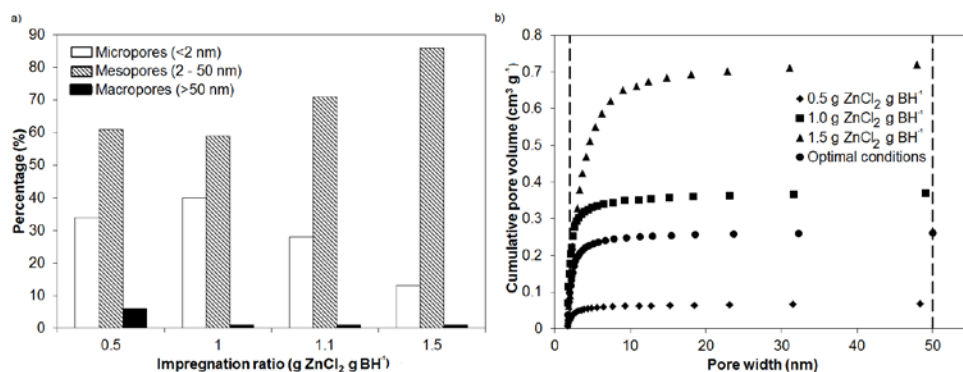
Fig. 8 The pore size Distribution (a) and Cumulative Pore Volume (b) for BHAC Produced Under Optimal Conditions (Activation time of 20 min, Temperature of 436 °C, and Impregnation Ratio of 1.1 g ZnCl$_2$ g BH^{-1}) and under Different Impregnation Ratios (with Activation time of 100 min and Temperature of 500 °C).

The high non-micropore volume content of the total pore volume makes BHAC a good adsorbent for aqueous phase applications. In adsorption studies, much attention has been paid in the steric effects. According to the results of Pelekani and Snoeyink [82] and Kasaoka *et al.* [83], the pore size of an adsorbent should be 1.2 to 1.7 times of the second widest dimension of the adsorbate molecule to allow effective adsorption. The calculations of Efremenko and Sheintuch [1] indicate that phenol adsorption in cylindrical pores smaller than 0.94 nm in diameter is limited by steric restrictions. Therefore, only micropores with diameter larger than 1 nm are available for phenol adsorption. From these studies, we conclude that more than 60% of the BHAC could be occupied by adsorbed phenol molecules.

3.3.2 Surface Charge Distribution

A solid adsorbent in aqueous solution acquires a positive or negative charge balance as a result of the interactions between the ions in the solution and the

functional groups on the surface of the adsorbent, such as amines, pyrones, ethers, carbonyls, carboxyl acids, phenols and lactones [28,32,35,84]. The electrostatic charges on the activated carbon surface can be elucidated by determining the pH at which the carbon surface is neutral; this pH value is called point of zero charge (pH$_{PZC}$). The pH$_{PZC}$ values for raw BH and BHAC (produced under optimal conditions) were 4.25 and 1.9, respectively. According to these values, raw BH and BHAC can be considered acidic. Some authors [85] proposed that the formation of acidic groups on activated carbon developed from lignocellulosic wastes activated with zinc chloride are due to the hydrolysis of the precursor under acidic conditions, which leads to the formation of carboxylic groups of different strengths and to reactions between the activating agent and precursor or the previously mentioned hydrolysis products.

3.3.3 FTIR Analysis

Infrared analysis was used to qualitatively identify the functional groups on the surface of BH and BHAC. Fig. 9 shows the FTIR spectra for BH and for BHAC produced under optimal conditions (436 °C, 1.1 g ZnCl$_2$ g BH^{-1}, and 20 min), and Fig. 10 shows BHAC produced at different temperatures (300, 500, and 700 °C) but at a fixed impregnation ratio and time (1.0 g ZnCl$_2$ g BH^{-1} and 100 min). The main differences between the BH and BHAC spectra are the decrease in the wide absorption band from 3000 to 3500 cm^{-1}, corresponding to the O – H stretching mode of the hydroxyl group, and the decrease in the bands with maxim at 2935 cm^{-1} and 1422 cm^{-1}, corresponding to the C – H stretching mode of the aliphatic groups. The decrease in the band from 3000 to 3500 cm^{-1} suggests the elimination of the OH groups from the biopolymers that compose BH during the activation process. Regarding the temperature effect on the BHAC surface chemistry, it can be observed that an increase in the

temperature leads to an enhancement in the elimination of hydrogen, which is reflected

in the elimination of the peak at approximately 1422 cm^{-1}.
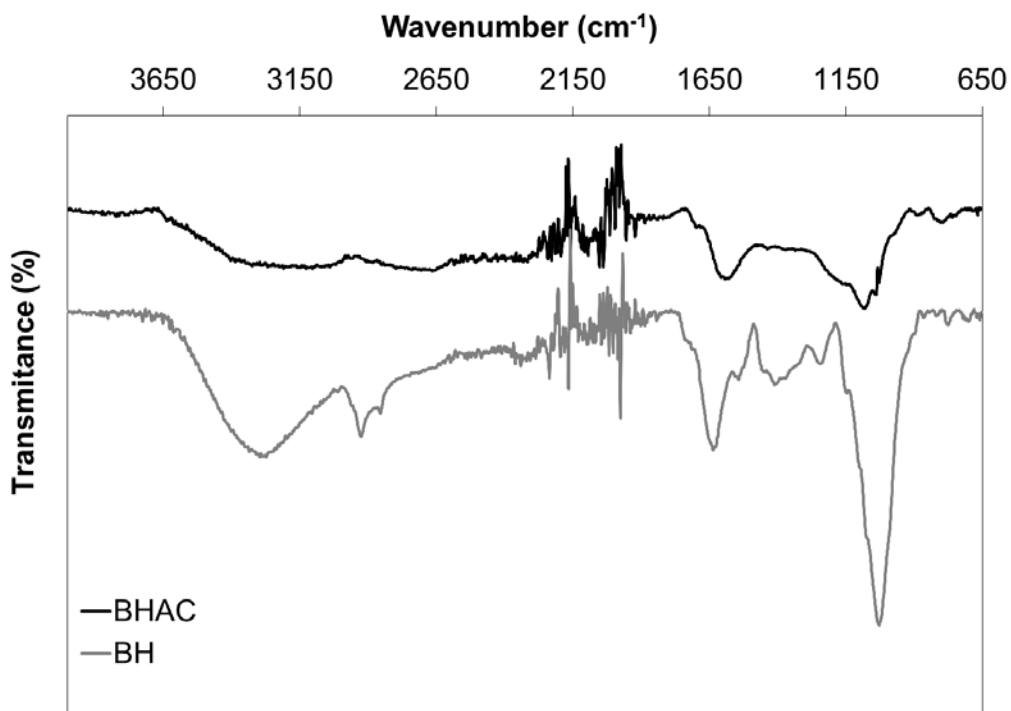
Fig. 9 FTIR Spectra of BH and BHAC Produced under Optimal Conditions (Activation time of 20 min, Temperature of 436 °C, and Impregnation Ratio of 1.1 g ZnCl$_2$ g BH^{-1}).
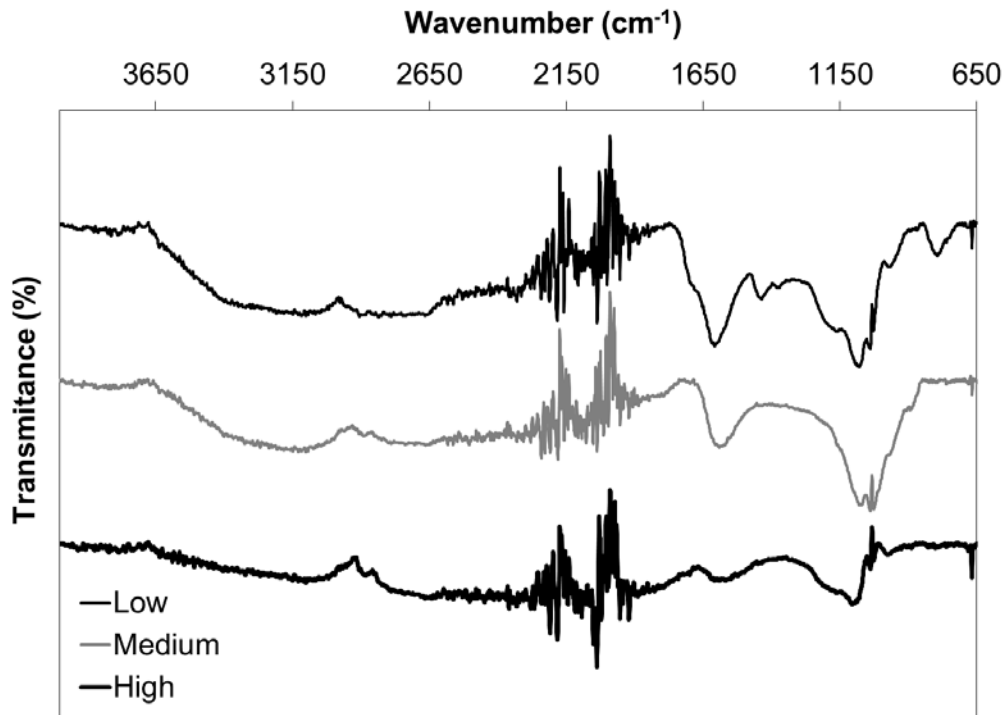
Fig. 10 FTIR Spectra for BHAC Produced at Different Temperatures (with Activation time of 100 min and Impregnation Ratio 1.0 g ZnCl$_2$ g BH[-1]).

3.3.4 Morphology of BHAC

Scanning electron microscopy (SEM) was used to observe the surface morphology of BHAC. Fig. 11 shows micrographs of BHAC produced at different conditions. As observed in these micrographs, chemical activation followed by pyrolysis was useful in developing pore structure within the carbon. At the lowest impregnation ratio (0.5 g ZnCl$_2$ g BH[-1]), the activated carbon shows a smooth surface (Fig. 11a), whereas at the highest impregnation ratio (1.5 g ZnCl$_2$ g BH[-1]), a highly porous surface was developed (Fig. 11b). These results are related to those reported in Fig. 8, where when the impregnation ratio increased from 0.5 to 1.5 g ZnCl$_2$ g BH[-1], the pore volume rose from 0.072 to 0.728 cm^3 g^{-1}. In addition, this increase in the impregnation ratio decreased the quantity of micropores 2.6 times, whereas the quantity of mesopores increased 1.4 times (Fig. 8). Similarly, the surface area increased by nearly 2 times

56

when the impregnation ratio increased 3 times (Fig. 8). The BHAC obtained under the optimal conditions shows a porous surface (Fig. 11b) with a pore volume of 0.263 cm^3 g^{-1} and principally a mesoporous structure (Fig. 8), resulting in a high surface area (811.44 m^2 g^{-1}). It is important to note that these values fall in the middle of the values obtained at the lowest and highest impregnation ratio.
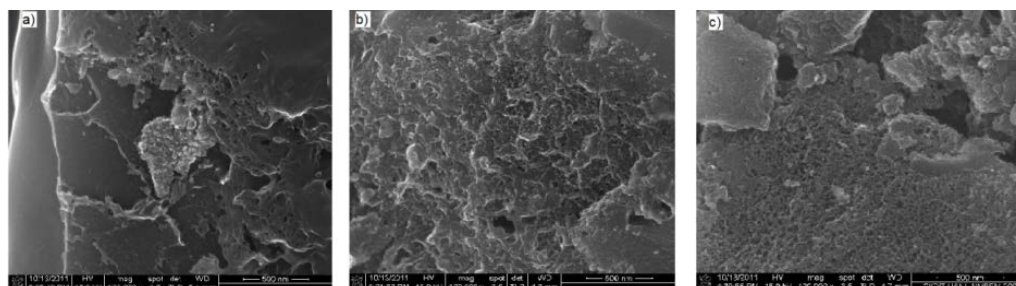
Fig. 11 SEM Micrographs of BHAC at (a) a low Impregnation Ratio (0.5 g ZnCl$_2$ g BH^{-1}; Activation time of 100 min and Temperature of 500 °C), (b) Optimal Conditions (Activation time of 20 min, Temperature of 436 °C, and Impregnation Ratio of 1.1 g ZnCl$_2$ g BH^{-1}) and (c) a high Impregnation Ratio (1.5 g ZnCl$_2$ g BH^{-1}; Activation time of 100 min and Temperature of 500 °C).

3.4 Effect of Adsorbent Concentration on Phenol Adsorption onto BHAC

Fig. 12 indicates the effect of BHAC concentration on adsorption capacity and removal of phenol. The removal of phenol increases from 10 to 75% by increasing BHAC concentration from 0.8 to 10 mg L^{-1}. This can be explained by the fact that the increase in adsorbent concentration resulted in more available sites to adsorb phenol from aqueous solution. On the other hand, adsorption capacity decreases from 70 to 35 mg g^{-1} when BHAC concentration was increased in the same range, because not all available sites for the adsorbate are occupied at high adsorbent concentrations. Thus, a BHAC dosage of 0.8 mg L^{-1} was used for further studies.
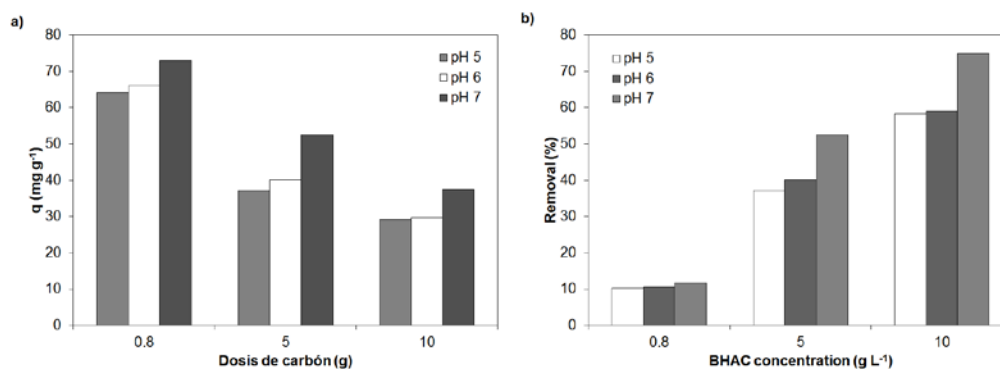
Fig. 12 The Effect of the BHAC Concentration on the Adsorption Capacity (mg g^{-1}) and Phenol Removal (%).

3.5 Effect of pH on Phenol Adsorption onto BHAC

The effect of pH on the adsorption of phenol from aqueous solution is the result of the combined effects of pH solution on the ionization of phenol, the inorganic acids and bases present used to adjust pH, and the surface charge distribution [86]. Fig. 13 depicts the effect of pH solution on adsorption capacity of phenol. The effect of pH was studied in the pH range of 3 to 11 with 0.8 g BHAC L^{-1}, contact time of 24 h, stirring speed of 200 min^{-1}, and temperature of 25 °C. The adsorption capacity of phenol onto BHAC increased when the pH solution was augmented from 3 to 7. At pH 7, the highest adsorption capacity of phenol onto BHAC was achieved, and then it decreased as pH value increased up to pH 11. This behavior can be explained in terms of the dissociation constant of phenol (pK_a = 9.89 [87]) and the pH of the point of zero charge (pH_{PZC} = 1.9). At solution pH higher than the pK_a of phenol, the adsorbent is primarily present in aqueous phase as phenolate (negatively charged species) and, additionally, BHAC net surface charge is predominantly negative; therefore, the electrostatic repulsive forces between phenolate and the negative surface of carbon may cause a decrement in the phenol adsorption capacity at pH values higher than 9.89. The

observed reduction in adsorption capacity at pH lower than 7 suggests that additional protons added in the phenol solution to obtain the pH values of 3, 4, and 5 compete with phenol for carbonyl oxygen sites, where the adsorption occurs by an electron donor-acceptor complex formation at the carbon surface. This complex is formed for the oxygen of the surface carbonyl group (electron donor) and the phenol aromatic ring (electron acceptor) [88].
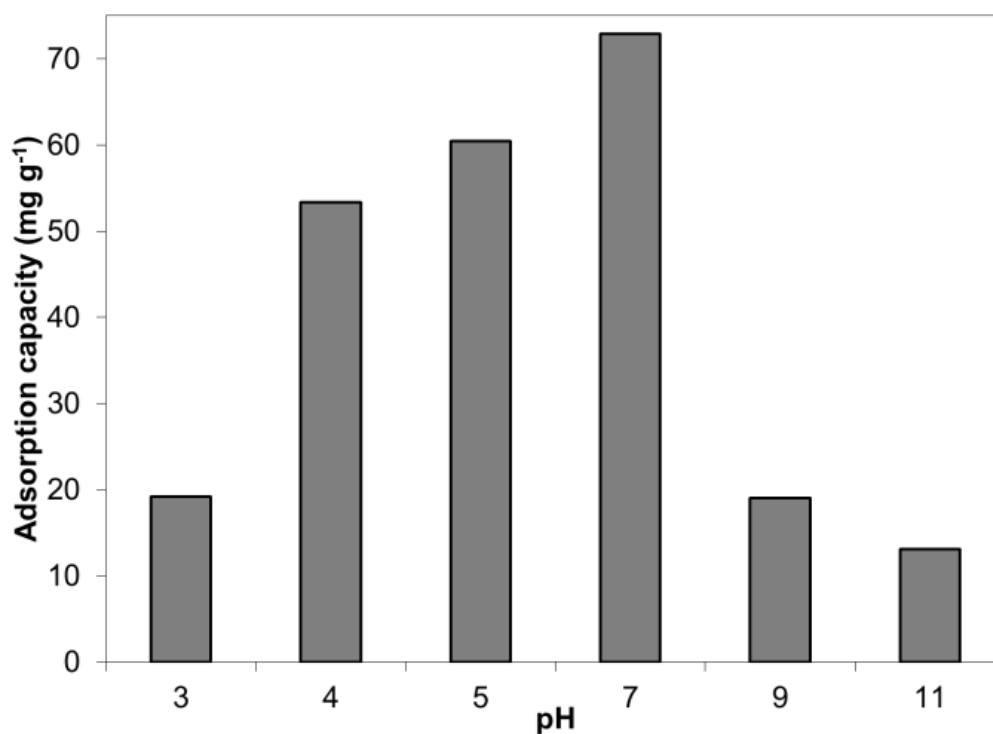
Fig. 13 The Effect of pH on the Phenol Adsorption Capacity onto BHAC (mg g^{-1})

3.6 Equilibrium Adsorption Experiments

The equilibrium isotherms of phenol at pH 7 and temperatures of 25, 35, and 45 °C are presented in Fig. 14. The maximum experimental adsorption capacity of phenol onto BHAC decreased from 98.83 to 75.28 mg g^{-1} when temperature increased from 25 to 35 °C (Fig. 14). This increase could be related to the combined effects of a decrease of the vibrational energy of the adsorbed molecules, which results in less desorption of

phenol from the BHAC surface, and a decrease in phenol solubility in water, which results in a lower degree of attraction of the phenol by water [28]. A further increase in temperature to 45°C did not caused a decrease in the adsorption capacity. The maximum experimental adsorption capacity value determined for phenol onto BHAC is similar or higher than those reported for activated carbon produced from other lignocellulosic precursors (Table 11).
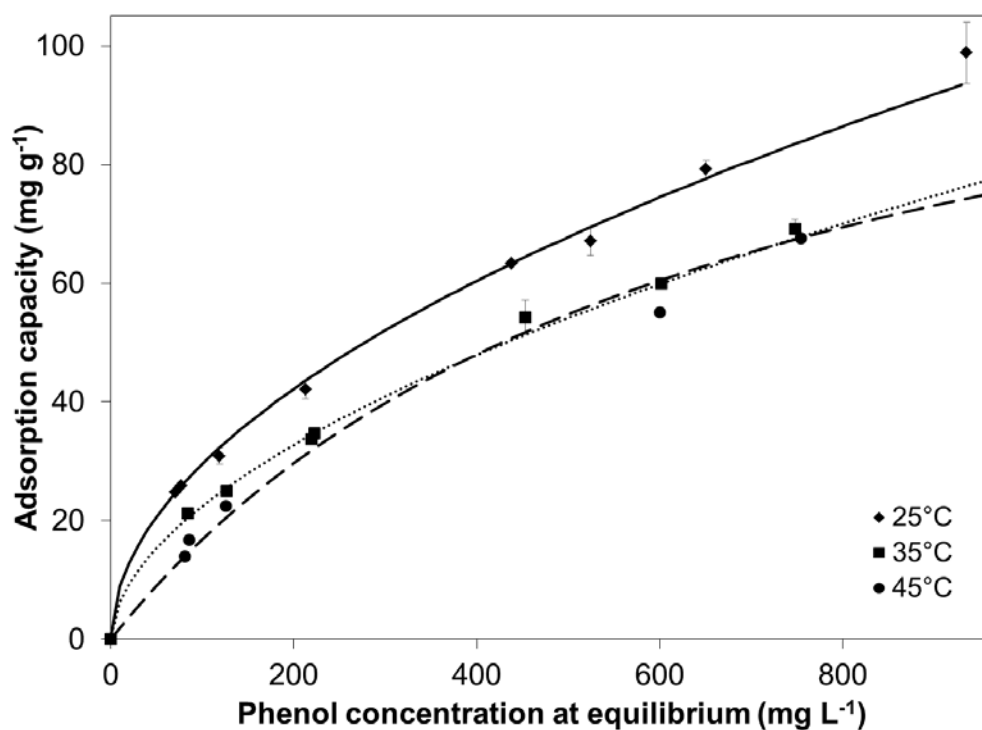
Fig. 14 The Adsorption Isotherms of Phenol onto BHAC at pH 7 and 25, 35, and 45 °C. Symbols Represent the Experimental data and the Lines Indicate the Freundlich Model Prediction for 25 and 35 °C and Langmuir Model for 45 °C.

Table 11 Phenol Adsorption Capacities for Activated Carbons Derived from Lignocellulosic By-products.

Precursor	Surface area $(m^2\ g^{-1})$	Phenol initial concentration $(mg\ L^{-1})$	Maximum adsorption capacity $(mg\ g^{-1})$	Reference
Nutshells of *Sterculia alata*	712	100	11.16	[20]
Nuts of *Terminalia Arjuna*	1260	100	11.18	[19]
Pecan shells	-	35	18.00	[40]
Rice husks	438.9	300	22.09	[41]
Rice husk	-	100	75.15	[42]
Kenaf	1021	188	80.00	[43]
Cofee residue	520	170	84.02	[18]
Green gram husk	-	100	90.94	[42]
Oreganum stalks	719	200	94.34	[25]
Barley husks	**811.44**	**1000**	**98.83**	**This work**
Black gram husk	-	100	109.92	[42]
Vetiver root	1170	100	122.00	[44]
Black stone cherries	-	500	133.33	[45]
Date pit	490.1	100	262.30	[46]

The equilibrium adsorption data of phenol onto BHAC at 25 and 35 °C were satisfactorily predicted with the Freundlich isotherm, while at 45 °C the experimental data were well predicted by the Langmuir model (Table 12). In the theoretical derivation of the Freundlich model, there is not any requirement that the coverage must approach a constant value corresponding to one complete monomolecular layer. According to isotherm at 25 °C showed in Fig. 14, there is not a plateau in the studied range, which could suggest that the phenol is adsorbed in multi-layer onto BHAC as proposed in the Freundlich isotherm, or that the experiments were conducted in the linear region of the Langmuir isotherm. Also, the Freundlich isotherm equation implies that the energy distribution for the adsorption sites is an exponential type. This leads to the possibility of non-linear energy distribution for the adsorption sites of BHAC, which is consistent with

a heterogeneous surface as that of an activated carbon produced from lignocellulosic materials, consisting of basal planes and edges of the microcrystallites [89].

Table 12 Isotherm Parameters Estimated from Experimental data of Phenol Adsorption onto BHAC at pH 7.

Temperature	Langmuir			Freundlich		
(°C)	q_{max}	b	ARE (%)	K	1/n	ARE (%)
25	132.94	0.002	11.12	2.73	0.52	2.36
35	95.95	0.003	5.07	1.79	0.55	2.41
45	125.63	0.002	7.95	0.68	0.69	11.35

As observed in Fig. 14 an increase in temperature reduces the adsorption capacity of phenol onto BHAC. This behavior could be explained as follows: the adsorbed molecules have vibrational energies at 35 and 45 °C greater than at 25 °C and, therefore, these are more likely to desorb from the BHAC surface, in particular those adsorbed on the external layers, which results in a lower phenol adsorption capacity. Moreover, solubility of phenol in water increases from 82.89 g L^{-1} at 25 °C to 98.97 and 101.87 g L^{-1} at 35 and 45 °C, respectively [2], which increase the attraction of the phenol by water causing a decrease in adsorption capacity. The increase in solubility when temperature rose from 25 to 35 °C (16.08 g L^{-1}) is higher than the increase of solubility when temperature augmented from 35 to 45 °C (2.9 g L^{-1}). For this reason adsorption capacity decreases when temperature increases from 25 to 35 °C but a further increase in temperature from 35 to 45 °C did not decreased the adsorption capacity.

Fig. 15 shows the phenol adsorption isotherm onto CAC and BHAC at 25 °C. It can be observed that the quantity of phenol adsorbed onto CAC is greater than that adsorbed by BHAC at equilibrium phenol concentrations lower than 950 mg L^{-1}.

However, both adsorption data for CAC and BHAC tends to converge at equilibrium concentrations greater than 950 mg L^{-1}. The difference between the adsorption capacities of BHAC and CAC could be explained on the basis of different surface areas and total surface acidic sites. The BHAC used in these studies had a surface area of 811.44 m^2 g^{-1} and 2.4 meq H^+ g^{-1}, while CAC was 1620 m^2 g^{-1} and 1.55 meq H^+ g^{-1} (Table 13). Based on surface area, the adsorption capacity of CAC might be expected to be greater than that of the BHAC as evidenced in the low concentration region ($C_0 <$ 950 mg L^{-1}) shown in Fig. 15. Moreover, it is proposed that the observed decrease in adsorption capacity at low concentration range is also related to water adsorption, as proposed by Coughlin and Ezra [90] and other researchers [88,91-94]. As water comes in contact with the adsorbent surface, it adsorbs on the acidic sites located at the entrance of the carbon pores, reducing the accessibility of the phenol molecules to the inner pore structure. Consequently, high surface acidic sites content in BHAC leads to a lower phenol adsorption capacity because the number of sites for H-bonding is increased, and it is to be expected that adsorption of water molecules on these groups is higher than the adsorption of phenol molecules. Nonetheless, at higher concentrations of phenol ($C_0 >$ 950 mg L^{-1}) the number of water molecules decrease, increasing the accessibility of the phenol molecules to the micropores and the adsorption on carbonyl active sites.
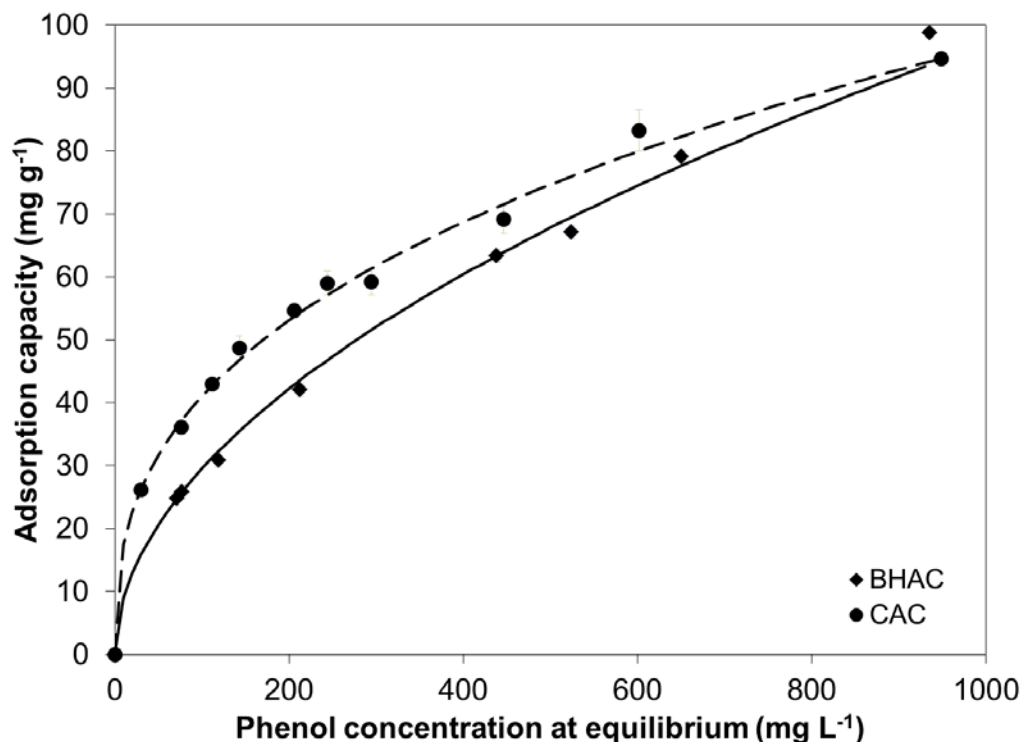
Fig. 15 The Adsorption Isotherms of Phenol onto BHAC and CAC at pH 7 and 25 °C.
Symbols Represent the Experimental data and the Lines Indicate the Freundlich
Model Prediction.

Table 13 Physico-chemical Characteristics of BHAC and CAC

Parameter	Value	
	BHAC	CAC
pH_{PZC}	1.9	4.2
Total surface acidid sites (meq g^{-1})	2.4	1.55
BET surface area ($m^2 g^{-1}$)	811.44	1347.05
Total pore volume ($cm^3 g^{-1}$)	0.26	0.96
Average pore width (nm)	2.56	3.13

3.7 Kinetic Adsorption Experiments

The results and discussion of the adsorption reaction models [51,52] and
adsorption intraparticle diffusion models [54,55] are presented in Section 3.7.1 and
3.7.2, respectively.

3.7.1 Adsorption Reaction Models

Both, the pseudo-first and pseudo-second order reaction models were used to predict the adsorption kinetics of phenol onto BHAC. Table 14 presents the adsorption rate constants, equilibrium adsorption capacities, and the ARE of these models. Based on the ARE, the pseudo-first order reaction model (ARE ≤ 5.16%) predicted the experimental results better than the pseudo-second order reaction model (ARE ≤ 8.25%), except for the experimental run carried out at 300 min^{-1} and the one carried out at 30 °C. Few examples of satisfactory fitting of kinetics experimental data with pseudo-first order model have been reported [56,95,96].

Table 14 Comparison of the Pseudo-first and Pseudo-second Order Kinetic Models for the Phenol Adsorption onto BHAC at Different Experimental Conditions.

Stirring speed (min^{-1})	Mean particle diameter (cm)	C_0 (mg L^{-1})	Temperature (°C)	Pseudo-first order			Pseudo-second order		
				k_1 (g mg^{-1} min^{-1})	q_e (mg g^{-1})	ARE (%)	k_2 (g mg^{-1} min^{-1})	q_e (mg g^{-1})	ARE (%)
300	0.04	1000	35	0.04	75.76	7.68	0.0005	84.57	5.31
400	0.04	1000	35	0.12	79.34	1.94	0.002	88.11	6.51
500	0.04	1000	35	0.18	77.10	2.39	0.003	83.20	3.67
400	0.01	1000	35	0.13	78.75	3.37	0.002	87.62	3.90
400	0.04	500	35	0.09	49.74	3.06	0.002	56.13	3.73
400	0.04	250	35	0.08	38.25	3.12	0.003	40.65	6.40
400	0.04	1000	30	0.07	80.25	4.53	0.0009	89.88	2.78

Fig. 16 shows the experimental results of the adsorption kinetics of phenol onto BHAC at different stirring speed and the predicted values with the pseudo-first order model. The phenol removal increased with time and attained equilibrium at approximately 40 minutes at stirring speed of 400 and 500 min^{-1}, and 120 minutes at 300 min^{-1}. This behavior is due to the decreasing of external mass transfer resistance at stirring speed higher than 400 min^{-1}, therefore phenol molecules are transferred fast to the external surface of the adsorbent. A further increase in the stirring speed was not necessary to reduce the time required to achieve the equilibrium in the adsorption of

phenol onto BHAC. For this reason, the subsequent adsorption kinetics experiments of phenol onto BHAC were only performed at 400 min^{-1}.
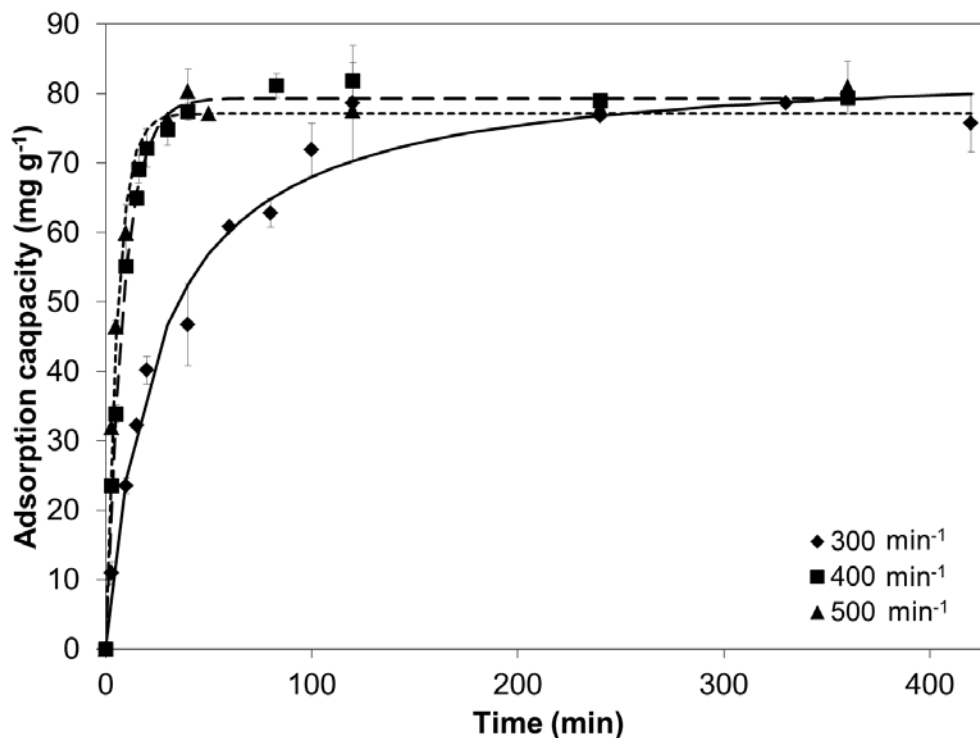
Fig. 16 Adsorption Kinetics of Phenol onto BHAC at pH 7 and 35 °C, Using 80 mg L^{-1} of BHAC and Different Stirring Speeds. Symbols Represent the Experimental Results and the Lines the Predicted Values by the Pseudo-first Order Reaction Model.

Fig. 17 shows the experimental adsorption capacity of phenol onto BHAC at two mean particle size (0.01 and 0.04 cm) and the adsorption capacity predicted by the pseudo-first order model. The phenol equilibrium adsorption was attained at approximately 40 minutes in both cases; reduction of mean particle size does not improve the intraparticle diffusion because external mass transfer had been already minimized at 400 min^{-1}. Therefore the time needed to achieve equilibrium cannot be decreased at mean particle size lower than 0.01 cm.
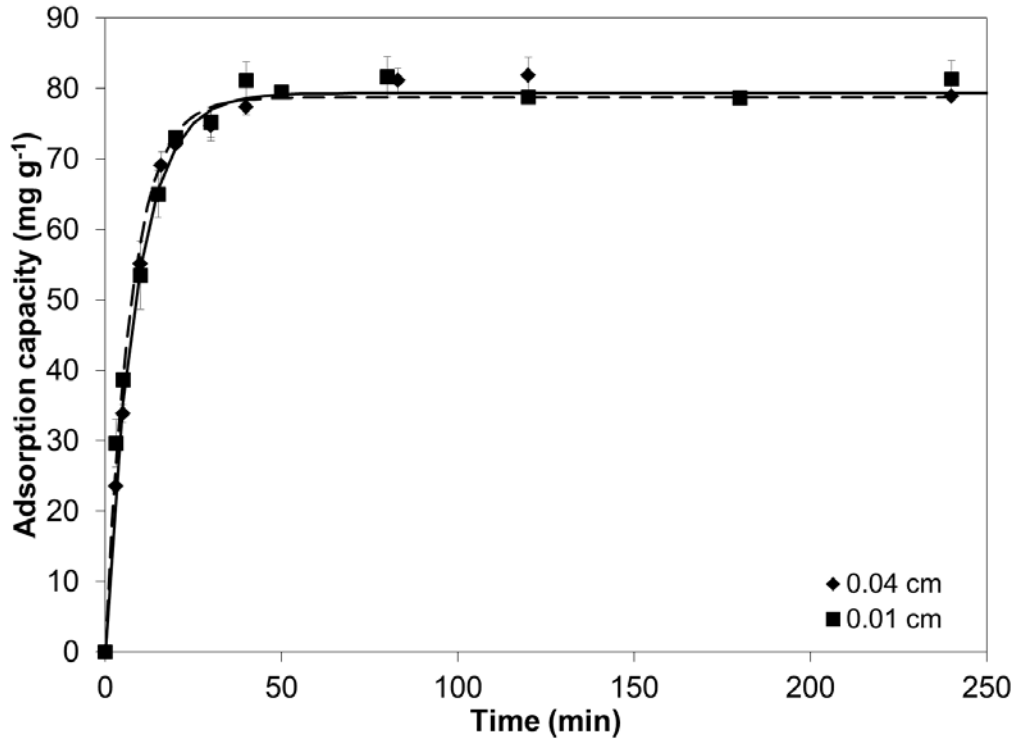
Fig. 17 Adsorption Kinetics of Phenol onto BHAC at pH 7 and 35 °C, Using 80 mg L^{-1} of BHAC and Different mean Particle size. Symbols Represent the Experimental Results and the Lines the Predicted Values by the Pseudo-first Order Model.

Fig. 18 shows the experimental adsorption capacity of phenol onto BHAC at three phenol initial concentrations (250, 500, and 1000 mg L^{-1}) and the adsorption capacity predicted by the pseudo-first order model. The initial phenol concentration determines both the equilibrium concentration and the adsorption rate of phenol. The phenol removal attained equilibrium at approximately 40 minutes at initial concentration of 1000 mg L^{-1}, and 60 minutes at 500 and 250 mg L^{-1}. It was also observed that rising initial phenol concentration from 250 to 1000 mg L^{-1} increased twofold the equilibrium adsorption capacity. The increase of the equilibrium adsorption capacity is related to the increase concentration gradient which is the driving force for mass transfer of phenol through the film and pores of adsorbent particles [73,97,98].
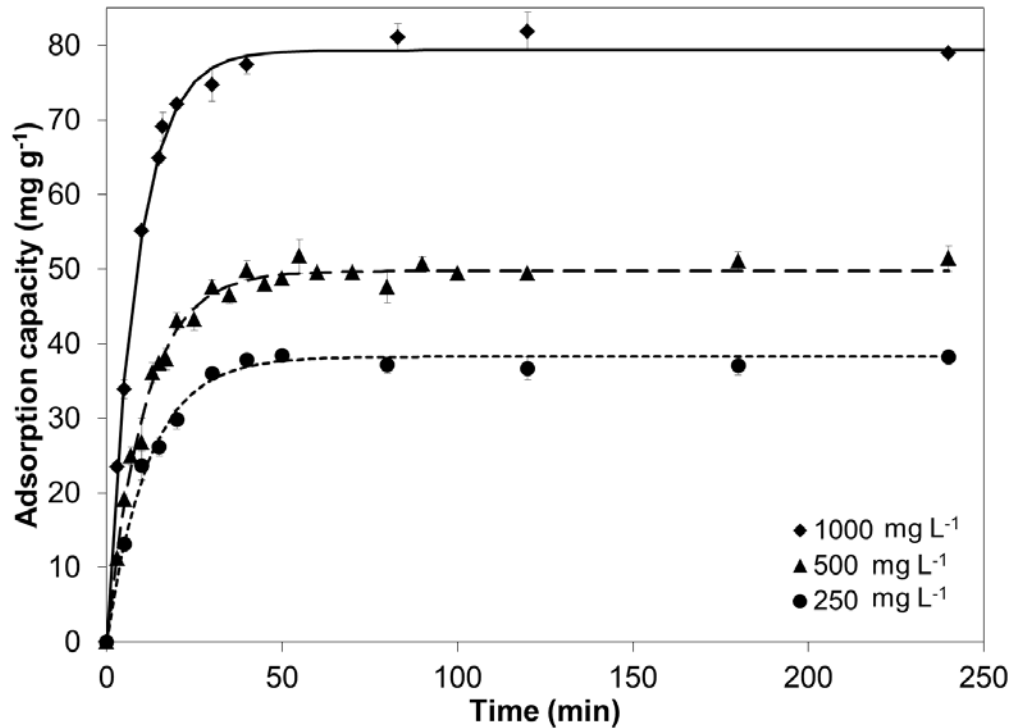
Fig. 18 Adsorption Kinetics of Phenol onto BHAC at pH 7 and 25 °C, Using 80 mg L^{-1} of BHAC and Different Phenol Initial Concentration. Symbols Represent the Experimental Results and the Lines the Predicted Values by the Pseudo-first Order Reaction Model.

Fig. 19 shows the experimental adsorption capacity of phenol onto BHAC at 30 and 35 °C and the adsorption capacity predicted by the pseudo-second and pseudo-first order model, respectively. The adsorption temperature had an effect in both the equilibrium concentration and the adsorption rate of phenol. The equilibrium adsorption capacity at 35 °C was approximately 80 mg g^{-1}, while for 30 °C was approximately 90 mg g^{-1} because an increase in vibrational energy of phenol molecules which can cause desorption from the BHAC surface. It was also observed that an increase in temperature from 30 to 35 °C decreased the time required to attain equilibrium from 200 min to 40 min, due to an increase in diffusion of phenol through the film and pores of adsorbent particles.
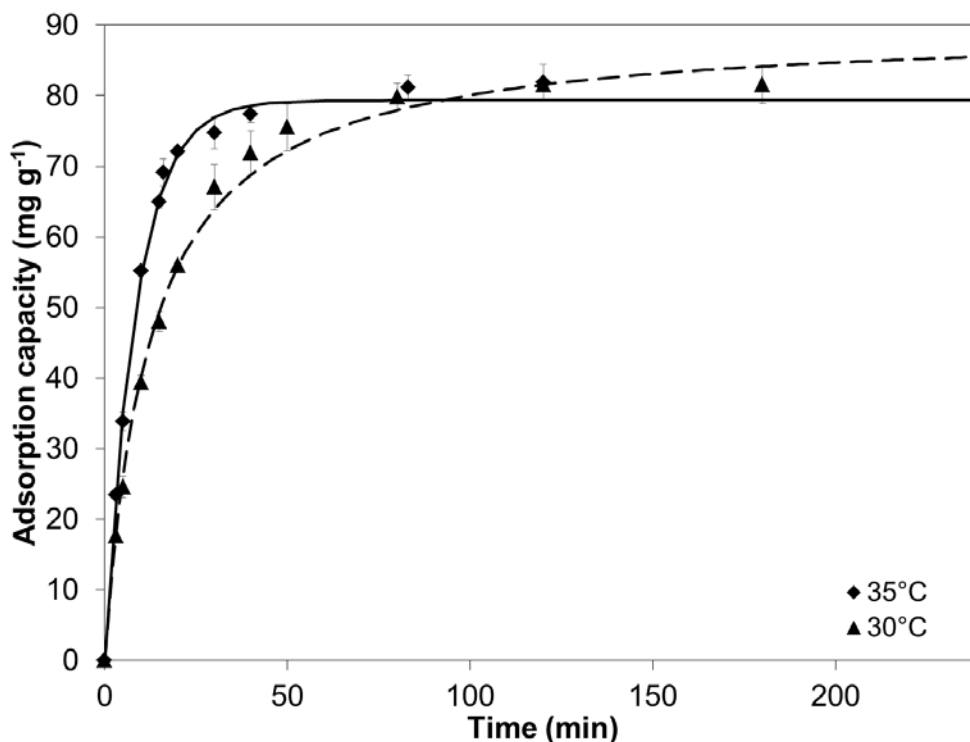
Fig. 19 Adsorption Kinetics of Phenol onto BHAC at pH 7 Using 80 mg L^{-1} of BHAC and Different Temperatures. Symbols Represent the Experimental Results and the Lines the Predicted Values by the Pseudo-first Order Reaction Model for 35 °C and Pseudo-second order for 30 °C.

3.7.2 Adsorption Intraparticle Diffusion Models

The phenol adsorption data were plotted according to Eq. 8 for different stirring speed (300, 400, and 500 min^{-1}), mean particle size (0.01 and 0.04 cm), phenol initial concentration (250, 500, and 1000 mg L^{-1}), and temperature (30 and 35 °C), and the results are showed in Fig. 20 to 23. These figures show two linear sections, the first linear section intercepts the origin suggesting that the intraparticle diffusion is the only rate-limiting step [99]. The second linear section does not intercept the origin, which implies that more than one diffusion mechanism is occurring at the same time in the adsorption process of phenol onto BHAC. Similar behavior for adsorption process of other adsorbates has been reported in few previous studies [100,101]. The initial slope

represents the intraparticle diffusion process according to Eq. 8 and the plateau portion corresponds to the final equilibrium process. In the first stage, the phenol diffusion is primarily restricted by the highly porous structure of the BHAC (Table 3), and during the next stage the diffusion is predominantly retarded by the surface diffusion of phenol species along the pore surface.
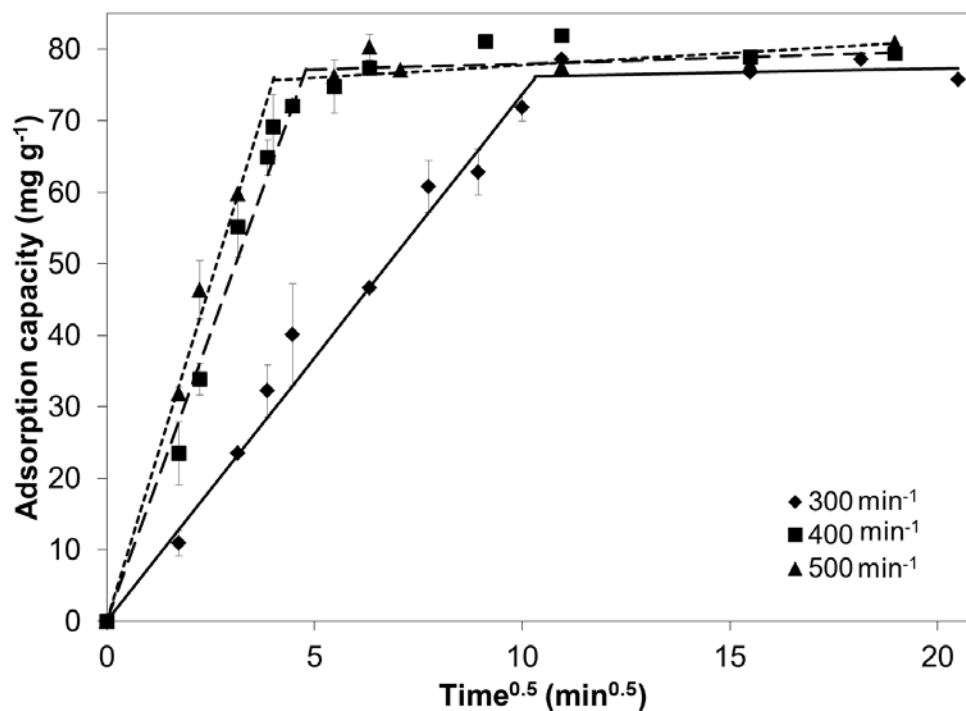
Fig. 20 Adsorption Kinetics of Phenol onto BHAC at pH 7 and 35 °C Using 80 mg L^{-1} and Different Stirring Speed. Symbols Represent Experimental Results and the Lines the Predicted Values by the Intraparticle Diffusion Model.
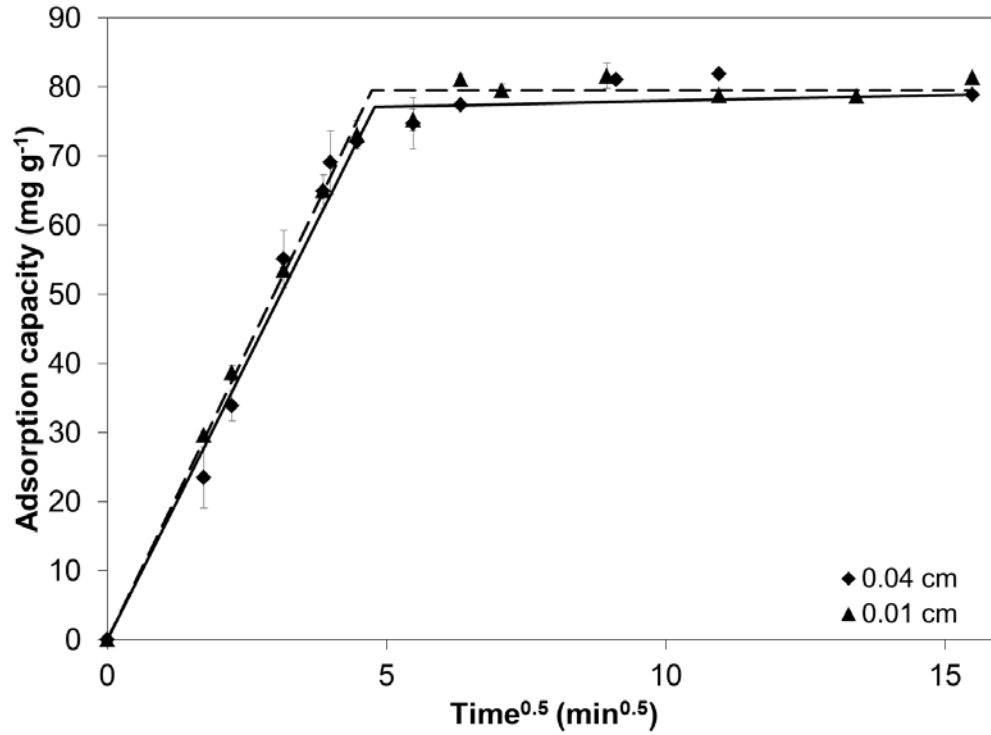
Fig. 21 Adsorption Kinetics of Phenol onto BHAC at pH 7 and 35 °C, Using 80 mg L^{-1} of BHAC and Different mean Particle size. Symbols Represent the Experimental Results and the Lines the Predicted Values by the Intraparticle Diffusion Model.
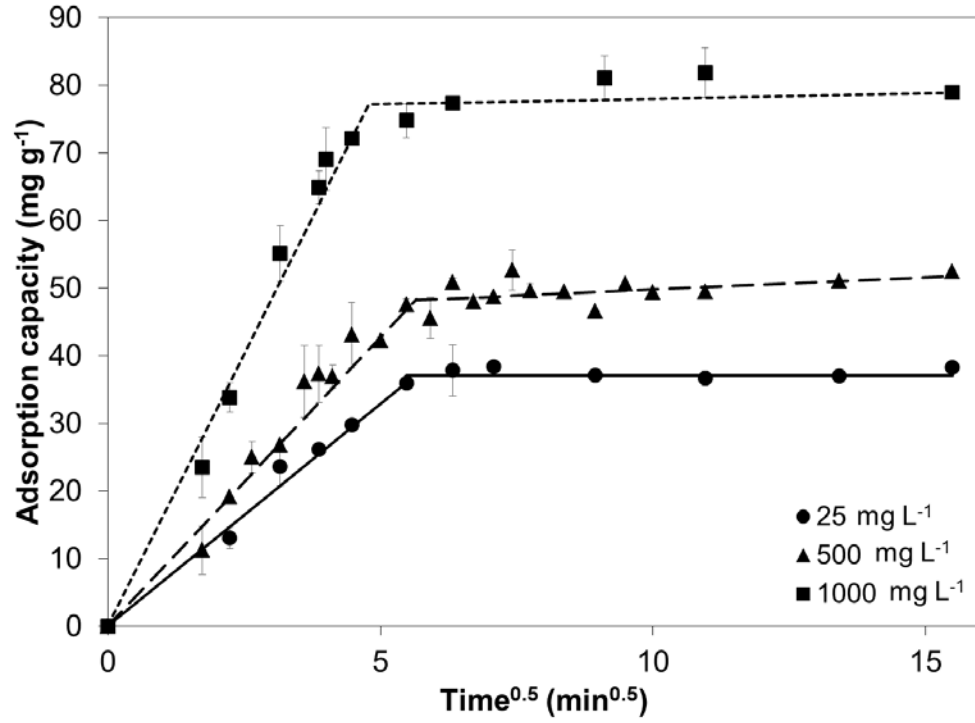
Fig. 22 Adsorption Kinetics of Phenol onto BHAC at pH 7 and 35 °C, Using 80 mg L^{-1} of BHAC and Different Phenol Initial Concentration. Symbols Represent the Experimental Results and the Lines the Predicted Values by the Intraparticle Diffusion Model.
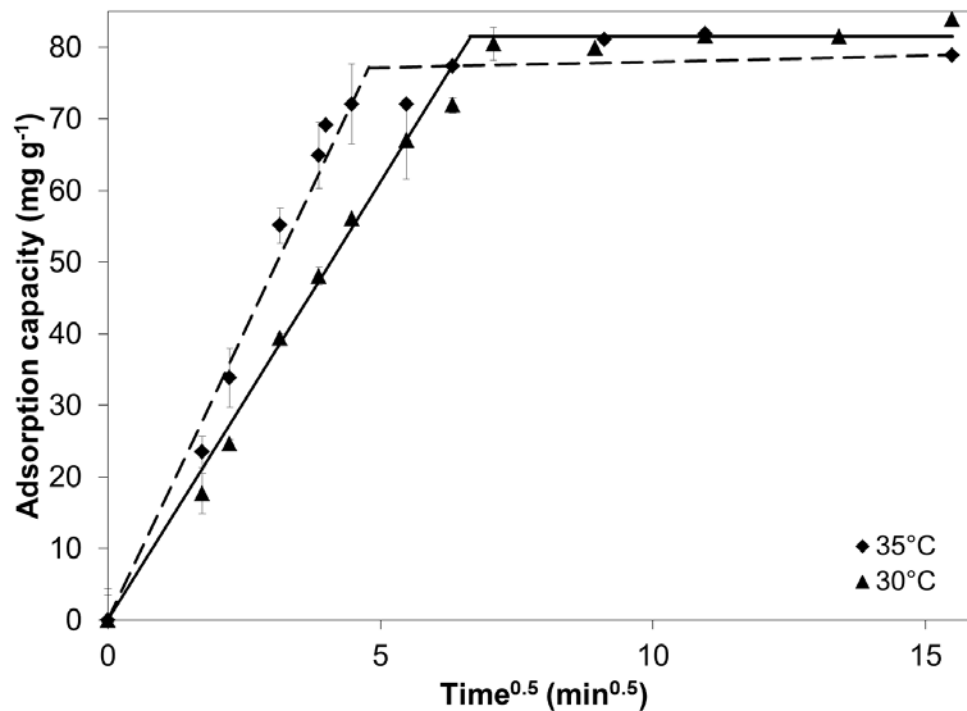
Fig. 23 Adsorption Kinetics of Phenol onto BHAC at pH 7, Using 80 mg L^{-1} of BHAC and Different Temperatures. Symbols Represent the Experimental Results and the Lines the Predicted Values by the Intraparticle Diffusion Model.

Table 15 presents the parameters of the intraparticle diffusion model calculated with the intraparticle diffusion model and the Vermeulen's approximation (Eq. 6 and Eq. 9, respectively). It can be noted that diffusivities for the first linear part of the plot and diffusivities calculated from Eq. 6 and Eq. 9 are in an order of magnitude of 10^{-12} m^2 s^{-1}, which is lower than the diffusivities on liquid phase at ordinary temperatures [31], and it can be related to BHAC porosity as well as tortuosity factor [102].

Table 15 Fitting Parameters for Intraparticle Diffusion Model and the Diffusion Coefficient Values for Phenol Adsorption onto BHAC.

Stirring Speed (min^{-1})	Mean particle diameter (cm)	C_0 (mg L^{-1})	Temperature (K)	Weber & Morris intraparticle diffusion model								Vermeulen's approximation D_i (x10^{-12} $m^2 s^{-1}$)
				First linear part of the curve				Second linear part of the curve				
				k_p (mg $g^{-1}min^{-0.5}$)	I (mg g^{-1})	ARE (%)	D_i (x10^{-12} $m^2 s^{-1}$)	k_p (mg $g^{-1}min^{-0.5}$)	I (mg g^{-1})	ARE (%)	D_i (x10^{-14} $m^2 s^{-1}$)	
300	0.04	1000	308	7.38	0.00	7.00	5.44	0.11	75.06	1.33	0.12	3.50
400	0.04	1000	308	16.12	0.00	7.21	32.83	0.17	76.35	2.02	0.35	30.67
500	0.04	1000	308	18.92	0.00	3.89	47.83	0.35	74.30	1.91	1.61	39.33
400	0.01	1000	308	16.79	0.00	5.09	3.32	0.00	79.55	1.47	0.00	1.33
400	0.04	500	308	8.55	0.00	8.67	7.33	0.37	46.14	1.99	1.34	28.00
400	0.04	250	308	6.57	0.00	6.39	4.33	0.00	37.12	1.54	0.00	7.83
400	0.04	1000	303	12.24	0.00	6.31	14.67	0.00	81.54	2.58	0.00	11.00

3.8 Desorption Studies

The Fig. 24 shows the effect of distilled water, HCl, NaOH, and ethanol/water solutions in the phenol desorption from BHAC. According to the results shown in Fig. 24, it is observed that water is not the best eluent to desorb phenol species from BHAC, and it could be because the relatively low solubility of phenol in this eluent (8.2 g 100 g^{-1} solution) [4], and the interactions between phenol and the functional groups on the BHAC surface. On the other hand, the highest desorption capacity (68.79 mg g^{-1}) was obtained with 10% V/V ethanol solutions because phenol can be dissolved in pure ethanol [4]. Although is well known that regenerant solution pH can strongly influence desorption by changing the speciation of the adsorbate and the adsorbent surface charge distribution, when 0.1 N HCl and 0.1 N NaOH were used as eluent the desorption capacities reached were 55.44 and 63.00 mg g^{-1} respectively, which are lower than those found for 10% V/V ethanol solutions. Fig. 25 shows the results of five cycles of adsorption/desorption of phenol on BHAC using 10% V/V ethanol solution as the regenerating agent. The adsorption capacity of phenol onto BHAC decreased from 98.33 to 73.33 mg g^{-1} from the first cycle to the fifth cycle, which indicates that the adsorption sites on the BHAC surface were occupied with non-desorbed phenol molecules, gradually saturated with phenol. Therefore, further research should be carried out using higher concentration ethanol solutions, in order to enhance the solubility of phenol in the regeneration solution.
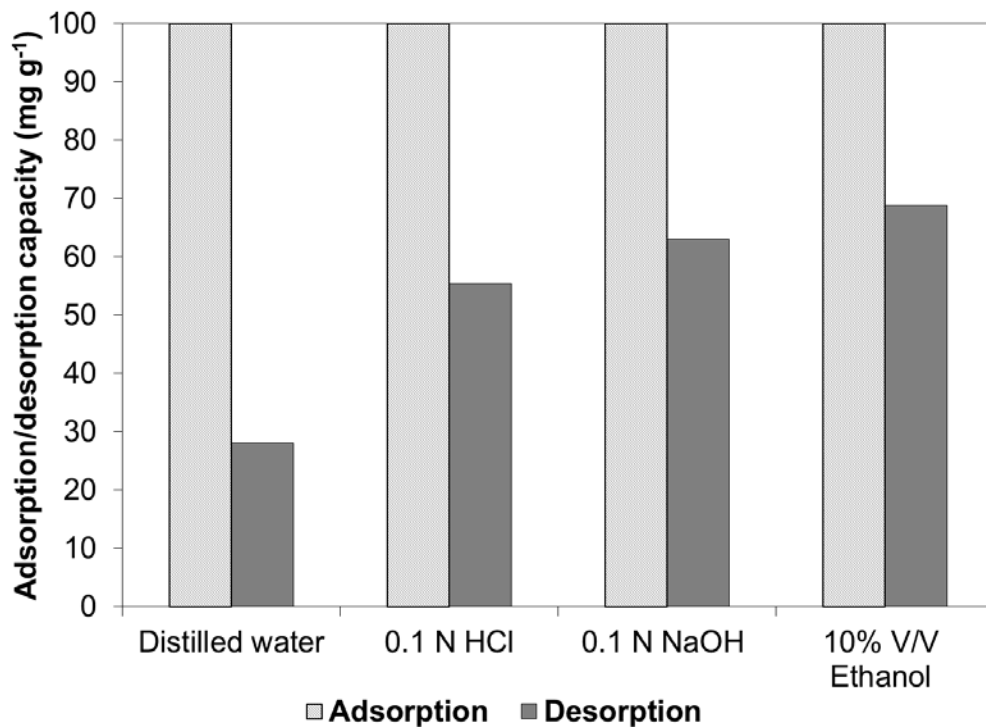
Fig. 24 The effect of Different Eluting Agents on Regeneration of Spent BHAC.
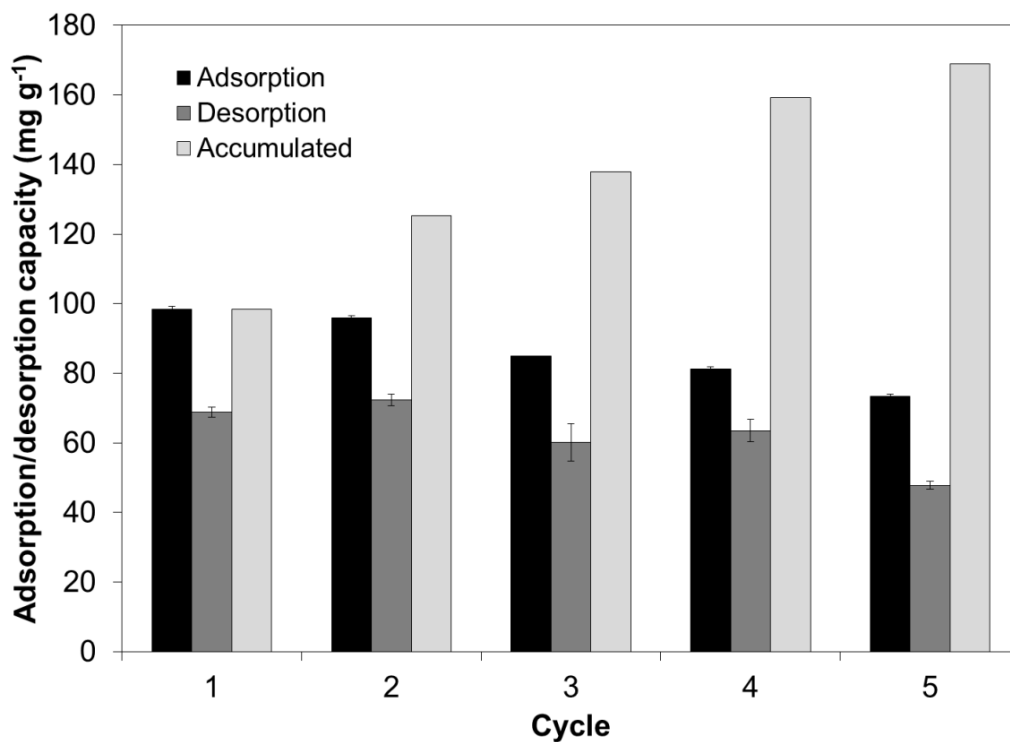
Fig. 25 Five Repetitive Cycles of Adsorption and Desorption of Phenol onto BHAC with 10% V/V Ethanol Solution as Regenerating Agent.

3.9 Modeling of Breakthrough Curves with Artificial Neural Networks

One input neuron (time) was supplied to a feed-forward back propagation ANN. This ANN was tested with different quantities of neurons in the hidden layer to predict the output neuron (C/C_0) for each experimental set as listed in Table 3. Mean square errors were used to compare the performance of the ANN based on the experimental and predicted data of C/C_0 (Fig. 26). The MSE of the ANN with 2 neurons was lower lower (1.67×10^{-4} – 7.52×10^{-4}) than the MSE of the ANN with 1 neuron (2.22×10^{-4} – 9.80×10^{-4}) for all the data sets, but MSE did not decrease when the number of neurons increased up to 20. Consequently, ANN with 2 neurons in the hidden layer will be used in the subsequent experiments. Figures 27 to 30 show the breakthrough experimental data as well as the predicted results by using the ANN architecture. All ANNs described the experimental data adequately, with regression coefficients higher than 0.99 for all cases.
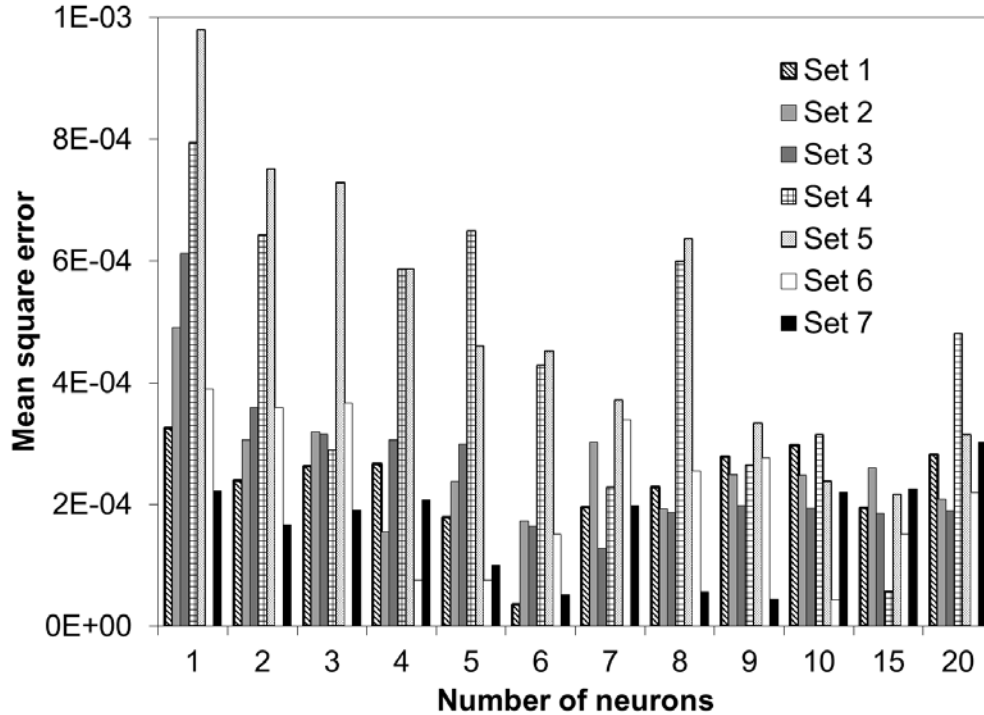
Fig. 26 Mean square error (MSE) estimated by using an ANN varying the number of neurons in the hidden layer for predicting C/C_0.

The effect of the air flow rate, phenol initial concentration, BHAC dosage and influent flow rate is shown in Fig. 27, 28, 29, and 30, respectively. The adsorption process of phenol onto BHAC did not occur very fast; this can be concluded from the behavior of the curves that did not show a linear vertical behavior between the breakthrough point and the saturation point. The breakthrough point can be taken as the point at which the effluent phenol concentration reaches a particular concentration. The drinking water standards and health advisories of the U.S. Environmental Protection Agency (EPA) derived an oral reference dose of 2 mg L^{-1} for lifetime consumption of phenol [103]. Therefore, an effluent phenol concentration of 2 mg L^{-1} was used to calculate the breakthrough time.

The effect of air stripping in the phenol removal was studied in the airlift reactor without using BHAC. The experimental study demonstrated that the phenol removal

due to air stripping was up to 0.05% at an air flow rate of 10 L min^{-1}. Although there is an effect of air stripping, it is much less compared to that of adsorption by BHAC, because air stripping is effective at very high gas velocities and high phenol concentrations [56].

Fig. 27 shows that the time required to achieve the breakthrough time does not significantly change when the air flow rate increases from 1 to 3 L min^{-1} and from 1 to 10 L min^{-1}. The breakthrough curve obtained at 10 L min^{-1} shows a sharper shape than the curve obtained at the lower air flow rate. At low air flow rate the time required for complete BHAC saturation is longer due to a less turbulent flow and this time decreased with increasing air flow rate.
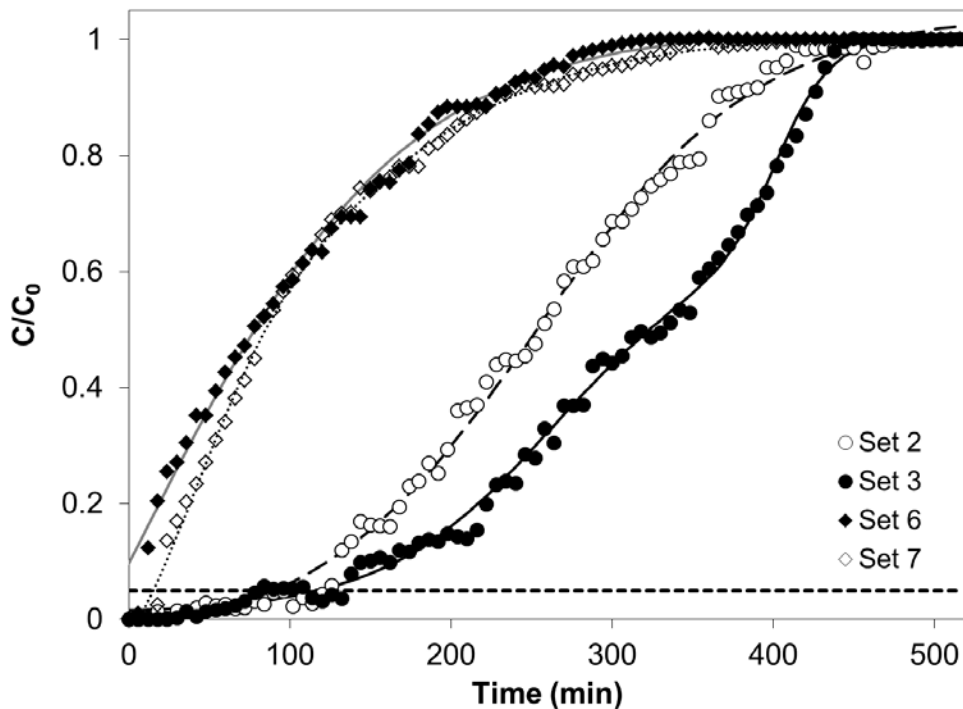
Fig. 27 Effect of the air flow rate on breakthrough curves at feed concentration of 40 mg L^{-1}, (a) BHAC dosage of 2 g L^{-1} and phenol feed rate of 3 L h^{-1}, and (b) BHAC dosage of 5 g L^{-1} and phenol feed rate of 2 L h^{-1}. Symbols represent the experimental data and lines show the predicted results by ANN.

The breakthrough curve shifted towards the origin when increasing the phenol feed concentration, as shown in Fig. 28. The breakthrough times for C_0 values of 40 and 250 mg L^{-1} were found to be 90 and 0 min, respectively. A decrease in the breakthrough time and the saturation time at higher C_0 could be related to the rapid exhaustion of adsorption sites. Also, because the total amount of sites available for phenol adsorption is finite, an increase in C_0 results in a decrease in the adsorption of phenol.
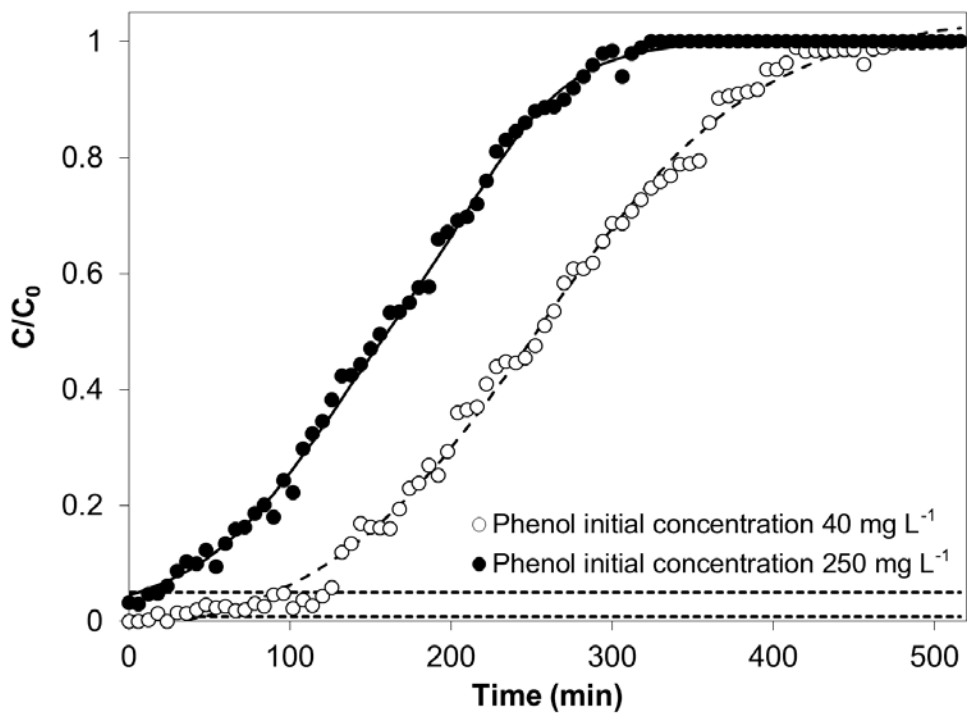
Fig. 28 Effect of phenol initial concentration on breakthrough curves at a BHAC dosage of 5 g L^{-1}, air flow rate of 10 L min^{-1} and phenol feed rate of 2 L h^{-1}.

Fig. 29 shows the breakthrough curve of phenol onto BHAC obtained at 2 and 5 g BHAC L^{-1}. The time needed to reach the breakthrough point increased from 36 to 90 min when BHAC dosage increased from 2 to 5 g L^{-1}. This can be explained by the fact that a higher concentration of BHAC creates a greater surface area of contact with phenol molecules, increasing the quantity of adsorbate removed from the solution.

Consistent findings were reported by Filipkowska and Waraksa [58], who demonstrated that in an airlift reactor under dynamic conditions, the adsorption capacity of chitosan depended on adsorbent dosage.
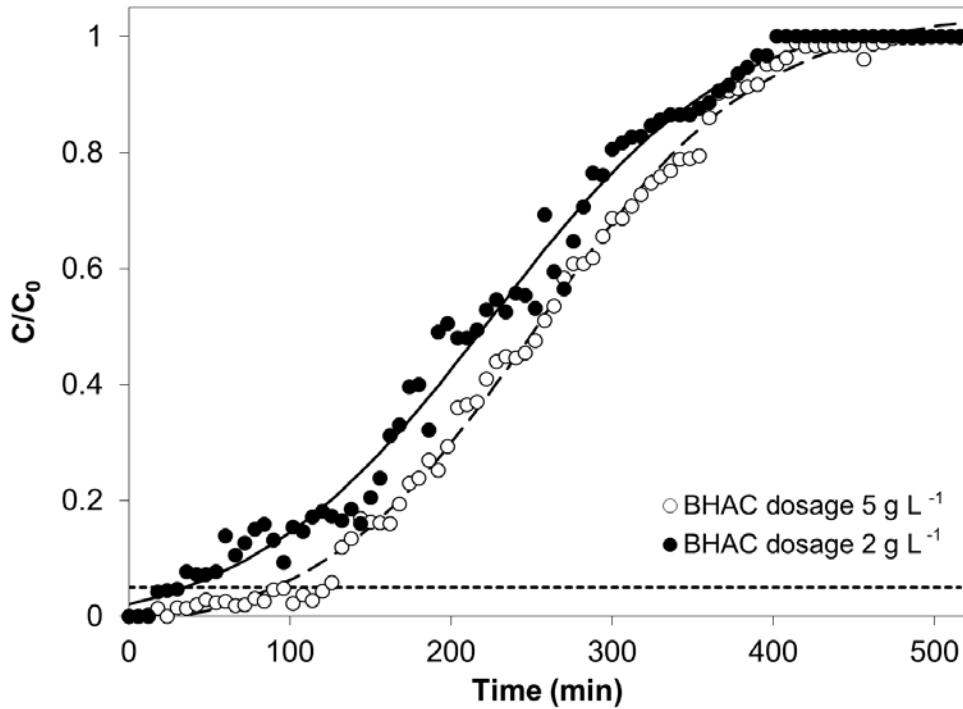
Fig. 29 Effect of BHAC Dosage on Breakthrough Curves at Phenol Initial Concentration of 40 mg L^{-1}, Air Flow Rate of 10 L min^{-1}, and Influent Flow Rate of 2 L h^{-1}.

The breakthrough curves at phenol inlet flow rate of 2 and 3 L h^{-1} are shown in Fig. 30 where it can be seen that the time needed to reach saturation increased from 342 to 468 min with a decrease in the flow rate, because at a low rate of influent phenol molecules had more time to be in contact with BHAC. Filipskowska and Waraksa [58], based on investigation of a reactive dye onto chitosan in an airlift reactor, also reported that the inlet flow rate affected the accumulated adsorption capacity. Additionally, an increase in the inlet flow rate increases the sharpness of the breakthrough curve. According to Cooney [104], the slow approach of C/C$_0$ toward 1 is commonly observed

in liquid-phase adsorption where intraparticle diffusion is the rate-limiting transport process.
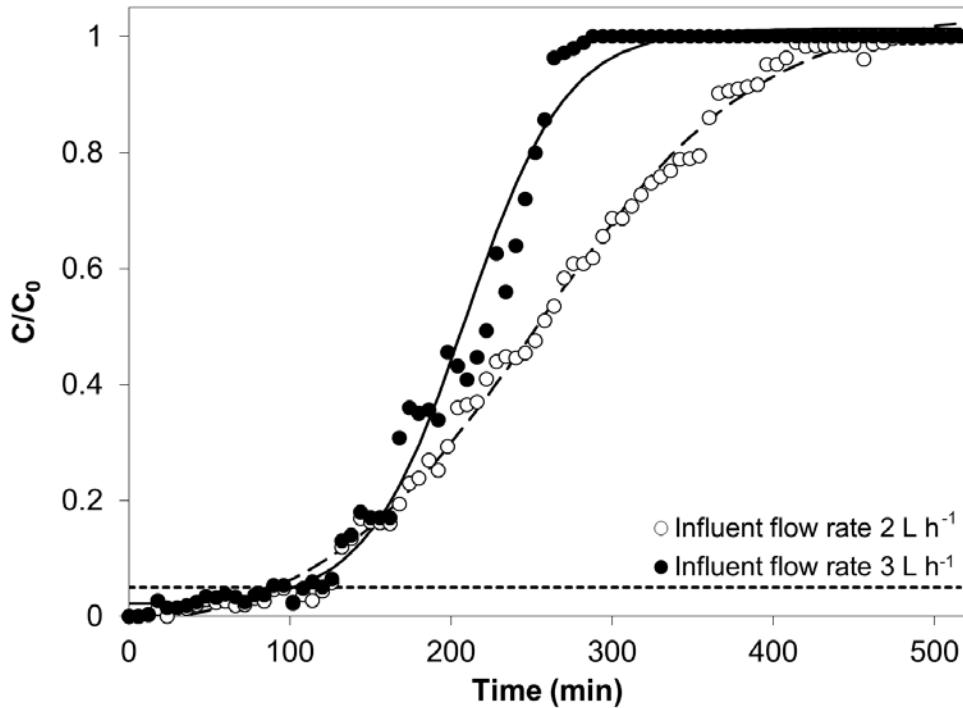
Fig. 30 Effect of Influent Flow Rate on Breakthrough Curves at Phenol Initial Concentration of 40 mg L^{-1}, BHAC Dosage of 5 g L^{-1}, and Influent Flow Rate of 2 L h^{-1}.

In the single-input single-output study, a feed-forward back propagation ANN with 2 neurons in the hidden layer was able to satisfactorily predict C/C_0 respect to time. For the multi-input single-output study, the objective was to predict one of the experimental breakthrough curves in Table 3 by training an ANN with the remaining experimental sets. The performance of an ANN, in terms of its generalization and prediction qualities, depends significantly on the training cases it is presented with and the domain these training cases cover. To determine the extent of the domain of the experimental breakthrough data, tangents were plotted at $C/C_0 = 0.5$ for all experimental series listed in Table 3. Values of tangent coefficients m (slope) and b (the y-intercept of the line) are presented in Table 16.

Table 16 Values of Slope and y-Intercept of Tangents Plotted at $C/C_0 = 0.5$ for Experimental Breakthrough Curves

Experimental Set	m	b
1	0.004	-0.154
2	0.004	-0.504
3	0.002	-0.287
4	0.008	-1.164
5	0.004	-0.294
6	0.004	0.153
7	0.005	0.072

The experimental sets 2, 5, 6, and 7 have similar tangent slope values, while a distinct tendency was observed for tangent slope of experimental sets 3 and 4 (Table 16). As a consequence, it is expected a decrease in the ability of an ANN to predict breakthrough curves of sets 3 and 4, because the domain of the training data do not cover the behavior of said sets. Therefore, only experimental sets 2, 5, 6, and 7 were used in the multi-input single-output study.

Four input neurons (air flow rate, inlet flow rate, phenol initial concentration, and BHAC dosage) were supplied to an Adaline neural network. Fig. 31 shows the experimental sets 2, 5, 6, and 7 and the simulation obtained with the Adaline neural network. All ANNs described the experimental data adequately.
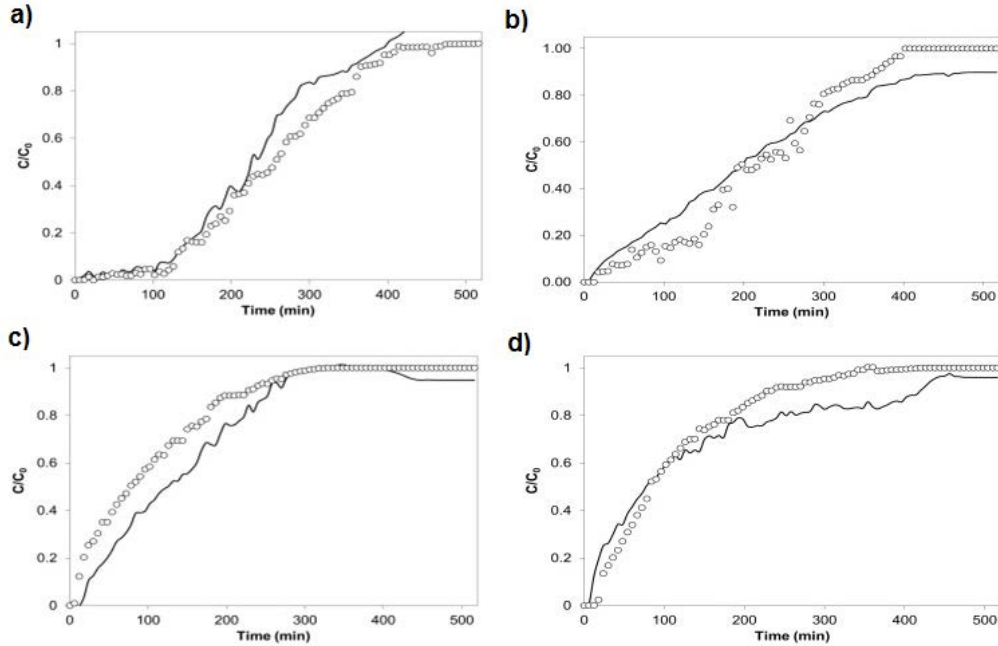
Fig. 31 Breakthrough curves of phenol onto BHAC at experimental conditions specified on Table 3. Symbols represent the experimental data and lines show the predicted results by ANN as a multi-input single-output problem for experimental sets a)2, b)5, c)6, and d)7.

In spite of the high regression coefficients obtained in the ANN simulation of experimental sets 2, 5, 6, and 7, it is expected to obtain a better correlation between experimental and simulated data using the ANN approach. For instance, input neurons can be varied to cover a wide range of values. This should yield a larger database where the effects of all inputs can be included in the developed predictive network. Besides improve the current simulations, the increase in the range of values would allow to simulate experimental set 1, which presented an extremely low regression coefficient, since the value of one of the input neurons (phenol initial concentration) was not included in the training sets. More generalizations can also be achieved upon the modification of the architecture of the ANN.

84

CHAPTER 4

4. CONCLUSIONS

Activated carbons were produced from barley husks by chemical activation with ZnCl$_2$. Like in most manufacturing processes, the production of quality activated carbon involves balancing the production conditions to get the desired characteristics of the output. The desired characteristics not only refer to the requirements of the end-users such as high surface area, but also refer to the producer side. Higher yield obtained at lower operating and energy cost is always preferred for the manufacturer. Therefore, the optimization of activated carbon production was carried out by means of the desirability function approach, a useful tool that is rarely used in activated carbon production. This study demonstrates the usefulness of a central composite design to determine the optimal conditions to improve both the surface area and yield in the production of activated carbon from BH. Dual optimization is better than single optimization because both the yield and surface area are very important parameters in manufacturing activated carbon from lignocellulosic precursors.

After the simultaneous dual optimization, the optimal conditions were obtained at 436 °C, an activation time of 20 min, and an impregnation ratio of 1.1 g ZnCl$_2$ g BH^{-1}. At these conditions, the predicted responses for the iodine number and yield were 829.58 ± 78.30 mg g^{-1} and 46.82 ± 2.64%, respectively, that are similar to the experimental

results (901.86 mg g^{-1} and 48.48% for the iodine number and yield, respectively). The BHAC produced under the optimal conditions determined by the simultaneous dual optimization showed a porous surface, with a significant fraction of the volume corresponding to micropores and mesopores, and had a surface area of 811.44 m^2 g^{-1}, which is similar to commercial activated carbons and lignocellulosic-based activated carbons. The pH$_{PZC}$ value for BHAC was 1.9, which indicates that is suitable for adsorption of negative charged species. The physicochemical characterization and iodine number of BHAC are indicatives of its potential use as a good adsorbent to remove pollutants.

Equilibrium and kinetics data for the adsorption of phenol onto BHAC were determined and these results were used to obtain the parameters of different isotherm and kinetic models. Based on the low deviation between the experimental and predicted data, Freundlich and Langmuir models were adequate to predict the experimental data, whereas both pseudo-first order and intraparticle diffusion models were capable of modeling the adsorption kinetics of phenol onto BHAC. The highest adsorption capacity of phenol onto BHAC was achieved at pH 7, and it decreased as pH value increased up to pH 11 probably due to electrostatic repulsion between phenolate and ionized groups onto BHAC. The maximum adsorption capacity of phenol onto BHAC is quite similar to those values reported for commercial and lignocellulosic-based activated carbons.

Adsorption equilibrium was reached within 40 and 200 min at pH 7, initial phenol concentration of 1000 mg L^{-1}, and at 35 °C and 30 °C, respectively. The experimental adsorption data as well as intraparticle diffusion models were used to estimate the effective diffusion coefficients, a key parameter for subsequent design calculations in adsorption processes. The obtained diffusion coefficients were lower than the diffusivities on liquid phase at ordinary temperatures, which are related to BHAC porosity and the tortuosity factor. The two linear sections in the adsorption intraparticle

diffusion model proved that the external mass transfer did not play an active role in the adsorption process, but that the adsorption is predominantly controlled by intraparticle diffusion. The efficiency of the phenol loaded BHAC regeneration was investigated. It has been demonstrated that the spent BHAC can be regenerated by 10% V/V ethanol/water solutions as eluent and this adsorbent can be used up to five adsorption/desorption cycles.

Adsorption of phenol onto BHAC from aqueous solutions was investigated at 30 °C in a continuous airlift reactor. The effects of air flow rate, initial phenol concentration, BHAC dosage, and influent flow rate on the breakthrough characteristics were investigated. Phenol initial concentration affected the breakthrough time of the reactor. With an increasing phenol initial concentration, the breakthrough time decreased. Artificial neural network predicts the experimental data adequately. The optimal neural network structure for single-input single-output problem consists of 1 input neuron, 2 neurons in the hidden layer, and 1 output neuron, while for multi-input single-output problem consists of an Adaline network trained with sequence of inputs. Generalizations to improve the simulation of breakthrough curves are under further investigation by the author.

In summary, since the results show that the phenol adsorption capacity of BHAC is comparable to other adsorbents, it can also be concluded that it can be considered as a low-cost alternative to commercial activated carbons for the phenolic wastewater treatment.

4.1 Future Work

This work presented the modeling of batch and continuous adsorption of phenol onto BHAC at a specific range of experimental conditions. The obtained results have

led to a number of open questions that should be answered to allow a better understanding of the phenol adsorption process. The following paragraphs briefly discuss the recommended future investigations.

It was discussed in Section 3.6 that there was not a plateau in the adsorption isotherms of phenol onto BHAC and CAC in the studied range. Therefore, phenol initial concentration needs to be increased in equilibrium experiments to determine if the absence of the plateau is due to a multi-layer phenol adsorption onto BHAC and CAC or if the experiments were conducted in the linear region of the Langmuir isotherm. These experiments will lead either to a single or multiple plateau isotherms, evidence of single or multilayer adsorption, respectively. The calculation of the equivalent surface monolayer could also help to elucidate the mechanism of adsorption of phenol onto BHAC and CAC.

As stated in Sections 3.7.1 and 3.7.2, few previous studies have reported satisfactory fitting of kinetics experimental data with pseudo-first order model and interception with the origin in the intraparticle diffusion models. This behavior is due to the decreasing of external mass transfer resistance when working with a rotating-basket reactor at stirring speed higher than 400 min^{-1}. Batch kinetic experiments in airlift reactor and an impeller-mixed suspension would be useful to study the effect of reactor configuration in the external mass transfer resistance in adsorption processes.

It is shown in Fig. 25 that phenol adsorption onto ethanol-regenerated BHAC is higher than the expected adsorption capacity derived from the calculated desorption capacity. This leads to the possibility of either multilayer adsorption of phenol onto BHAC or the ethanol acting as a binding site for phenol adsorption. Pretreatment of BHAC with ethanol solutions can be conducted to determine the effect of eluent in adsorption capacity.

4.2 List of Publications and Attendance at Conferences

- Loredo-Cancino, M., E. Soto-Regalado, F. J. Cerino-Córdova, R. B. García-Reyes, A. M. García-León, and M. T. Garza-González, **Determining Optimal Conditions to Produce Activated Carbon from Barley Husks Using Single or Dual Optimization**. J. Environ. Manage., 125 (2013) 117–125.

- **Looking for Optimal Conditions to Manufacture Activated Carbon from Barley Husk by Single- or Dual-Optimization**, Poster presentation, AIChE Annual Meeting, Pittsburgh, PA, USA, October 31, 2012.

- **Determinación de las Condiciones Óptimas de Producción de Carbón Activado de Cascarilla de Cebada Mediante Optimización Individual o Simultánea**, Congreso Internacional de Química e Ingeniería Verde, Poster presentation, Monterrey, NL, México, October 25, 2012.

- **Barley Husks: A Precursor of Activated Carbon and its Application for Phenol Removal from Aqueous Solutions**, Oral Presentation, XXII International Materials Research Congress, Cancún, QR, México, August 2013.

REFERENCES

1. Efremenko, I., Sheintuch, M., *Predicting solute adsorption on activated carbon: Phenol.* Langmuir, 2006. **22**: p. 3614-3621.
2. Krasil'nikova, O., N. Kazbanov,V. Gur'yanov, *Effect of temperature on adsorption of phenol on microporous activated FAS-type carbons.* Prot. Met. 2009. **45**(5): p. 518-524.
3. László, K., *Adsorption from aqueous phenol and 2,3,4-trichlorophenol solutions on nanoporous carbon prepared from poly(ethylene terephthalate)*, in *Adsorption and Nanostructure*, I. Dékány, Editor. 2002, Springer Berlin / Heidelberg. p. 5-12.
4. Green, D.W., R.H. Perry, *Perry's Chemical Engineers' Handbook (8th Edition).* 2008, McGraw-Hill. p. 43,76.
5. Busca, G., Berardinelli, S., Resini, C., Arrighi, L., *Technologies for the removal of phenol from fluid streams: A short review of recent developments.* J. Hazard. Mat. 2008. **160**(2-3): p. 265-288.
6. Bruce, R.M., Santodonato, J., Neal, M. W., *Summary review of the health effects associated with phenol.* Toxicol. Ind. Health, 1987. **3**(4): p. 535-568.
7. Saha, N.C., Bhunia, F., Kaviraj, A., *Toxicity of Phenol to Fish and Aquatic Ecosystems.* Bull. Environ. Contam. Toxicol. 1999. **63**(2): p. 195-202.
8. Dong, Y., Wang, G., Jiang, P., Zhang, A., Yue, L., Zhang, X., *Catalytic ozonation of phenol in aqueous solution by Co_3O_4 nanoparticles.* Bull. Korean Chem. Soc. 2010. **31**(10): p. 2830 - 2834.
9. Annadurai, G., Lee, J. F., *Application of artificial neural network model for the development of optimized complex medium for phenol degradation using Pseudomonas pictorum (NICM 2074).* Biodegradation, 2007. **18**(3): p. 383-392.
10. Annadurai, G., Rajesh Babu, S., Mahesh, K. P. O., Murugesan, T., *Adsorption and bio-degradation of phenol by chitosan-immobilized Pseudomonas putida (NICM 2174).* Bioprocess Biosyst. Eng. 2000. **22**(6): p. 493-501.
11. Chen, Y.X., Liu, H., Chen, H. L., *Characterization of phenol biodegradation by Comamonas testosteroni ZD4-1 and Pseudomonas aeruginosa ZD4-3.* Biomed. Environ. Sci. 2003(16): p. 163-172.
12. Mollaei, M., S. Abdollahpour, S. Atashgahi, H. Abbasi, F. Masoomi, I. Rad, A.S. Lotfi, H.S. Zahiri, H. Vali,K.A. Noghabi, *Enhanced phenol degradation by Pseudomonas sp. SA01: Gaining insight into the novel single and hybrid immobilizations.* J. Hazard. Mat. 2010. **175**(1–3): p. 284-292.
13. Jiang, Y., X. Cai, D. Wu,N. Ren, *Biodegradation of phenol and m-cresol by mutated Candida tropicalis.* J. Environ. Sci. 2010. **22**(4): p. 621-626.
14. Galíndez-Mayer, J., J. Ramón-Gallegos, N. Ruiz-Ordaz, C. Juárez-Ramírez, A. Salmerón-Alcocer, H.M. Poggi-Varaldo, *Phenol and 4-chlorophenol biodegradation by yeast Candida tropicalis in a fluidized bed reactor.* Biochem. Eng. J. 2008. **38**: p. 147–157.
15. Molva, M., *Removal of phenol from industrial wastewaters using lignitic coals*, in *Environmental Engineering.* 2004, Izmir Institute of Technology: Izmir, Turquía. p. 90.
16. Radushev, A., A. Plotnikov,V. Tyryshkina, *Regeneration methods of decontamination of phenol-containing waste waters.* Theor. Found. Chem. Eng. 2008. **42**(5): p. 781-794.

17. Alhamed, Y.A., *Adsorption kinetics and performance of packed bed adsorber for phenol removal using activated carbon from dates' stones.* J. Hazard. Mat. 2009. **170**(2-3): p. 763-770.

18. Khenniche, L.,F. Benissad-Aissani, *Adsorptive Removal of Phenol by Coffee Residue Activated Carbon and Commercial Activated Carbon: Equilibrium, Kinetics, and Thermodynamics.* J. Chem. Eng. Data, 2010. **55**(11): p. 4677-4686.

19. Mohanty, K., M. Jha, B.C. Meikap,M.N. Biswas, *Preparation and Characterization of Activated Carbons from Terminalia Arjuna Nut with Zinc Chloride Activation for the Removal of Phenol from Wastewater.* Ind. Eng. Chem. Res. 2005. **44**(11): p. 4128-4138.

20. Mohanty, K., D. Das,M. Biswas, *Preparation and characterization of activated carbons from Sterculia alata nutshell by chemical activation with zinc chloride to remove phenol from wastewater.* Adsorption, 2006. **12**(2): p. 119-132.

21. Nieto-Delgado, C.,J.R. Rangel-Mendez, *Production of activated carbon from organic by-products from the alcoholic beverage industry: Surface area and hardness optimization by using the response surface methodology.* Ind. Crops Prod. 2011. **34**(3): p. 1528-1537.

22. Yang, J., Qiu, K., *Experimental Design To Optimize the Preparation of Activated Carbons from Herb Residues by Vacuum and Traditional $ZnCl_2$ Chemical Activation.* Ind. Eng. Chem. Res. 2011. **50**(7): p. 4057-4064.

23. Sahu, J.N., J. Acharya,B.C. Meikap, *Optimization of production conditions for activated carbons from Tamarind wood by zinc chloride using response surface methodology.* Biores. Technol. 2010. **101**(6): p. 1974-1982.

24. Namasivayam, C., D. Sangeetha, *Recycling of agricultural solid waste, coir pith: Removal of anions, heavy metals, organics and dyes from water by adsorption onto $ZnCl_2$ activated coir pith carbon.* J. Hazard. Mat. 2006. **B**(135): p. 449 - 452.

25. Timur, S., E. Ikizoglu,J. Yanik, *Preparation of Activated Carbons from Oreganum Stalks by Chemical Activation.* Energy Fuels, 2006. **20**(6): p. 2636-2641.

26. Lua, A.C.,T. Yang, *Characteristics of activated carbon prepared from pistachio-nut shell by zinc chloride activation under nitrogen and vacuum conditions.* J. Colloid Interface Sci. 2005. **290**(2): p. 505-513.

27. Leng, C.-C.,N.G. Pinto, *An Investigation of the Mechanisms of Chemical Regeneration of Activated Carbon.* Ind. Eng. Chem. Res. 1996. **35**(6): p. 2024-2031.

28. Cooney, D.O., *Adsorption design for wastewater tratment.* 1998: Lewis Publishers. 27 - 36.

29. Ruthven, D., *Fundamentals of Adsorption Equilibrium and Kinetics in Microporous Solids*, in *Adsorption and Diffusion*, H. Karge and J. Weitkamp, Editors. 2008, Springer Berlin / Heidelberg. p. 1-43.

30. Erbil, H.Y., *Solid Surfaces*, in *Surface Chemistry*. 2009, Blackwell Publishing Ltd. p. 277-307.

31. Ruthven, D.M., *Principles of adsorption and adsorption processes.* 1984: Wiley - Interscience 29 - 30.

32. Leyva Ramos, R., *Importancia y aplicaciones de la adsorción en fase líquida*, in *Sólidos porosos. Preparación, caracterización y aplicaciones.*, J.C.M. Piraján, Editor. 2007, Ediciones Uniandes: Bogotá, Colombia. p. 155 - 211.

33. Sing, K.S.W., Everett, D. H., Haul, R. A. W., Moscou, L., Pierotti, R. A., Rouquerol, J., Siemieniewska, T., *Reporting physisorption data for gas/solid*

systems with special reference to the determination of surface area and porosity. Pure Appl. Chem. 1985. **57**(4): p. 603 - 619.

34. Mohamed, A.R., M. Mohammadi,G.N. Darzi, *Preparation of carbon molecular sieve from lignocellulosic biomass: A review.* Renew. Sust. Energ. Rev. 2010. **14**(6): p. 1591-1599.

35. Yang, R.T., *Adsorbents: Fundamentals and applications*, ed. J.W. Sons. 2003, Hoboken, New Jersey: John Wiley & Sons. 79-130.

36. Timur, S., I.C. Kantarli, S. Onenc,J. Yanik, *Characterization and application of activated carbon produced from oak cups pulp.* J. Anal. Appl. Pyrol. 2010. **89**(1): p. 129-136.

37. Cerino-Córdova, F.J., García-León, A.M., García-Reyes, R.B., Garza-González, M.T., Soto-Regalado, E., Sánchez-González, M.N., Quezada-López, I., *Response surface methodology for lead biosorption on Aspergillus terreus.* Int. J. Environ. Sci. Tech., 2011. **8**(4): p. 695-704.

38. Guijarro-Aldaco, A., V. Hernández-Montoya, A. Bonilla-Petriciolet, M.A. Montes-Morán,D.I. Mendoza-Castillo, *Improving the Adsorption of Heavy Metals from Water Using Commercial Carbons Modified with Egg Shell Wastes.* Ind. Eng. Chem. Res. 2011. **50**(15): p. 9354-9362.

39. Hernández-Montoya, V., L.A. Ramírez-Montoya, A. Bonilla-Petriciolet,M.A. Montes-Morán, *Optimizing the removal of fluoride from water using new carbons obtained by modification of nut shell with a calcium solution from egg shell.* Biochem. Eng. J. 2012. **62**(0): p. 1-7.

40. Shawabkeh, R., Abu-Nameh, E., *Absorption of phenol and methylene blue by activated carbon from pecan shells.* Colloid J. 2007. **69**(3): p. 355-359.

41. Kennedy, L.J., J.J. Vijaya, K. Kayalvizhi,G. Sekaran, *Adsorption of phenol from aqueous solutions using mesoporous carbon prepared by two-stage process.* Chem. Eng. J., 2007. **132**(1-3): p. 279-287.

42. Srihari, V.,A. Das, *The kinetic and thermodynamic studies of phenol-sorption onto three agro-based carbons.* Desalination, 2008. **225**(1-3): p. 220-234.

43. Nabais, J.M.V., Gomes, J.A., Suhas, Carrott, P.J.M., Laginhas, C.,Roman, S., *Phenol removal onto novel activated carbons made from lignocellulosic precursors: Influence of surface properties.* J. Hazard. Mat. 2009. **167**: p. 904-910.

44. Altenor, S., Carene, B., Emmanuel, E., Lambert, J., Ehrhardt, J. J., Gaspard, S., *Adsorption studies of methylene blue and phenol onto vetiver roots activated carbon prepared by chemical activation.* J. Hazard. Mat. 2009. **165**(1-3): p. 1029-1039.

45. Rodríguez Arana, J.M.R., Reyes Mazzoco, R., *Adsorption studies of methylene blue and phenol onto black stone cherries prepared by chemical activation.* J. Hazard. Mat. 2010. **180**: p. 656-661.

46. El-Naas, M.H., Al-Zuhair, S., Alhaija, M. A., *Removal of phenol from petroleum refinery wastewater through adsorption on date-pit activated carbon.* Chem. Eng. J. 2010. **162**(3): p. 997-1005.

47. Kilduff, J.E.,C.J. King, *Effect of Carbon Adsorbent Surface Properties on the Uptake and Solvent Regeneration of Phenol.* Ind. Eng. Chem. Res. 1997. **36**(5): p. 1603-1613.

48. Lorenc-Grabowska, E., Gryglewicz, G., Machnikowski, J., *p-Chlorophenol adsorption on activated carbons with basic surface properties.* Appl. Surf. Sci. 2010. **256**(14): p. 4480-4487.

49. Langmuir, I., *The adsorption of gases on plane surfaces of glass, mica and platinum.* J. Am. Chem. Soc. 1918. **40**(9): p. 1361-1403.

50. Krishna, R., *A unified approach to the modelling of intraparticle diffusion in adsorption processes.* Gas Sep. Purif. 1993. **7**(2): p. 91-104.
51. Lagergren, S.Y., *Zur Theorie der sogenannten Adsorption gelöster Stoffe.* 1898.
52. Ho, Y.S.,G. McKay, *The sorption of lead(II) ions on peat.* Water Res. 1999. **33**(2): p. 578-584.
53. Crank, J., *The Mathematics Diffusion.* 1979: Oxford University Press, Incorporated.
54. Vermeulen, T., *Theory for Irreversible and Constant-Pattern Solid Diffusion.* Ind. Eng. Chem. 1953. **45**(8): p. 1664-1670.
55. Weber, W.J., Morris, J.C., *Kinetics of adsorption on carbon from solution.* J. Sanitary Eng. Div. 1963. **89**(2): p. 31-60.
56. Mohanty, K., Das, D., Biswas, M. N. , *Treatment of phenolic wastewater in a novel multi-stage external loop airlift reactor using activated carbon.* Sep. Purif. Technol. 2008. **58**(3): p. 311-319.
57. Filipkowska, U., *Efficiency of Black DN Adsorption onto Chitin in an Air-Lift Reactor.* Polish J. Environ. Studies, 2004. **13**(5): p. 503-508.
58. Filipkowska, U., Waraksa, K. , *Adsorption of reactive dye on chitosan in air-lift reactor.* Adsorption, 2008. **14**(6): p. 815-821.
59. Mohammed, F.M., E.P.L. Roberts, A. Hill, A.K. Campen,N.W. Brown, *Continuous water treatment by adsorption and electrochemical regeneration.* Water Res. 2011. **45**(10): p. 3065-3074.
60. Himmelblau, D.M., *Accounts of Experiences in the Application of Artificial Neural Networks in Chemical Engineering.* Ind. Eng. Chem. Res. 2008. **47**(16): p. 5782-5796.
61. SIAP, *Anuario Estadístico de la Producción agrícola.* 2012, SIAP (Servicio de Información Agroalimentaria y Pesquera).
62. COFUPRO, *Identificación de las Demandas Tecnológicas de la Cadena Agroalimentria de Cebada*, A.C. Coordinadora Nacional de las Fundaciones Produce, Editor. 2002, Coordinadora Nacional de las Fundaciones Produce, A.C.
63. Palmarola-Adrados, B., Galbe, M., Zacchi, G., *Pretreatment of barley husk for bioethanol production.* J. Chem. Technol. Biotechnol. 2005. **80**: p. 85 - 91.
64. Krawczyk, H., Persson, T., Andersson, A., Jönsson, A.-S., *Isolation of hemicelluloses from barley husks.* Food Bioprod. Process, 2008. **86**(1): p. 31-36.
65. ASTM, *D3172 Standard Practice for Proximate Analysis of Coal and Coke.* 2007, ASTM: West Conshohocken, PA.
66. ASTM, *Standard Test Method for Determination of Iodine Number of Activated Carbon.* 2011, American Society for Testing and Materials.
67. Noh, J.S., Schwarz, J. A., *Estimation of the point of zero charge of simple oxides by mass titration.* J. Colloid Interface Sci., 1989. **130**(1): p. 157 - 164.
68. Al-Degs, Y., M.A.M. Khraisheh, S.J. Allen,M.N. Ahmad, *Effect of carbon surface chemistry on the removal of reactive dyes from textile effluent.* Water Res. 2000. **34**(3): p. 927-935.
69. Montgomery, D.C., *Diseño y análisis de experimentos.* 2nd ed. 2010, México, D.F.: Limusa Wiley. 686.
70. Kim, K.J., Lin, D. K. J., *Simultaneous optimization of mechanical properties of steel by maximizing exponential desirability functions.* Appl. Stat. 2000. **49**(3): p. 311 - 325.
71. StatEase, *Design Expert 7 User's Guide.* 2005.

72.   Dávila-Guzmán, N.E., F. de Jesús Cerino-Córdova, E. Soto-Regalado, J.R. Rangel-Mendez, P.E. Díaz-Flores, M.T. Garza-Gonzalez,J.A. Loredo-Medrano, *Copper Biosorption by Spent Coffee Ground: Equilibrium, Kinetics, and Mechanism.* CLEAN – Soil, Air, Water, 2013.

73.   Garcia-Reyes, R.B., Rangel-Mendez, J.R., *Adsorption kinetics of chromium(III) ions on agro-waste materials.* Biores. Technol. 2010. **101**: p. 8099-8108.

74.   Robinson, J.P., S. W. Kingman, R. Barranco, C. E. Snape, and H. Al-Sayegh, *Microwave Pyrolysis of Wood Pellets.* Ind. Eng. Chem. Res. 2010. **49**: p. 459-463.

75.   Mahvi, A.H., Maleki, A., Eslami, A., *Potential of rice husk and rice husk ash for phenol removal in aqueous systems.* Am. J. Appl. Sci. 2004. **1**(4): p. 321 - 326.

76.   Sricharoenchaikul, V., Chiravoot Pechyen, Duangdao Aht-ong, and Duangduen Atong, *Preparation and Characterization of Activated Carbon from the Pyrolysis of Physic Nut (Jatropha curcas L.) Waste.* Energy Fuels, 2008. **22**: p. 31-37.

77.   Duman, G., Y. Onal, C. Okutucu, S. Onenc,J. Yanik, *Production of Activated Carbon from Pine Cone and Evaluation of Its Physical, Chemical, and Adsorption Properties.* Energy Fuels, 2009. **23**(4): p. 2197-2204.

78.   Yang, T.,A.C. Lua, *Textural and chemical properties of zinc chloride activated carbons prepared from pistachio-nut shells.* Mater. Chem. Phys. 2006. **100**(2-3): p. 438-444.

79.   Demiral, H.,G. Gündüzoğlu, *Removal of nitrate from aqueous solutions by activated carbon prepared from sugar beet bagasse.* Biores. Technol. 2010. **101**(6): p. 1675-1680.

80.   Temdrara, L., A. Khelifi, A. Addoun,N. Spahis, *Study of the adsorption properties of lignocellulosic material activated chemically by gas adsorption and immersion calorimetry.* Desalination, 2008. **223**(1-3): p. 274-282.

81.   Loredo-Cancino, M., Soto-Regalado, E., Cerino-Córdova, F. J., García-Reyes, R. B., García-León, A. M., Garza-González, M. T., *Determining Optimal Conditions to Produce Activated Carbon from Barley Husk using Single or Dual Optimization.* J. Environ. Manage. 2013. **125:** p. 117–125

82.   Pelekani, C., V.L. Snoeyink, *Competitive adsorption between atrazine and methylene blue on activated carbon: the importance of pore size distribution.* Carbon, 2000. **38**: p. 1423-1436.

83.   Kasaoka, S., Y. Sakata, E. Tanaka, R. Naitoh, *Design of molecular-sieve carbon. Studies on the adsorption of various dyes in the liquid phase.* Int. Chem. Eng. 1989. **29**: p. 734-742.

84.   Snoeyink, V.L., Weber, W. J., *The surface chemistry of active carbon: A discussion of structure and surface functional groups.* Environ. Sci. Technol. 1967. **1**(3): p. 228 - 234.

85.   Boudrahem, F., A. Soualah,F. Aissani-Benissad, *Pb(II) and Cd(II) Removal from Aqueous Solutions Using Activated Carbon Developed from Coffee Residue Activated with Phosphoric Acid and Zinc Chloride.* J. Chem. Eng. Data, 2011. **56**(5): p. 1946-1955.

86.   Snoeyink, V.L., Weber, W.J., Mark, H.B., *Sorption of Phenol and Nitrophenol by Active Carbon.* Environ. Sci. Technol. 1969. **3**(10): p. 918-92.

87.   Morrison, R.T., Boyd, R.N., *Química orgánica.* First ed. 1998, Naucalpan de Juarez, Edo. de México: Addison Wesley Longman de México, S. A. de C. V.

88.   Mattson, J.S., Mark, H.B., Malbin, M.D., Weber, W.J., Crittenden, J.C., *Surface chemistry of active carbon: specific adsorption of phenols.* J. Colloid Interface Sci. 1969. **31**(1): p. 116-130.

89. Rudzinski, W., Plazinski, W., *Studies of the Kinetics of Solute Adsorption at Solid/Solution Interfaces: On the Possibility of Distinguishing between the Diffusional and the Surface Reaction Kinetic Models by Studying the Pseudo-First-order Kinetics.* J. Phys. Chem. 2007. **111**(41): p. 15100-15110.

90. Coughlin, R.W., F.S. Ezra, *Role of surface acidity in the adsorption of organic pollutants on the surface of carbon.* Environ. Sci. Technol. 1968. **2**(4): p. 291-297.

91. Arafat, H.A., M. Franz, N.G. Pinto, *Effect of salt on the mechanism of adsorption of aromatics on activated carbon.* Langmuir **15**(18) Third international symposium on effects of surface heterogeneity in adsorption and catalysis on solids, Torun (PL), 08/09/1998--08/16/1998.

92. Mahajan, O.P., C. Moreno-castilla, P.L. Walker, *Surface-Treated Activated Carbon for Removal of Phenol from Water.* Sep. Sci. Technol. 1980. **15**(10): p. 1733-1752.

93. Müller, E.A., K.E. Gubbins, *Molecular simulation study of hydrophilic and hydrophobic behavior of activated carbon surfaces.* Carbon, 1998. **36**(10): p. 1433-1438.

94. Franz, M., H.A. Arafat, N.G. Pinto, *Effect of chemical surface heterogeneity on the adsorption mechanism of dissolved aromatics on activated carbon.* Carbon, 2000. **38**(13): p. 1807-1819.

95. Chang, M.-Y., R.-S. Juang, *Adsorption of tannic acid, humic acid, and dyes from water using the composite of chitosan and activated clay.* J. Colloid Interface Sci., 2004. **278**(1): p. 18-25.

96. Bhattacharyya, K.G., A. Sharma, *Kinetics and thermodynamics of Methylene Blue adsorption on Neem (Azadirachta indica) leaf powder.* Dyes Pigm. 2005. **65**(1): p. 51-59.

97. Mohd Din, A.T., Hameed, B.H., Ahmad, A.L., *Batch adsorption of phenol onto physiochemical-activated coconut shell.* J. Hazard. Mat., 2009. **161**: p. 1522-1529.

98. Hameed, B.H., Chin, L. H., Rengaraj, S., *Adsorption of 4-chlorophenol onto activated carbon prepared from rattan sawdust.* Desalination, 2008. **225**(1-3): p. 185-198.

99. Qiu, H., L. Lv, B.-c. Pan, Q.-j. Zhang, W.-m. Zhang, Q.-x. Zhang, *Critical review in adsorption kinetic models.* J. Zhejiang University Sci. A, 2009. **10**(5): p. 716-724.

100. Cheung, W.H., Y.S. Szeto, G. McKay, *Intraparticle diffusion processes during acid dye adsorption onto chitosan.* Biores. Technol. 2007. **98**(15): p. 2897-2904.

101. Liu, Q.-S., T. Zheng, P. Wang, J.-P. Jiang,N. Li, *Adsorption isotherm, kinetic and mechanism studies of some substituted phenols on activated carbon fibers.* Chem. Eng. J., 2010. **157**(2–3): p. 348-356.

102. Crittenden, J.C., R.R. Trussell, D.W. Hand, K.J. Howe,G. Tchobanoglous, *Adsorption*, in *MWH's Water Treatment.* 2012, John Wiley & Sons, Inc. p. 1117-1262.

103. EPA, *Toxicological review of phenol.* 2002: Washington DC.

104. Cooney, D.O., *The importance of axial dispersion in liquid-phase fixed-bed adsorption operations.* Chem. Eng. Commun., 1991. **110**: p. 217-231.

APPENDIX A

The mass titration method proposed by Noh and Schwarz [67] is a suitable tool in determination the point of zero charge (pH_{PZC}) of materials. It was originally developed for pure metal oxides and later extended so that it can be used also for activated carbon. Results of the acid-base titrations experiments (Fig. A1) were used to determine the pH_{PZC} (Fig. A2).
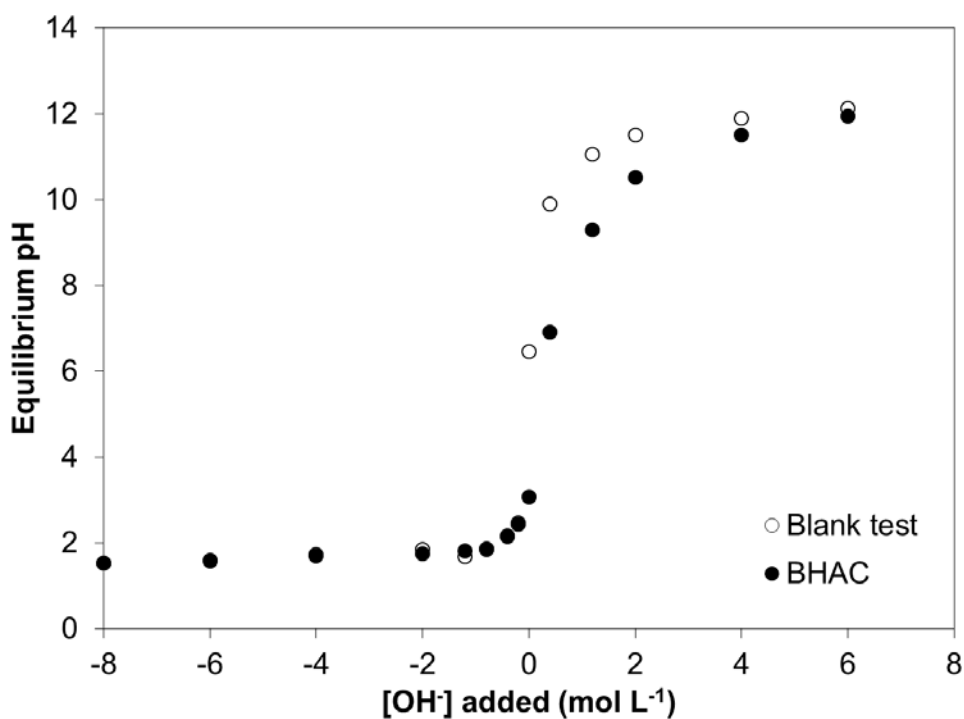
Fig. A1 Potentiometric titrations of BHAC.
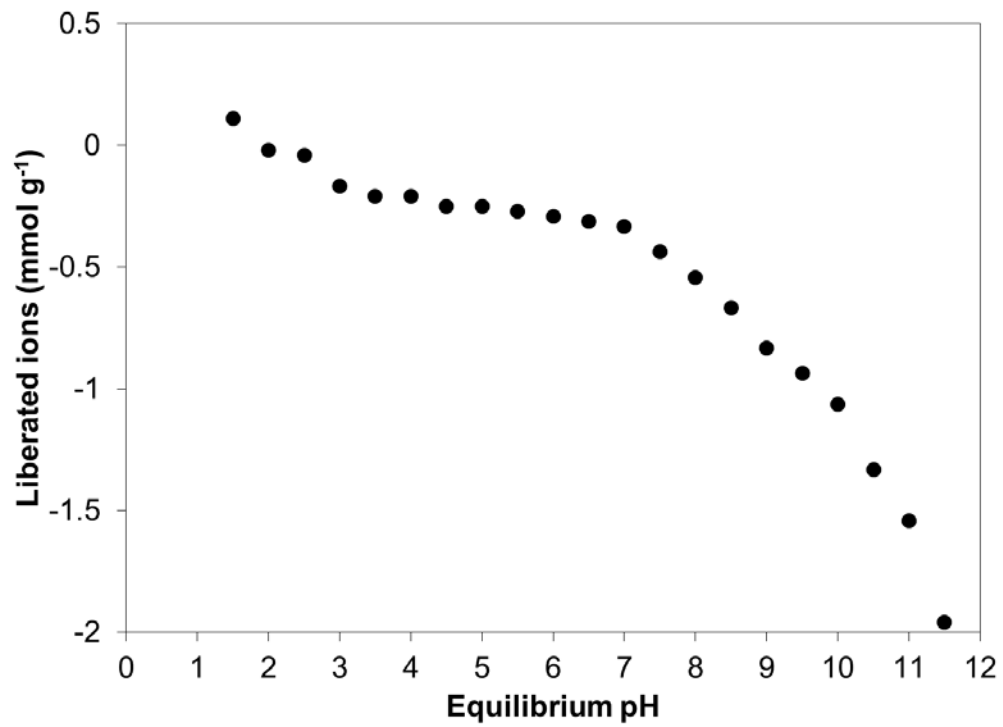
Fig A2 pH in the point of zero charge (pH$_{PZC}$) of BHAC.

APPENDIX B

The values tested for the input variables (BHAC dosage, phenol initial concentration, air flow rate, and influent flow rate) of the multi-input single-output problem are summarized in Table B1. For each set, the output is the variation of effluent phenol concentration with the running time (the breakthrough curve).

Set	BHAC dosage (g L^{-1})	C_0 phenol (mg L^{-1})	Air flow rate (L min^{-1})	Influent flow rate (L h^{-1})	Time (min)	C/C_0
1	5	250	10	2	0	0.03
1	5	250	10	2	6	0.03
1	5	250	10	2	12	0.05
1	5	250	10	2	18	0.05
1	5	250	10	2	24	0.06
1	5	250	10	2	30	0.09
1	5	250	10	2	36	0.10
1	5	250	10	2	42	0.10
1	5	250	10	2	48	0.12
1	5	250	10	2	54	0.09
1	5	250	10	2	60	0.13
1	5	250	10	2	66	0.16
1	5	250	10	2	72	0.16
1	5	250	10	2	78	0.19
1	5	250	10	2	84	0.20
1	5	250	10	2	90	0.18
1	5	250	10	2	96	0.24
1	5	250	10	2	102	0.22
1	5	250	10	2	108	0.30
1	5	250	10	2	114	0.32
1	5	250	10	2	120	0.35
1	5	250	10	2	126	0.38
1	5	250	10	2	132	0.42
1	5	250	10	2	138	0.42
1	5	250	10	2	144	0.44
1	5	250	10	2	150	0.47
1	5	250	10	2	156	0.50
1	5	250	10	2	162	0.53
1	5	250	10	2	168	0.53
1	5	250	10	2	174	0.55
1	5	250	10	2	180	0.58
1	5	250	10	2	186	0.58
1	5	250	10	2	192	0.66
1	5	250	10	2	198	0.67
1	5	250	10	2	204	0.69

1	5	250	10	2	210	0.70
1	5	250	10	2	216	0.72
1	5	250	10	2	222	0.76
1	5	250	10	2	228	0.81
1	5	250	10	2	234	0.83
1	5	250	10	2	240	0.85
1	5	250	10	2	246	0.86
1	5	250	10	2	252	0.88
1	5	250	10	2	258	0.89
1	5	250	10	2	264	0.89
1	5	250	10	2	270	0.90
1	5	250	10	2	276	0.92
1	5	250	10	2	282	0.94
1	5	250	10	2	288	0.96
1	5	250	10	2	294	0.98
1	5	250	10	2	300	0.99
1	5	250	10	2	306	0.94
1	5	250	10	2	312	0.98
1	5	250	10	2	318	0.99
1	5	250	10	2	324	1.00
1	5	250	10	2	330	1.00
1	5	250	10	2	336	1.00
1	5	250	10	2	342	1.00
1	5	250	10	2	348	1.00
1	5	250	10	2	354	1.00
1	5	250	10	2	360	1.00
1	5	250	10	2	366	1.00
1	5	250	10	2	372	1.00
1	5	250	10	2	378	1.00
1	5	250	10	2	384	1.00
1	5	250	10	2	390	1.00
1	5	250	10	2	396	1.00
1	5	250	10	2	402	1.00
1	5	250	10	2	408	1.00
1	5	250	10	2	414	1.00
1	5	250	10	2	420	1.00
1	5	250	10	2	426	1.00
1	5	250	10	2	432	1.00
1	5	250	10	2	438	1.00
1	5	250	10	2	444	1.00
1	5	250	10	2	450	1.00
1	5	250	10	2	456	1.00
1	5	250	10	2	462	1.00
1	5	250	10	2	468	1.00
1	5	250	10	2	474	1.00
1	5	250	10	2	480	1.00
1	5	250	10	2	486	1.00
1	5	250	10	2	492	1.00
1	5	250	10	2	498	1.00
1	5	250	10	2	504	1.00
1	5	250	10	2	510	1.00

1	5	250	10	2	516	1.00
2	5	40	10	2	0	0.00
2	5	40	10	2	6	0.00
2	5	40	10	2	12	0.00
2	5	40	10	2	18	0.01
2	5	40	10	2	24	0.00
2	5	40	10	2	30	0.01
2	5	40	10	2	36	0.01
2	5	40	10	2	42	0.02
2	5	40	10	2	48	0.03
2	5	40	10	2	54	0.02
2	5	40	10	2	60	0.03
2	5	40	10	2	66	0.02
2	5	40	10	2	72	0.02
2	5	40	10	2	78	0.03
2	5	40	10	2	84	0.03
2	5	40	10	2	90	0.05
2	5	40	10	2	96	0.05
2	5	40	10	2	102	0.02
2	5	40	10	2	108	0.04
2	5	40	10	2	114	0.03
2	5	40	10	2	120	0.04
2	5	40	10	2	126	0.06
2	5	40	10	2	132	0.12
2	5	40	10	2	138	0.13
2	5	40	10	2	144	0.17
2	5	40	10	2	150	0.16
2	5	40	10	2	156	0.16
2	5	40	10	2	162	0.16
2	5	40	10	2	168	0.19
2	5	40	10	2	174	0.23
2	5	40	10	2	180	0.24
2	5	40	10	2	186	0.27
2	5	40	10	2	192	0.25
2	5	40	10	2	198	0.29
2	5	40	10	2	204	0.36
2	5	40	10	2	210	0.36
2	5	40	10	2	216	0.37
2	5	40	10	2	222	0.41
2	5	40	10	2	228	0.44
2	5	40	10	2	234	0.45
2	5	40	10	2	240	0.45
2	5	40	10	2	246	0.45
2	5	40	10	2	252	0.48
2	5	40	10	2	258	0.51
2	5	40	10	2	264	0.54
2	5	40	10	2	270	0.58
2	5	40	10	2	276	0.61
2	5	40	10	2	282	0.61
2	5	40	10	2	288	0.62
2	5	40	10	2	294	0.65

2	5	40	10	2	300	0.69
2	5	40	10	2	306	0.69
2	5	40	10	2	312	0.71
2	5	40	10	2	318	0.73
2	5	40	10	2	324	0.75
2	5	40	10	2	330	0.76
2	5	40	10	2	336	0.77
2	5	40	10	2	342	0.79
2	5	40	10	2	348	0.79
2	5	40	10	2	354	0.79
2	5	40	10	2	360	0.86
2	5	40	10	2	366	0.90
2	5	40	10	2	372	0.91
2	5	40	10	2	378	0.91
2	5	40	10	2	384	0.91
2	5	40	10	2	390	0.92
2	5	40	10	2	396	0.95
2	5	40	10	2	402	0.95
2	5	40	10	2	408	0.96
2	5	40	10	2	414	0.99
2	5	40	10	2	420	0.98
2	5	40	10	2	426	0.98
2	5	40	10	2	432	0.98
2	5	40	10	2	438	0.98
2	5	40	10	2	444	0.99
2	5	40	10	2	450	0.99
2	5	40	10	2	456	0.96
2	5	40	10	2	462	0.99
2	5	40	10	2	468	0.99
2	5	40	10	2	474	1.00
2	5	40	10	2	480	1.00
2	5	40	10	2	486	1.00
2	5	40	10	2	492	1.00
2	5	40	10	2	498	1.00
2	5	40	10	2	504	1.00
2	5	40	10	2	510	1.00
2	5	40	10	2	516	1.00
3	5	40	1	2	0	0.00
3	5	40	1	2	6	0.00
3	5	40	1	2	12	0.00
3	5	40	1	2	18	0.00
3	5	40	1	2	24	0.00
3	5	40	1	2	30	0.00
3	5	40	1	2	36	0.01
3	5	40	1	2	42	0.00
3	5	40	1	2	48	0.01
3	5	40	1	2	54	0.02
3	5	40	1	2	60	0.02
3	5	40	1	2	66	0.02
3	5	40	1	2	72	0.03
3	5	40	1	2	78	0.05

3	5	40	1	2	84	0.06
3	5	40	1	2	90	0.05
3	5	40	1	2	96	0.05
3	5	40	1	2	102	0.05
3	5	40	1	2	108	0.06
3	5	40	1	2	114	0.04
3	5	40	1	2	120	0.03
3	5	40	1	2	126	0.04
3	5	40	1	2	132	0.04
3	5	40	1	2	138	0.08
3	5	40	1	2	144	0.10
3	5	40	1	2	150	0.10
3	5	40	1	2	156	0.11
3	5	40	1	2	162	0.10
3	5	40	1	2	168	0.12
3	5	40	1	2	174	0.12
3	5	40	1	2	180	0.13
3	5	40	1	2	186	0.14
3	5	40	1	2	192	0.13
3	5	40	1	2	198	0.15
3	5	40	1	2	204	0.14
3	5	40	1	2	210	0.14
3	5	40	1	2	216	0.15
3	5	40	1	2	222	0.20
3	5	40	1	2	228	0.23
3	5	40	1	2	234	0.24
3	5	40	1	2	240	0.23
3	5	40	1	2	246	0.28
3	5	40	1	2	252	0.28
3	5	40	1	2	258	0.33
3	5	40	1	2	264	0.30
3	5	40	1	2	270	0.37
3	5	40	1	2	276	0.37
3	5	40	1	2	282	0.37
3	5	40	1	2	288	0.44
3	5	40	1	2	294	0.45
3	5	40	1	2	300	0.44
3	5	40	1	2	306	0.45
3	5	40	1	2	312	0.49
3	5	40	1	2	318	0.50
3	5	40	1	2	324	0.49
3	5	40	1	2	330	0.49
3	5	40	1	2	336	0.51
3	5	40	1	2	342	0.53
3	5	40	1	2	348	0.53
3	5	40	1	2	354	0.59
3	5	40	1	2	360	0.60
3	5	40	1	2	366	0.62
3	5	40	1	2	372	0.65
3	5	40	1	2	378	0.67
3	5	40	1	2	384	0.70

3	5	40	1	2	390	0.71
3	5	40	1	2	396	0.74
3	5	40	1	2	402	0.78
3	5	40	1	2	408	0.81
3	5	40	1	2	414	0.83
3	5	40	1	2	420	0.87
3	5	40	1	2	426	0.91
3	5	40	1	2	432	0.95
3	5	40	1	2	438	0.98
3	5	40	1	2	444	1.00
3	5	40	1	2	450	1.00
3	5	40	1	2	456	1.00
3	5	40	1	2	462	1.00
3	5	40	1	2	468	1.00
3	5	40	1	2	474	1.00
3	5	40	1	2	480	1.00
3	5	40	1	2	486	1.00
3	5	40	1	2	492	1.00
3	5	40	1	2	498	1.00
3	5	40	1	2	504	1.00
3	5	40	1	2	510	1.00
3	5	40	1	2	516	1.00
4	5	40	10	3	0	0.00
4	5	40	10	3	6	0.00
4	5	40	10	3	12	0.00
4	5	40	10	3	18	0.03
4	5	40	10	3	24	0.01
4	5	40	10	3	30	0.01
4	5	40	10	3	36	0.02
4	5	40	10	3	42	0.02
4	5	40	10	3	48	0.03
4	5	40	10	3	54	0.03
4	5	40	10	3	60	0.04
4	5	40	10	3	66	0.03
4	5	40	10	3	72	0.02
4	5	40	10	3	78	0.04
4	5	40	10	3	84	0.04
4	5	40	10	3	90	0.05
4	5	40	10	3	96	0.05
4	5	40	10	3	102	0.02
4	5	40	10	3	108	0.05
4	5	40	10	3	114	0.06
4	5	40	10	3	120	0.05
4	5	40	10	3	126	0.06
4	5	40	10	3	132	0.13
4	5	40	10	3	138	0.14
4	5	40	10	3	144	0.18
4	5	40	10	3	150	0.17
4	5	40	10	3	156	0.17
4	5	40	10	3	162	0.17
4	5	40	10	3	168	0.31

4	5	40	10	3	174	0.36
4	5	40	10	3	180	0.35
4	5	40	10	3	186	0.36
4	5	40	10	3	192	0.34
4	5	40	10	3	198	0.46
4	5	40	10	3	204	0.43
4	5	40	10	3	210	0.41
4	5	40	10	3	216	0.45
4	5	40	10	3	222	0.49
4	5	40	10	3	228	0.63
4	5	40	10	3	234	0.56
4	5	40	10	3	240	0.64
4	5	40	10	3	246	0.72
4	5	40	10	3	252	0.80
4	5	40	10	3	258	0.86
4	5	40	10	3	264	0.96
4	5	40	10	3	270	0.97
4	5	40	10	3	276	0.98
4	5	40	10	3	282	0.99
4	5	40	10	3	288	1.00
4	5	40	10	3	294	1.00
4	5	40	10	3	300	1.00
4	5	40	10	3	306	1.00
4	5	40	10	3	312	1.00
4	5	40	10	3	318	1.00
4	5	40	10	3	324	1.00
4	5	40	10	3	330	1.00
4	5	40	10	3	336	1.00
4	5	40	10	3	342	1.00
4	5	40	10	3	348	1.00
4	5	40	10	3	354	1.00
4	5	40	10	3	360	1.00
4	5	40	10	3	366	1.00
4	5	40	10	3	372	1.00
4	5	40	10	3	378	1.00
4	5	40	10	3	384	1.00
4	5	40	10	3	390	1.00
4	5	40	10	3	396	1.00
4	5	40	10	3	402	1.00
4	5	40	10	3	408	1.00
4	5	40	10	3	414	1.00
4	5	40	10	3	420	1.00
4	5	40	10	3	426	1.00
4	5	40	10	3	432	1.00
4	5	40	10	3	438	1.00
4	5	40	10	3	444	1.00
4	5	40	10	3	450	1.00
4	5	40	10	3	456	1.00
4	5	40	10	3	462	1.00
4	5	40	10	3	468	1.00
4	5	40	10	3	474	1.00

4	5	40	10	3	480	1.00
4	5	40	10	3	486	1.00
4	5	40	10	3	492	1.00
4	5	40	10	3	498	1.00
4	5	40	10	3	504	1.00
4	5	40	10	3	510	1.00
4	5	40	10	3	516	1.00
5	2	40	10	2	0	0.00
5	2	40	10	2	6	0.00
5	2	40	10	2	12	0.00
5	2	40	10	2	18	0.04
5	2	40	10	2	24	0.05
5	2	40	10	2	30	0.05
5	2	40	10	2	36	0.08
5	2	40	10	2	42	0.07
5	2	40	10	2	48	0.07
5	2	40	10	2	54	0.08
5	2	40	10	2	60	0.14
5	2	40	10	2	66	0.11
5	2	40	10	2	72	0.13
5	2	40	10	2	78	0.15
5	2	40	10	2	84	0.16
5	2	40	10	2	90	0.13
5	2	40	10	2	96	0.09
5	2	40	10	2	102	0.15
5	2	40	10	2	108	0.15
5	2	40	10	2	114	0.17
5	2	40	10	2	120	0.18
5	2	40	10	2	126	0.17
5	2	40	10	2	132	0.16
5	2	40	10	2	138	0.18
5	2	40	10	2	144	0.16
5	2	40	10	2	150	0.20
5	2	40	10	2	156	0.24
5	2	40	10	2	162	0.31
5	2	40	10	2	168	0.33
5	2	40	10	2	174	0.40
5	2	40	10	2	180	0.40
5	2	40	10	2	186	0.32
5	2	40	10	2	192	0.49
5	2	40	10	2	198	0.50
5	2	40	10	2	204	0.48
5	2	40	10	2	210	0.48
5	2	40	10	2	216	0.49
5	2	40	10	2	222	0.53
5	2	40	10	2	228	0.55
5	2	40	10	2	234	0.53
5	2	40	10	2	240	0.56
5	2	40	10	2	246	0.55
5	2	40	10	2	252	0.53
5	2	40	10	2	258	0.69

5	2	40	10	2	264	0.59
5	2	40	10	2	270	0.56
5	2	40	10	2	276	0.65
5	2	40	10	2	282	0.71
5	2	40	10	2	288	0.76
5	2	40	10	2	294	0.76
5	2	40	10	2	300	0.81
5	2	40	10	2	306	0.82
5	2	40	10	2	312	0.83
5	2	40	10	2	318	0.83
5	2	40	10	2	324	0.85
5	2	40	10	2	330	0.86
5	2	40	10	2	336	0.86
5	2	40	10	2	342	0.87
5	2	40	10	2	348	0.87
5	2	40	10	2	354	0.88
5	2	40	10	2	360	0.89
5	2	40	10	2	366	0.91
5	2	40	10	2	372	0.92
5	2	40	10	2	378	0.94
5	2	40	10	2	384	0.95
5	2	40	10	2	390	0.97
5	2	40	10	2	396	0.97
5	2	40	10	2	402	1.00
5	2	40	10	2	408	1.00
5	2	40	10	2	414	1.00
5	2	40	10	2	420	1.00
5	2	40	10	2	426	1.00
5	2	40	10	2	432	1.00
5	2	40	10	2	438	1.00
5	2	40	10	2	444	1.00
5	2	40	10	2	450	1.00
5	2	40	10	2	456	1.00
5	2	40	10	2	462	1.00
5	2	40	10	2	468	1.00
5	2	40	10	2	474	1.00
5	2	40	10	2	480	1.00
5	2	40	10	2	486	1.00
5	2	40	10	2	492	1.00
5	2	40	10	2	498	1.00
5	2	40	10	2	504	1.00
5	2	40	10	2	510	1.00
5	2	40	10	2	516	1.00
6	2	40	3	3	0	0.00
6	2	40	3	3	6	0.01
6	2	40	3	3	12	0.12
6	2	40	3	3	18	0.20
6	2	40	3	3	24	0.25
6	2	40	3	3	30	0.27
6	2	40	3	3	36	0.30
6	2	40	3	3	42	0.35

6	2	40	3	3	48	0.35
6	2	40	3	3	54	0.39
6	2	40	3	3	60	0.43
6	2	40	3	3	66	0.45
6	2	40	3	3	72	0.47
6	2	40	3	3	78	0.51
6	2	40	3	3	84	0.52
6	2	40	3	3	90	0.54
6	2	40	3	3	96	0.57
6	2	40	3	3	102	0.58
6	2	40	3	3	108	0.61
6	2	40	3	3	114	0.64
6	2	40	3	3	120	0.63
6	2	40	3	3	126	0.67
6	2	40	3	3	132	0.69
6	2	40	3	3	138	0.69
6	2	40	3	3	144	0.69
6	2	40	3	3	150	0.74
6	2	40	3	3	156	0.76
6	2	40	3	3	162	0.75
6	2	40	3	3	168	0.77
6	2	40	3	3	174	0.79
6	2	40	3	3	180	0.84
6	2	40	3	3	186	0.85
6	2	40	3	3	192	0.87
6	2	40	3	3	198	0.88
6	2	40	3	3	204	0.88
6	2	40	3	3	210	0.88
6	2	40	3	3	216	0.89
6	2	40	3	3	222	0.89
6	2	40	3	3	228	0.91
6	2	40	3	3	234	0.91
6	2	40	3	3	240	0.93
6	2	40	3	3	246	0.93
6	2	40	3	3	252	0.93
6	2	40	3	3	258	0.95
6	2	40	3	3	264	0.96
6	2	40	3	3	270	0.95
6	2	40	3	3	276	0.97
6	2	40	3	3	282	0.98
6	2	40	3	3	288	0.98
6	2	40	3	3	294	0.99
6	2	40	3	3	300	0.99
6	2	40	3	3	306	0.99
6	2	40	3	3	312	1.00
6	2	40	3	3	318	1.00
6	2	40	3	3	324	1.00
6	2	40	3	3	330	1.00
6	2	40	3	3	336	1.00
6	2	40	3	3	342	1.00
6	2	40	3	3	348	1.00

6	2	40	3	3	354	1.00
6	2	40	3	3	360	1.00
6	2	40	3	3	366	1.00
6	2	40	3	3	372	1.00
6	2	40	3	3	378	1.00
6	2	40	3	3	384	1.00
6	2	40	3	3	390	1.00
6	2	40	3	3	396	1.00
6	2	40	3	3	402	1.00
6	2	40	3	3	408	1.00
6	2	40	3	3	414	1.00
6	2	40	3	3	420	1.00
6	2	40	3	3	426	1.00
6	2	40	3	3	432	1.00
6	2	40	3	3	438	1.00
6	2	40	3	3	444	1.00
6	2	40	3	3	450	1.00
6	2	40	3	3	456	1.00
6	2	40	3	3	462	1.00
6	2	40	3	3	468	1.00
6	2	40	3	3	474	1.00
6	2	40	3	3	480	1.00
6	2	40	3	3	486	1.00
6	2	40	3	3	492	1.00
6	2	40	3	3	498	1.00
6	2	40	3	3	504	1.00
6	2	40	3	3	510	1.00
6	2	40	3	3	516	1.00
7	2	40	1	3	0	0.00
7	2	40	1	3	6	0.00
7	2	40	1	3	12	0.00
7	2	40	1	3	18	0.03
7	2	40	1	3	24	0.13
7	2	40	1	3	30	0.17
7	2	40	1	3	36	0.20
7	2	40	1	3	42	0.23
7	2	40	1	3	48	0.27
7	2	40	1	3	54	0.31
7	2	40	1	3	60	0.34
7	2	40	1	3	66	0.38
7	2	40	1	3	72	0.41
7	2	40	1	3	78	0.45
7	2	40	1	3	84	0.52
7	2	40	1	3	90	0.53
7	2	40	1	3	96	0.56
7	2	40	1	3	102	0.59
7	2	40	1	3	108	0.61
7	2	40	1	3	114	0.64
7	2	40	1	3	120	0.66
7	2	40	1	3	126	0.69
7	2	40	1	3	132	0.70

7	2	40	1	3	138	0.70
7	2	40	1	3	144	0.74
7	2	40	1	3	150	0.74
7	2	40	1	3	156	0.75
7	2	40	1	3	162	0.76
7	2	40	1	3	168	0.78
7	2	40	1	3	174	0.78
7	2	40	1	3	180	0.78
7	2	40	1	3	186	0.81
7	2	40	1	3	192	0.82
7	2	40	1	3	198	0.84
7	2	40	1	3	204	0.85
7	2	40	1	3	210	0.86
7	2	40	1	3	216	0.87
7	2	40	1	3	222	0.88
7	2	40	1	3	228	0.90
7	2	40	1	3	234	0.90
7	2	40	1	3	240	0.92
7	2	40	1	3	246	0.92
7	2	40	1	3	252	0.92
7	2	40	1	3	258	0.92
7	2	40	1	3	264	0.92
7	2	40	1	3	270	0.92
7	2	40	1	3	276	0.94
7	2	40	1	3	282	0.94
7	2	40	1	3	288	0.95
7	2	40	1	3	294	0.95
7	2	40	1	3	300	0.95
7	2	40	1	3	306	0.95
7	2	40	1	3	312	0.96
7	2	40	1	3	318	0.97
7	2	40	1	3	324	0.97
7	2	40	1	3	330	0.97
7	2	40	1	3	336	0.98
7	2	40	1	3	342	0.99
7	2	40	1	3	348	0.99
7	2	40	1	3	354	1.00
7	2	40	1	3	360	1.00
7	2	40	1	3	366	0.99
7	2	40	1	3	372	0.99
7	2	40	1	3	378	0.99
7	2	40	1	3	384	0.99
7	2	40	1	3	390	0.99
7	2	40	1	3	396	0.99
7	2	40	1	3	402	1.00
7	2	40	1	3	408	1.00
7	2	40	1	3	414	1.00
7	2	40	1	3	420	1.00
7	2	40	1	3	426	1.00
7	2	40	1	3	432	1.00
7	2	40	1	3	438	1.00

7	2	40	1	3	444	1.00
7	2	40	1	3	450	1.00
7	2	40	1	3	456	1.00
7	2	40	1	3	462	1.00
7	2	40	1	3	468	1.00
7	2	40	1	3	474	1.00
7	2	40	1	3	480	1.00
7	2	40	1	3	486	1.00
7	2	40	1	3	492	1.00
7	2	40	1	3	498	1.00
7	2	40	1	3	504	1.00
7	2	40	1	3	510	1.00
7	2	40	1	3	516	1.00

AUTOBIOGRAPHIC SUMMARY

Margarita Loredo Cancino

Doctoral candidate in the Sustainable Processes orientation

Dissertation title: ARTIFICIAL NEURAL NETWORK MODELING OF PHENOL ADSORPTION ONTO BARLEY HUSKS ACTIVATED CARBON IN AN AIRLIFT REACTOR

Orientation: Sustainable processes

Biography: Born in Rioverde, San Luis Potosi on October 15, 1980, daughter of Ponciano Loredo Martinez and Martha Cancino Hernandez.

Education: Graduated from Universidad Autonoma de San Luis Potosi with a Bachelor degree in Chemical Engineering in 2001, and a Master of Science degree in Hydrosystems in 2005.

Professional Experience: Environmental Analyst in ArvinMeritor from 2002 to 2004, Environmental Leader in AFL Telecommunications from 2005 to 2006, and Quality and Environmental Systems Specialist in Philips® from 2006 to 2009.